Electroosmotic Flow Characterization and Enhancement in PDMS Microchannels

by

Zeyad Almutairi

A thesis
presented to the University of Waterloo
in fulfillment of the
thesis requirement for the degree of
Master of Applied Science
in
Mechanical Engineering

Waterloo, Ontario, Canada, 2008

I hereby declare that I am the sole author of this thesis. This is a true copy of the thesis, including any required final revisions, as accepted by my examiners.

I understand that my thesis may be made electronically available to the public.

Abstract

Electroosmotic flow is widely used as a solution pumping method in numerous microfluidic applications. This type of flow has several advantages over other pumping techniques, such as the fast response time, the ease of control and integration in different microchannel designs. The flow utilizes the scaling of channel dimensions, which enhances the effects of the electrostatic forces to create flow in microchannels under an electrical body force. However, the electrostatic properties of the solution/wall material pairings are unique and must be experimentally measured. As a consequence, accurate knowledge about the electrostatic properties of the solution and wall material pairings is important for the optimal design of microfluidic devices using electroosmotic flow. Moreover, the introduction of new solutions and new channel materials for different applications is common in the microfluidics area. Therefore, any improvement on the experimental techniques used to examine the electrostatic properties of microchannels is beneficial to the research community.

In this work, an improvement to the current-monitoring technique for studying the electrokinetic properties of microchannels is achieved by replacing the conventional straight channel design with a new Y-channel design. The errors from both the undesired pressure driven flow and solution electrolysis were addressed and significantly reduced. The new design offers high accuracy in finding the electrokinetic properties of microchannels. The experimental outcome from the new channel design is better compared to the outcomes of the straight channel, which helps in distinguishing the important electroosmotic pumping regions from the current-time plot. Moreover the time effectiveness in performing the experiments with the new channel design is better compared to that for the straight channel design.

A modified analysis approach is also presented and validated for finding the electrokinetic properties from the outcomes of the current-monitoring technique, which is called the current-slope method. This approach is validated by comparing its findings with the results of the conventional length method. It was found for most situations that the discrepancy between the two methods, the current-slope and total length method, are within the uncertainty of the experimental measurements, thus validating the new analysis approach. In situations where it is hard to distinguish the start and end of solution replacement from the current-time plot of the current-monitoring technique, the current-slope method is advised.

With the new design, different parametric studies of electroosmotic flow in PDMS based microchannels are estimated. At first the zeta potential of biological buffers are studied. Moreover the effect of continuous electroosmotic pumping, the chip substrate

structure, and temperature on the average zeta potential of microchannels are examined. It was found that for air plasma treated PDMS microchannels the chip substrate material does not have an effect on the average zeta potential of the microchannels.

The following chemical treatments are attempted with the aim of improving the surface and electrostatic properties of PDMS based microchannels: prepolymer additive with acrylic acid, extraction of PDMS, and both heat and plasma induced HEMA (Hydroxyethyl methacrylate) grafting on the surface of PDMS. Extensive characterization is performed with different experimental methods. The stability of the artificial hydrophilic properties of the PDMS microchannels with time was improved with both the extraction and HEMA grafting techniques. On the other hand, there was no evidence of any improvement in the zeta potential of microchannels with the surface treatments.

Acknowledgements

In the name of God the most gracious the most merciful.

First I would like to thank both of my supervisors Prof. Ren and Prof. Johnson for their help and support during my quest for the master degree. The research attitude, and the encouragement from Prof. Ren has changed my research approach to a better state and are well appreciated. My sincere gratitude to Prof. Johnson for his professional advises and ideas regarding my research. At one point during the master program he stood by my side and helped me to overcome serious problems that were hindering my progresses in the research. I'm very grateful to him.

I would like to thank Prof. Culham and Prof. Yarusevych for agreeing to be the committee members of the MSc degree. Their comments and suggestions have helped in improving the thesis structure.

Special thanks to Prof. Leonardo Simon from the chemical engineering department for his assistance, discussion and support with the ATR-FTIR system. Also thanks and appreciation to Prof. P. Chen from the chemical engineering department for allowing the use of his contact angle measurement system.

Special appreciation is directed to the group members at the Microfluidics lab at the University of Waterloo. Lab members that I worked closely with and deserve recognition are Tom Glawdel, Razim Sami, Jay Taylor, and Sean Wang.

I would like to thank my sponsor King Saud University for their financial support during my graduate studies. Also I wish to thank the Saudi Cultural Bureau in Canada for their endless efforts for assisting the Saudi students in Canada. Their work is in the shadow and I would like to thank them for it.

Special thanks for my dear friends here in Waterloo who made the work in last two years somewhat enjoyable. I gained great friends that I would like to dedicate them with special appreciation whom are Mubarak Almutairi (My Cousin), Fawaz Alsolami, Abdulaziz Alkhoraidly, Ammar Altaf and Khalid Almutairi.

Last but not least, I would like to thank my dear family who supported and encouraged me to stay with my choices. Special appreciation and respect to my father, who is my main inspirer. He raised me on looking for the hard path, pursue new adventures, and not to be short-sighted about different issues. Sincere appreciation to my mother, since her love and support was there when I need it. I'm indebted for the affection of my siblings, especially my younger sister Tahani.

Dedication

To My Father and Mother.

Contents

List of Tables

List of Figures

Nomenclature

Acronyms

AA	Acrylic acid
ATR-FTIR	Attenuated total reflectance Fourier transform infrared spectroscopy
EDL	Electric double layer
FTIR	Fourier transform infrared spectroscopy
GUI	Graphical user interface
H-S	Helmholtz-Smoluchowski
HEMA	Hydroxyethyl methacrylate
IR	Infrared beam
PCR	Polymerase chain reaction
PDMS	Polydimethylsilicone
P/G , P/g	PDMS/glass hybrid microchip
P/P	PDMS/PDMS microchip
P/SU8	PDMS/SU8 hybrid chip
TCMS	Trimethlylchlorosilane
UDA	Undecylenic acid

Mathematical Symbols

A_{ab}	Absorbance of infra red beam
A_c	Microchannel cross sectional area (m^2)
A_{c_exp}	Expected microchannel cross sectional area (m^2)
c_p	Specific heat of the solution $(J/kg \cdot K)$

c_i	Molar concentration of species i (mol/L)
C	Concentration of chemical compound (mol/L)
C_{light}	Speed of light (m/s)
D_i	Diffusion coefficient of species i (m^2/s)
D_h	Hydraulic diameter of microchannel $\left(= \frac{4 \cdot A_c}{P}\right)$
e	Electron charge (C)
$\vec{E}, E$	Applied electric field (V/m)
E_x, E_y, E_z	Applied electric field at different coordinates (V/m)
E_s	Streaming potential (V)
f	Form factor of channel or capillary (m^{-1})
$\vec{F_b}$	External body force in vector notation (N/m^3)
h	Channel height (m)
I	Electrical current (A)
I_1, I_2	Steady current values at the start and end of replacement (A)
I_{bulk_cond}	Current carried from the bulk conductivity of the solution (A)
I_{surf_cond}	Surface current carried within the EDL (A)
I_{total}	Total current draw during electroosmotic flow (A)
k	Spring constant (N/m)
k_b	Boltzmann constant (m^2kg/s^2K)
l	Path length of the infra red beam (m)
L	Channel length (m)
$L_{channel}$	Total channel length (m)
L_d	Displacement length in the microchannel in the Y-channel design (m)
L_{side}	Side channel length of the Y-channel design (m)
m	Mass (kg)
M	Solution concentration (mol/L)
n_i	Ionic number
$n_{i\infty}$	Ionic concentration at natural state
P	Channel perimeter (m)
$\triangle p, \vec{p}$	Pressure (Pa)
Re	Reynolds number
$R_{electrical}$	Electrical resistance of the solution in the microchannel (Ohm)
R_i	Rate of generation of species i due to chemical reaction
R_1, R_2	Meniscus radius (m)
$R1, R2, R3$	Reservoirs of the microchannel
t_1, t_2	Start and end of replacement times (s)
$\triangle t$	Time difference (s)

T	Absolute temperature in kelvin (K)
$\vec{T}$	Temperature field (K)
T_{tran}	Transmittance of infrared beam
$\vec{u}$	Velocity field (m/s)
u_{av}	Average velocity in microchannel (m/s)
u_{slip}	Slip velocity at shear layer in the EDL (m/s)
u_{emo}	Average electroosmotic velocity in the microchannel (m/s)
w	Channel width (m)
W	Wave number (cm^{-1})
z_i	Valence of ion specie i

Greek Symbols

α	Concentration coefficient
ε	Solution permittivity (dielectric constant) (C/Vm)
ε_o	Vacuum permittivity (C/Vm)
ε_r	Solution relative permittivity $\left(= \frac{\varepsilon}{\varepsilon_o}\right)$
ϕ	Applied electric potential ($Volt$)
κ^{-1}	Debye length (m)
λ_b	Solution conductivity (S/m)
λ_s	Surface conductance (S - Siemens)
ω	Frequency of vibration (Hz)
ψ	Electrostatic potential from the surface charge ($Volt$)
μ	Solution viscosity ($Pa \cdot s$)
μ_{emo}	Electroosmotic mobility ($m^2/V \cdot s$)
ρ	Solution density (kg/m^3)
ρ_f	Charge density
σ	Fluid surface tension (N/m)
σ_{sg}	Solid-gas interfacial energy (N/m)
σ_{sl}	Solid-liquid interfacial energy (N/m)
θ	Contact angle ($Degree$)
ζ	Zeta potential ($Volt$)

Chapter 1

Introduction

1.1 Background

The area of microfluidics has attracted an increased interest in recent years from researchers in chemistry, biomedical and engineering sciences [1, 2, 3, 4, 5]. The area attracted research since it offered different features that are beneficial for many applications [1, 2, 3, 4, 5]. Controlling the environmental domain in microdevices, such as the mass flow, and temperature, can be achieved with high precision [4, 5]. Moreover, reducing the volumes of reagents, shortening the experimental time, and increasing the detection accuracy are reasons for the interest in microfluidics [4, 5].

Microfluidics is a multidisciplinary field where researchers combine their efforts to successfully manufacture devices for desired applications [5]. The design of microfluidic devices may require the integration of different physical phenomena and will go through stages (such as device analysis, numerical simulations, prototyping, and validation studies) before the final micro device is produced. Currently the micro total analysis (μTAS) has the largest research interest, where different applications are integrated and optimized in one chip [1, 3, 5]. The fabrication of a successful μTAS-chip for an application may involve: flow pumping, reagent mixing, flow control, and detection processes [5]. The μTAS analysis is also referred to as *Lab-on-Chip*. The main applications for research in *Lab-on-Chip* are in biomedical diagnostics.

The global market for technologies related to the microfluidics area was approximated to be 3 billion dollars in 2006, and it is expected to grow [1, 3]. The main area of research is the *Lab-on-Chip* applications which are related to the health sciences [1, 3, 6, 7]. The objective is to successively manufacture chips that will perform different biomedical analyses with high accuracy and short operation time. However, other areas

related to microfluidics, such as chemical synthesis and sensors, also received a large interest [1, 2, 5, 8, 9].

Throughout the applications of microfluidics, electroosmotic flow is extensively used in various functions, such as sample transport, micromixing, and reagent delivery [4, 10]. Various aspects of electroosmotic flow such as the ease of control, fast response time, and ease of integration, are reasons that attracted researchers to use it in numerous applications [4, 10]. Electroosmotic flow can be created in microchannels since the effects of electrostatic forces are increased in the microscale, and under an applied electric field flow is achieved. As a consequence, accurate knowledge about the electrostatic properties of the solution and wall material pairing is important for the optimal design of microfluidic devices using electroosmotic flow [4, 10].

As microfluidics evolves, different channel material and new solutions are frequently introduced in numerous applications. One example is polydimethylsilicone (PDMS), which is an elastomeric polymer widely used as a microchannel substrate material because of the ease and cost of manufacturing. Also, PDMS supports electroosmotic pumping in microchannels. However, the electrostatic properties of PDMS are lower than that of glass or silicon. PDMS also has several disadvantages, such as the hydrophobic nature and the sample adsorption, which hinder the use of PDMS in different microfluidic applications. Thus, the area of treating PDMS for different applications has gained an interest from different researchers with an aim of improving the electrostatic properties of PDMS.

1.2 Research Motivator

In different microfluidic applications electroosmotic flow is used as a pumping technique to drive fluid and transfer species through channel geometries [4, 10]. Electroosmotic flow utilizes the geometrical scaling effects of microscale channels which will enhance the effects of electrostatic forces [4, 10]. To this end, different experimental techniques are available to study different electrostatic properties of microchannel walls and solutions, and the most common technique in the microfluidics community is the current-monitoring technique. If correctly used, the current-monitoring technique is simple and reliable. However, for microchannels in chip format the technique has some practical weaknesses that will affect its results. Problems such as the solution electrolysis and undesired pressure driven flow can cause errors from the outcomes of the current-monitoring technique.

In the first part of the thesis the improvement on the current-monitoring technique is

presented with the use of a new Y-channel design. Also, a modified analysis approach, the current-slope approach, for the experimental outcomes of the current-monitoring technique is presented and validated.

In the microfluidic area, PDMS is widely used for different applications as a channel material in devices utilizing electroosmotic flow. PDMS is hydrophobic and has low electrostatic properties (the zeta potential ζ), compared to glass. For these reasons, the second motivator for this work is the enhancement of the electroosmotic flow and surface properties of PDMS based microchannels. Different chemical based surface treatments are attempted and a full scope characterization is done with experimental approaches.

1.3 Objective and Outline

The general scope of the thesis is divided into two main parts, first the study of the electrostatic properties of biological buffers in PDMS based microchannels, and second the enhancement of the electrostatic and surface properties of PDMS based microchannels. The main goals of this work are as follows:

1. Develop a simple and reliable channel design and improved experimental approach to study the electrostatic properties of microchannels.
2. Propose a new analysis approach, the current-slope approach, for the outcomes from the current-monitoring technique.
3. Measure the electrostatic properties of different biological buffers, MOPS, L15-ex, and HEPES, that have not been reported in the literature.
4. Perform different parametric studies on the electroosmotic flow in microchannels to find the effects of changing the experimental conditions on electroosmotic flow in PDMS microchannels.
5. Enhance the surface electrostatic properties of PDMS based microchannels with chemical treatments.
6. Perform a characterization study of the effects of the chemical treatments on the hydrophilic and zeta potential properties of PDMS based microchannels

The thesis is outlined as follows:

Chapter 2: An overview of the theory and basic concepts of microfluidics is presented. The chapter will also include a literature review on both the current-monitoring technique and the surface treatment of PDMS based microfluidic chips.

Chapter 3: The experimental setups used in this work will be presented in this chapter. Mainly, the solutions used, the chip and sample manufacturing, the current-monitoring setup, the contact angle system, the ATR-FTIR system, and the fluorescence microscopy system are discussed.

Chapter 4: In this chapter the new Y-channel design will be presented to study the electrostatic properties of microchannels with the current-monitoring technique. The different aspects of the design will be discussed. Moreover, the validation of the accuracy of the Y-channel design with different criteria will be examined.

Chapter 5: The chapter will first present the modified current-slope approach that was proposed for analyzing the outcomes of the current-monitoring technique. Also, different parametric studies on electroosmotic flow in PDMS microchannels will be presented.

Chapter 6: This chapter will discuss the different chemical based surface treatments used to modify and enhance the electrostatic properties of PDMS based microchannels. The characterization of the effects of the treatments will be presented with different experimental studies.

Chapter 7: In this chapter a summary of the results that were reached in the present work will be presented. Recommendations for further improvements on the current studies will also be presented.

Chapter 2

Literature Review

The design of microfluidic applications requires an understanding of physical phenomena in microscale [1, 3, 11, 8, 6, 7]. Due to dimensional scaling, certain phenomena diminish such as the convective momentum and the gravity force compared to others like the viscus and electrostatic forces. First a view of the different applications of microfluidics will be presented. A general overview of different transport phenomena in microscale is discussed in this chapter with the emphasis on the momentum transport phenomena. Also, the use of PDMS as a channel substrate material is discussed. Furthermore, the surface modifications that have been used to maintain desirable surface properties in PDMS based microchannels are reviewed.

2.1 Microfluidics Background

Microfluidics can be defined as the study of the transport and control of minute volumes of fluid in small scale devices [1]. The area was introduced following the establishment of MEMS (Microelectromechanical systems), which allowed manufacturing microchannels with high accuracy [1]. Microfluidics gained interest in different bio-medical diagnostics and chemical synthesis research because of its promising advantages such as handling minute samples, increasing the detection accuracy, and reducing the time needed to perform experiments were reasons that attracted research to microfluidics [5, 8, 12, 13, 14]. Moreover the ability and precision in controlling the experimental environment, such as temperature and flow rate, were other reasons for this interest [2, 5, 8, 6, 7, 15]. The microfluidics area is also facing great challenges, such as material challenges, flow control, mixing, and cost of devices [2, 5, 8]. Up to now most of the research that has been done in microfluidics is still in the proof of concept stage and validating its use in dif-

ferent applications [1, 5, 8, 13]. However, it is anticipated by numerous researchers that in the near future devices with microfluidic concepts for biomedical and life sciences applications will be available [1, 2, 5, 8, 7, 14].

Lab-on-Chip is the area that is concerned with studying and promoting the application of microfluidic concepts in biomedical applications [5, 7]. Microchip devices, such as cell sorter, cell culture, DNA, and protein separation and analysis, are examples of *Lab-on-Chip* devices [14, 16, 17, 18, 19, 20, 21]. Presently *Lab-on-Chip* applications is the area that has the highest attraction for research in microfluidics [5, 15]. The future goal of *Lab-on-Chip* is developing portable biomedical diagnostics devices with high accuracy and short analysis time. Achieving this goal needs cooperation between researchers from different scientific disciplines and it will involve the optimization of different physical phenomena.

An example of a micro device that is considered as a *Lab-on-Chip* device was presented by Dodge *et al.* [22]. The main operation of the chip was to isolate myoglobin, a single chain protein, from a bio-sample. The system involved the integration of flow controllers, pumps, and micromixers [22]. Another example for microfluidics application in the bio-medical area is the PCR chip (polymer chain reaction) for DNA. The PCR technique amplifies a DNA sample with heat controlled reactions. This is performed in microfluidic chips since precise temperature control and variation can be achieved with high precision [17, 18, 23]. Recently, Lui *et al.* [23] was able to integrate a chip with ITP-ZE (Isotachophoresis-Zone electrophoresis) to separate the Hepatitis B virus with high accuracy that competed with the accuracy of conventional macro devices [23].

Agilent Technologies successively produced a commercial product which was based on microfluidic concepts. The *Agilent HPLC-chip* is a microfluidic chip that is used along with the *Agilent 2100* bioanalyzer to perform liquid chromatography of bio samples. The HPLC-chip is polymeric based and reusable. Agilent states that the accuracy and the time for performing measurements with this chip are better than conventional methods [24].

In chemical synthesis applications, the microfluidics area is also promising since the precision of controlling the mass and thermal transport are high in the microscale [2, 8, 9, 12]. An example of a successive chemical synthesis application in microfluidics was presented by Miller *et al.* [12]. They successfully performed a carbonylation reaction in a glass microchip. This type of reaction in macro scale needs high pressure and special conditions, yet it was achieved in microscale with a reaction rate higher than that of a macroscale domain [12].

The first era of microfluidics started with microchips fabricated from glass and silicon. The fabrication process was time consuming and expensive [1, 3]. The introduction

of polymeric based materials to the microfluidics area was the period for which the research in microfluidics gained a lot of interest because of the simplicity and cost of manufacturing the chips. PDMS (polydimethylsilicone) is one polymeric material that attracted the attention of researchers because of its favorable properties that suit different microfluidic applications. On the other hand, PDMS needs to be treated for certain applications, as will be discussed later in this chapter.

Initially, microchips for microfluidic applications were fabricated from glass and silicon. The fabrication process was time consuming and expensive [1, 3]. The introduction of polymeric-based materials to the microfluidics area attracted a huge interest because of the simplicity and low cost of manufacturing the chips. PDMS (polydimethylsilicone) is one polymeric material that attracted the attention of researchers because of its favorable properties, such as optically transparent, ease of manufacturing, and low cost, which suits different microfluidic applications. On the other hand, PDMS needs to be treated for certain applications, as will be discussed later in this chapter.

For an integrated microfluidic chip, different processes may be incorporated and optimized in a single chip, such as sample transport, flow control, temperature control, and effective mixing [1, 2, 3, 8]. These goals are achieved by an understanding the transport phenomena of fluids in microscale [1, 2, 3, 8].

2.2 Microscale Transport Phenomena

An understanding of transport phenomena of mass, momentum, and heat in microscale is important for the design of microfluidic devices. In the literature there are several books that cover different transport phenomena in microfluidic applications [1, 3, 4].

For the liquid phase in a microchannel, the continuum approach is still valid as long as the characteristic length of the microchannel is large compared to the mean free path of the fluid molecules [1, 3, 4, 11, 8] [1]. This is the case for most microfluidic devices, and for the work that will be discussed in this thesis. Thus, the established macro scale mass, momentum, and energy conservation equations are appropriate to analyze the microfluidic systems. Moreover, solution properties, such as viscosity, density, and electrical conductivity are assumed to be identical to the values used in the macro scale analysis.

[1] The Knudson number relates the mean free path between the molecules of the fluid with the characteristic length of flow domain. The Knudson number gives a direction on how to analyze the fluid flow and if the continuum approach is valid. It is very important for gas dynamic analysis since the intermolecular distance of the gas molecules are higher than of liquids [3].

Due to the scaling of geometry and the large surface to volume ratio of channels, different phenomena will have considerable effects on the flow. First, the Reynolds number (Re) in microchannels is around unity and the flow is laminar [1, 3]. As a consequence, viscous forces play a significance role in the flow. Also, the mixing speed of non reacting solutions is low in the microscale, since the dominant mixing mechanism is the diffusion of the species [1, 3, 25]. Moreover, the electrostatic effects become significant in microscale. This comes in the formation of the electric double layer (EDL) of ions in a region close to the wall of the microchannel. Body forces also change in the microscale with the gravity effects diminishing compared to the electrostatic and capillary forces [1, 3, 4]. Electrostatic effects play a major role in flow development in microscale such as electroosmotic flow and electrophoreses [4, 11].

2.2.1 Electric Double Layer (EDL)

When a channel surface comes in direct contact with a solution that has polar properties and in the absence of chemical reactions, a static surface charge will build along the wall [4, 11, 26]. This build up of the electric potential can occur due to different chemical mechanisms, such as ionization of surface groups, specific ionic absorptions on the wall, or other mechanisms [4, 11, 3]. This surface charge will affect the solution ions. The ions that have the opposite charge of the wall will be attracted and the ones having the same charge as the wall will be repelled. This phenomenon takes place to neutralize the wall surface charge. The region close to the wall where the wall surface charge is affecting the solution ions is called the electric double layer (EDL). Figure 2.1 presents a schematic of the EDL.

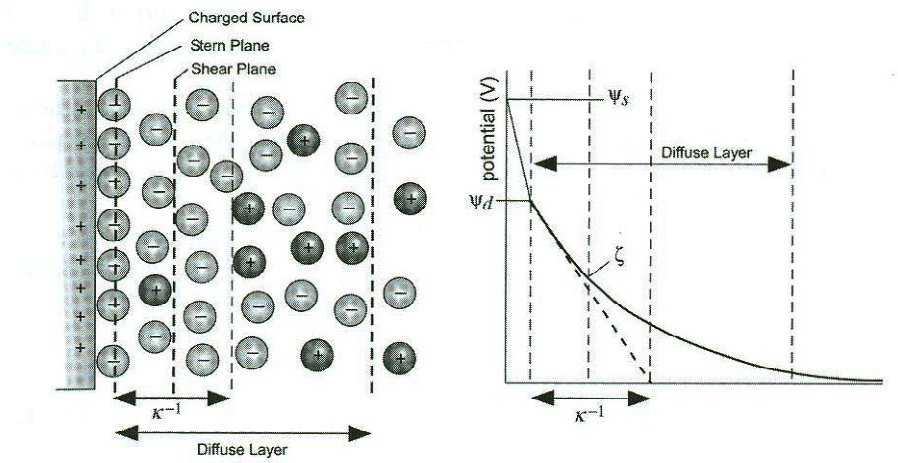

Figure 2.1: The electric double layer (EDL) [11].

As presented in Figure 2.1 there are two distinct regions in the EDL: a region containing immobile ions (stern layer), and the diffuse layer. The stern layer is the region where the ions are firmly attracted to the wall. The diffuse layer is the region in which the ions have some mobility of motion, such as diffusion, while still being affected by the wall charge. The thickness of the EDL is approximated to be in the same order as the Debye length [4, 11, 3]:

$$\kappa^{-1} = \left(\frac{\varepsilon \cdot k_b \cdot T}{2 \cdot e^2 \cdot z_i^2 \cdot n_{i\infty}} \right)^{1/2} \tag{2.1}$$

where κ^{-1} is the Debye length, ε is the solution permittivity, k_b is the Boltzmann constant, T is the absolute temperature, z_i is the valance of the species i, e is the electron charge, and $n_{i\infty}$ is the ionic concentration at natural state. The Debye length for a symmetric electrolyte with a valance of $z_+ = -z_- = z$ at a temperature of 25^oC can be approximated by [11]:

$$\kappa^{-1} = \frac{3.04}{z \cdot \sqrt{M}} \times 10^{-10} \tag{2.2}$$

where M is the solution concentration in mol/L. Equation 2.2 suggests that thickness of the EDL will decrease as the solution concentration increases because more ions are available to neutralize the wall surface charge.

The analysis of the electric potential carried within the EDL is important since it is a body force in the microscale cannot be neglected. To find the effect of applying an external body force on the EDL, the charge distribution of the ions in the EDL region must be found. The analysis of the electric charge potential follows the derivation presented in the literature [4, 11, 26]. It is assumed that the ionic distribution for a certain species follows a Boltzmann distribution and is presented by [4, 11, 26]:

$$n_i = n_{i\infty} \exp\left(-\frac{z_i e \psi}{k_b T} \right) \tag{2.3}$$

where n_i is the ionic concentration of species i, $n_{i\infty}$ is the ionic concentration at neutral state ($\psi = 0$), z_i is the valance of the ion, e is the charge of the electron, ψ is the electrostatic potential distribution from the wall, k_b is the Boltzmann constant, and T is the absolute temperature. The ionic charge density is found by:

$$\rho_f = \sum_i e \cdot z_i \cdot n_i \tag{2.4}$$

where ρ_f is the charge density of the ions. By assuming that the electric charge distribution is only affected by the wall charge equation 2.4 will reduce to:

$$\rho_f = -2 \cdot e \cdot z_i n_{i\infty} \cdot \sinh\left(\frac{z_i e \psi}{k_b T} \right) \tag{2.5}$$

The electrostatic potential distribution within the EDL could be found from the Poisson relation:

$$\frac{d^2\psi}{dy^2} = -\frac{\rho_f}{\varepsilon} \tag{2.6}$$

$$\frac{d^2\psi}{dy^2} = \frac{2 \cdot e \cdot z_i n_{i\infty}}{\varepsilon} \cdot \sinh\left(\frac{z_i e\psi}{k_b T}\right) \tag{2.7}$$

For a thin EDL the hyperbolic term will reduce to the first term of the Taylor expansion [3]:

$$\sinh\left(\frac{z_i e\psi}{k_b T}\right) \simeq \left(\frac{z_i e\psi}{k_b T}\right) \tag{2.8}$$

Thus, the electrostatic potential reduces to:

$$\frac{d^2\psi}{dy^2} = \kappa \cdot \psi \tag{2.9}$$

One important property of the EDL is the electrostatic potential at the imaginary shear plane in the EDL (figure 2.1 which is called the zeta potential ζ. The zeta potential is important since it relates the average electroosmotic pumping in microchannels with the applied electrical field, as will be presented in the an upcoming section [4, 11, 26].

When an external electrical body force is applied tangentially to the EDL, the mobile ions in the diffuse region of the EDL will move with a non uniform velocity distribution across the EDL thickness. This can be used as for solution pumping since the bulk solution in the region out of the EDL will be dragged by viscous forces. More details on this phenomenon will be presented in explaining the electroosmotic flow.

2.2.2 Thermal Transport

The thermodynamic state of a control volume in a microchannel is governed by the energy balance described previously in the literature for macro scale but with some modifications [1, 3, 8]. The energy conservation equation is presented next:

$$\rho \cdot c_p \left[\frac{\partial T}{\partial t} + \vec{u} \cdot \nabla\vec{T}\right] = \nabla \cdot \left(k\left(T\right) \cdot \vec{T}\right) + \lambda_b\left(T\right) \cdot \vec{E} \cdot \vec{E} \tag{2.10}$$

where ρ is the solution density, c_p is the specific heat of the solution, $\vec{T}$ is the absolute temperature field, $\lambda_b\left(T\right)$ is the solution conductivity as a function of temperature, and $\vec{E}$ is the applied electrical field. Due to scaling of the geometry the surface to volume ratio in microchannels is very high and the heat dissipation is large [1, 12]. This improves

precision in controlling the heat in the microscale domain [1, 8] and has been utilized in different microscale applications that need precise temperature control, such as PCR chips.

An important phenomenon that has crucial effects on the stability of electroosmotic pumping is the joule heating [27]. This phenomenon happens since the solution that is being pumped has an electric conductivity which will create an electric current. Thus, the presence of both the electrical current and the applied voltage creates internal heating. This will cause changes in the solution properties, moreover the flow pumping conditions will change. This will effect the outcome of the electroosmotic pumping. Therefore, it must be taken into consideration when electroosmotic pumping is used [27]. The final term of equation 2.10 is the internal heat generation in the presence of joule heating.

2.2.3 Mass Transport

The knowledge of the species distribution in microscale flow is important in different chemical synthesis and biological applications [11]. The mass conservation for a single specie in a flow field is governed by the advection-diffusion equation [11]:

$$\frac{\partial c_i}{\partial t} + \vec{u} \cdot (\nabla \vec{c_i}) = D_i \nabla^2 \vec{c_i} - \frac{D_i z_i e}{k_b T} \nabla \cdot \left(\vec{c_i} \vec{E} \right) + R_i \tag{2.11}$$

where c_i is the molar concentration of species i, D_i is the diffusion coefficient of species i, z_i is the valance of the specie, e is the electron charge, and R_i is the rate of generation of species i. In the absence of flow convection, the equation reduces to Fick's law [1, 2, 3, 11]. One of the challenges facing microfluidics is performing effective mixing of reagents to improve chemical synthesis and different biological reagent mixing [8, 28, 29]. Since the flow is laminar, the species diffusion is the dominant mass-mixing mechanism. In situations where chemical reactions are driven by diffusion, the rate of reaction in micro scale will improve [8]. In other applications, where the solutions are non-reacting, mixing enhancing procedures must be used.

2.2.4 Momentum Transport

The basic laws that govern the momentum transport in micro scale fluid flow are similar to the macro scale, which are the Navier-Stokes equations [1, 3, 4, 11]. The general momentum is governed by [1, 3, 4, 11]:

$$\rho \left[\frac{\partial \vec{u}}{\partial t} + (\vec{u} \cdot \nabla) \vec{u} \right] = -\nabla \vec{p} + \mu \nabla^2 \vec{u} + \vec{F_b} \tag{2.12}$$

where ρ is the solution density, μ is the solution viscosity, ∇p is the pressure gradient, and $\vec{F_b}$ is the applied body force. Body forces from gravity effects diminish in the flow field because of the scaling of geometry [2]. Thus, the electrostatic body force and the capillary effects will have an influence on the flow in microscale and must be considered [1, 3, 4, 10, 11].

In most cases the flow in microchannels is steady and laminar with Re less than unity (Re ≤ 0.1). Thus, the time dependent term will be eliminated. Moreover, the convection term in the equation 2.12 could be neglected compared to the viscous term [1, 3]. This leads to Stokes' approximation of the momentum conservation [1, 3]:

$$0 = -\nabla\vec{p} + \mu\nabla^2\vec{u} + \vec{F_b} \tag{2.13}$$

The three major pumping methods in microfluidic devices are: pressure driven flow, capillary driven, and electroosmotic driven flow. The main aspects of these methods will be presented next, with more elaboration on electroosmotic driven flow.

Pressure Driven Flow

Pressure driven flow is achieved by applying a pressure difference between the nodes (reservoirs) of the channel network with the aid of an external pressure source, such as syringe pumps [10]. The velocity field in the channels will have a parabolic profile, identical to the laminar Poiseuille flow profile [1, 3], across the cross section area of the channel [1, 3], which is unfavorable for sample transport and detection applications [30]. This Poiseuille flow profile will increase the sample dispersion and the lower the accurate detection of the analytes. Also, the need for an external pressure source complicates the hardware setup, and the portability of the devices is affected. Another issue with pressure driven flow is that immediate flow control is hard to achieve since valving elements are hard to integrate in microchips that use hard materials for channel substrates [1, 3, 31]. Thus, different means of flow control in pressure driven flow in microscale is still an open research problem [31].

Unger *et al.* [31] utilized the flexibility properties of PDMS microchannels to create pneumatic operated valves in microchips that allowed the control of the flow direction in microchips. The main issue with their system is that the controlling of the valves is achieved with a large external setup, which eliminates the portability of the device [10].

[2] The gravity force is scaled to the third power while the capillary force is scaled to the first power compared to the characteristic length . The decrease in the dimensions will reduce the gravity effects compared to the capillary and electrostatic forces [1].

A unique phenomena happens with pressure driven flow in shallow microchannels which is the electroviscous effects [4, 11, 26]. When fluid flows in a shallow microchannel, and due to the presence of EDL, this flow will cause the free ions in the EDL to move in the flow directions and accumulates. This accumulation of ions induces a potential field that creates a back flow in the microchannel. To an observer, the flow rate will be lower than the predicted flow rate from the traditional laminar Poiseuille flow equation. This is analogous to an increase in the viscosity of the solution in the microchannel; hence it is called the electroviscous effect. This effect has been utilized in the streaming potential technique to find the electrostatic properties of materials.

Capillary Driven Flow

Capillary driven flow uses the surface to volume ratio aspects of microchannels and the surface energy effects of the wall on the solution to create a passive pumping method. By utilizing the nature of the surface tension from channel walls, fluid flow could be achieved by creating gradients regions of hydrophilic channel patterns in the microchannels. This is achieved by creating meniscus shape differences between the two ends of the microchannel [1, 3, 32, 33, 34]. The flow in the capillary can be found by:

$$\triangle p = \sigma \left(\frac{1}{R_1} - \frac{1}{R_2} \right) \tag{2.14}$$

where σ is the fluid surface tension, and R_1 and R_2 are the solution radius of curvature of the gas liquid interface. This method of pumping is useful for passive continuous pumping of solutions in microchannels, but the limitations of immediate flow control is still apparent, similar to pressure driven flow.

In the literature, Berthier and Beebe [32] analyzed the stability conditions of a passive pump utilizing surface tension properties. Suk and Cho [34] used a scheme to pattern the microchannel with hydrophilic and hydrophobic regions to create a flow in the microchannel. Also they studied the effect of the ratio of hydrophilic to hydrophobic areas on the flow field [34].

Electroosmotic Driven Flow

Electroosmotic flow is an electrokinetic driven flow that utilizes the presence of the EDL in microchannels [4, 11, 26]. The flow is created by applying an external body force with an electric field that affects the free ions in the EDL causing them to migrate in a certain direction. The movement of the ions is affected by the sign of the surface charge and the

direction of the electric field. The electric field can be implemented by placing electrodes in direct contact with the solution. The migration of the ions within the EDL will cause the solution in the bulk region, away from the EDL, to move with same velocity due to viscous effects [4, 11, 26]. Figure 2.2 presents a schematic of the principle of the electroosmotic flow for a negatively charged surface under an applied external electric field.

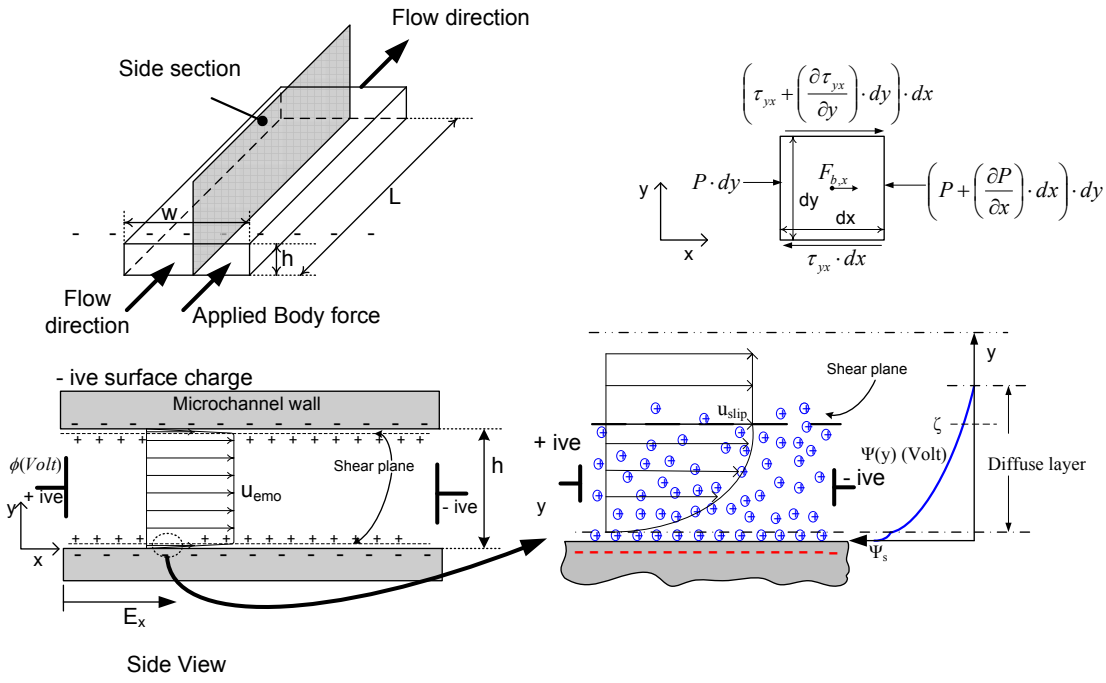

Figure 2.2: Schematic of electroosmotic flow in a microchannel.

The simplicity of incorporating electroosmotic flow in different microchannel designs, ease of control through complex channel geometry, and the fast response time are advantages of electroosmotic pumping which are hard to achieve with other pumping methods [4, 10, 11, 26]. Moreover, the velocity profile is plug like, which makes it attractive for sample transport and detection applications. Electroosmotic pumping has been widely used in several microfluidic applications such as micromixers [29]; cell sorters [16] , electroosmotic pumps [35], DNA stretching [36], and sample handling and separation [37, 38, 39]. On the other hand, electroosmotic flow is not without disadvantages. Problems, such as the occurrence of solution electrolysis and joule heating under certain operation conditions, will negatively affect the electroosmotic flow in microchannels [27, 40, 41].

The analysis of the momentum transport in is important to understand the velocity

flow field during electroosmotic pumping. A representative 2D control volume in solution is presented in figure 2.2 where the CV is under the influence of the pressure, viscous and body forces. The external body force originates from the applied electric potential that will affect the ions in the EDL. As discussed previously, the momentum conservation is governed by [1, 3, 4, 11]:

$$0 = -\nabla\vec{p} + \mu \cdot \nabla^2\vec{u} + \vec{F_b} \tag{2.15}$$

Under the assumption of the absence of pressure gradient, the equation reduces to:

$$0 = \mu\nabla^2\vec{u} + \vec{F_b} \tag{2.16}$$

where $\vec{F_b}$ is the body force coming from the effect of the external electric field on the free ions within the EDL. This body force is calculated by [11]:

$$\vec{F_b} = \rho_f \cdot \vec{E} \tag{2.17}$$

where ρ_f is the ionic charge density in the EDL, and $\vec{E}$ is the applied electrical field in vector notation. For a three dimensional applied electrical field:

$$E_x = \frac{\partial\phi}{\partial x}, E_y = \frac{\partial\phi}{\partial y}, \text{ and } E_z = \frac{\partial\phi}{\partial z}$$

where $E_x, E_y, and E_z$ are applied electric fields in the different directions, and ϕ is the applied potential between the electrodes. Recall from the EDL explanation, section 2.2.1, the net charge density ρ_f is related to the electrostatic surface charge by Poisson equation:

$$\frac{\partial^2\psi}{\partial y^2} = -\frac{\rho_f}{\varepsilon} \tag{2.18}$$

where ψ is the electrostatic potential due to the wall surface charge, and ε is the permittivity of the solution. By considering a flow in a microchannel where the electric field applied in the x-coordinate and the wall surface charge is affecting the ions in y-coordinate, the momentum equation can be reduced to:

$$\frac{d^2u}{dy^2} = \frac{\varepsilon E_x}{\mu}\frac{\partial^2\psi}{\partial y^2} \tag{2.19}$$

By following [1, 3, 4, 11, 26] the equation will reduce to:

$$u = \frac{\varepsilon E_x}{\mu}(\psi - \zeta) \tag{2.20}$$

where ζ is the electrostatic potential at the shear plane of the EDL. In the region away from the EDL $\psi = 0$, and the velocity is equal to the slip-velocity. Thus, equation 2.20 will reduce to:

$$u_{slip} = -\frac{\varepsilon E_x}{\mu}\zeta \tag{2.21}$$

equation 2.21 is known as the Helmholtz-Smoluchowski (H-S) slip velocity equation [1, 11, 26]. For a thin EDL compared to the channel thickness the average electroosmotic velocity in the microchannels is approximated by the H-S slip velocity. From this equation comes the importance of the zeta potential of microchannels since it relates the average velocity in the microchannel with electric field. Another commonly used term to describe electroosmotic flow in microchannels is the electroosmotic mobility $\mu_{emo} = \dfrac{-\zeta \cdot \varepsilon}{\mu}$ which is a regrouping of the zeta potential and the solution properties.

Electrical Current Draw During Electroosmotic Flow During electroosmotic pumping there will be an electrical current draw because of the presence of different ion flux phenomena. By assuming that the channel material is perfectly insulative and no current is carried within the stern layer of the EDL, the current draw has three main contributors. The main electric current components are: the current carried from the bulk solution conductivity, the current carried from the convection of the ions within the EDL, and the current from the diffusion of ions. The current carried from the diffusion of ions is very small compared to other terms, therefore it is neglected. The total current draw will reduce to the current carried from the bulk solution conductivity and the convection of ions in the EDL. Another terminology used to describe the current carried in the EDL is the surface conductance. Equation 2.22 presents the total current draw due to steady electroosmotic pumping of one solution in a microchannel [11]:

$$I_{total} = I_{bulk\_cond} + I_{surf\_cond} = \lambda_b \cdot A_c \cdot E + \lambda_s \cdot P \cdot E \tag{2.22}$$

where I_{total} is the total current draw, I_{bulk_cond} is the current carried from the bulk solution conductivity, I_{surf_cond} is the current carried within the EDL , λ_b (S/m) is the solution bulk conductivity, A_c (m2) is the cross sectional area of the microchannel, λ_s (S) is the surface conductance, P (m) is the perimeter, and E (V/m) is the applied electrical field. Since the solution conductivity could be measured the surface conductance can be determined by rearranging equation 2.22 into:

$$\lambda_s = \frac{I_{measured}}{P \cdot E} - \frac{\lambda_b \cdot A_c}{P} \tag{2.23}$$

where $I_{measured}$ is the steady current recorded during electroosmotic flow in a microchannel. In most cases, the current carried within the EDL is small compared to the current from the solution conductivity. Therefore, the measurement of the surface current needs special techniques and high precision equipment. Presently, the streaming potential is the most adopted method for finding the surface conductance [11, 26, 42, 43]. Recently, the current-monitoring technique was introduced to estimate the surface conductance during electroosmotic pumping [42].

2.3 Zeta Potential Measurements

The importance of the zeta potential is that it defines the electroosmotic flow in microchannels where the higher the zeta potential the faster the electroosmotic pumping. The zeta potential by nature is affected by different properties such as wall surface charge density, solution concentration, and the pH [44, 45], which makes it unique for the solution and material pairings. Furthermore, due to the nature of the microfluidics area new solutions and new materials are frequently introduced and the accurate knowledge of the zeta potential of the solution/wall pairing is important when electroosmotic pumping is used.

As an electrostatic property, the zeta potential can not be measured directly. However, it is inferred from the average flow velocity measurements in microchannels, and then approximated from the H-S equation [4, 11, 44, 45]. Different experimental techniques have been used in the literature to find the zeta potential, but the techniques are not without problems or limitations. The most common experimental methods used to measure the zeta potential are as follows: the current-monitoring technique [4, 46, 41, 42, 47, 48, 49, 50, 51, 52], the streaming potential [26, 43, 53], and direct velocity measurement with micro particle image velocimetry (μ-PIV) and fluorescein photobleaching [46, 54, 21, 51, 55, 56, 57]. These techniques will be presented in the next sections.

2.3.1 Streaming Potential Technique

The streaming potential technique relates the applied pressure difference to the measured streaming potential in order to estimate both the zeta potential and surface conductance of capillary and microchannels [4, 11, 26]. If a solution is forced to flow through a channel with an applied pressure difference, the free ions within the EDL will be carried in the same direction of the flow, creating a current flow. This current flow is called the streaming current (I_{st}). The moving ions accumulate within the EDL, causing an electric potential to build up, and eventually creating another flow in the direction opposite to the pressure driven flow. The flow that was created by the induced electric potential also carries an electrical current called the conduction current (I_{cond}). If the conduction current and the streaming current are equal $(I_{st} = I_{cond})$, then a steady state condition is reached. The electrostatic potential that is built up at the steady state condition is called the streaming potential [26]. By relating the streaming potential and the applied pressure difference both the zeta potential and the surface conductance could be found [26]. Equation 2.24 presents the relation used to analyze the experimental outcomes of

the streaming potential:

$$\frac{E_s}{\triangle p} = \frac{\varepsilon \zeta}{\mu} \frac{1}{(\lambda_b + f \cdot \lambda_s)} \tag{2.24}$$

where E_s is the measured streaming potential, $\triangle p$ is the applied pressure difference,ε is the dielectric constant of the solution, λ_b is the bulk solution conductivity, λ_s is the surface conductance, and f is the form factor of the channel or capillary (perimeter / cross sectional area) [26]. Since both the zeta potential and the surface conductance are unknown several measurements must be performed to find a relationship between $\triangle P$ and E_s. Erickson *et al.* [43] used this technique to find the zeta potential and surface conductance of different solutions in glass. Sze *et al.* [58] used the technique with the modified slope analysis to find the zeta potential of glass coated with PDMS.

The main issue with this technique is that it needs several points of measurements in order to get an estimate of the zeta potential. Moreover, the published results in the literature were not repeatable [43].

2.3.2 Direct Velocity Measurement

Another approach for finding the zeta potential of a microchannel is to quantitatively measure the actual velocity in the microchannel. This can be achieved with different techniques, such as μ-PIV [54, 56, 59], and fluorescent dye photobleaching [46, 51, 57]. Finding the channel zeta potential with direct velocity measurement is not a one step task and needs some advanced hardware and analysis. Nevertheless, these techniques give extra information about flow field by offering real time flow behavior during electroosmotic flow in microchannels [46, 51, 57].

μ-PIV is a quantitative method used to examine the actual flow field in microchannels by tracking fluorescent particles introduced in the flow [3]. The velocity field is found by capturing two consecutive images of the particles in the flow and then performing cross correlation analysis to the images to get information about the flow field. After finding the velocity field from the μ-PIV measurements the zeta potential is found from the H-S equation 2.21. A point of consideration when using the μ-PIV with the electroosmotic flow is that the particles are mostly charged and the applied electric field will cause particles to have an electrophoretic motion. Thus, the tracked velocity is made of the two components which are the electroosmotic velocity of the flow and the electrophoretic velocity of the particles. This issue must be taken with care when analyzing the μ-PIV outcomes with electroosmotic flow. Yan *et al.* [54] used the μ-PIV system to find the zeta potential of glass microchannels. The results of the zeta potential were comparable to results found in the literature. Hsieh *et al.* [59] used a μ-PIV system to find the

electroosmotic mobility of square PDMS microchannels and compared the results with results from the literature.

Another approach is to infer the electroosmotic velocity in a microchannel by tracing a photobleached region in the flow field. This is done by dying the solution with a fluorescent dye and then photobleaching a region of interest with an appropriate light source. The photobleached region will have the same velocity as the electroosmotic velocity. The average electroosmotic velocity could be found by tracking the photobleached region. Pittman *et al.* [46] performed photobleaching of neutral fluorophore to find the steady electroosmotic mobility in a cross microchannels manufactured in glass and compared it to the current-monitoring technique. It was found that the cross intersection will effect the electroosmotic flow in the microchannel. Wang [57] used the photobleaching technique to find the electroosmotic mobility with a glass Y-channel design.

2.3.3 Current-Monitoring Technique

The current-monitoring technique is the most adapted technique in the microfluidic community for finding the zeta potential of microchannels. Figure 2.3 presents a schematic of the operation principle for the current-monitoring technique. The current-monitoring technique is based on a simple concept which is monitoring the current change due to the solution conductivity change while performing electroosmotic pumping [4, 46, 41, 42, 47, 48, 49, 50, 51, 52]. This is achieved by replacing the solution that is being pumped with the same solution but with a slightly different conductivity (ie. 5 % conductivity difference). By monitoring the current change with time and finding the time needed to perform the full replacement the average velocity is estimated.

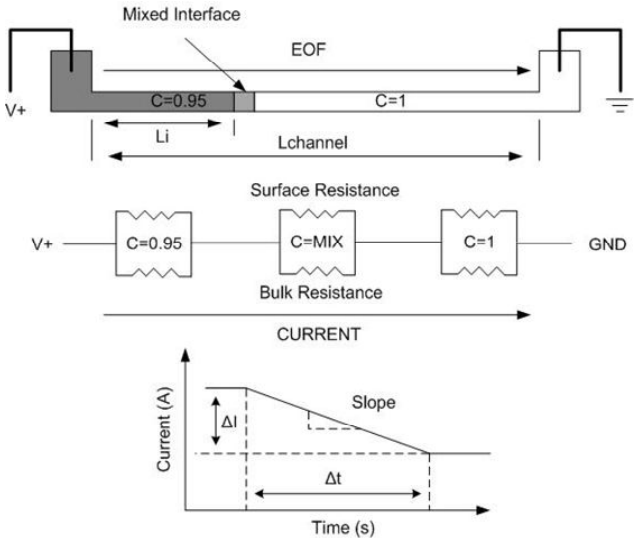

Figure 2.3: The basic concept of the current-monitoring technique [19].

The average velocity is found from:

$$u_{av} = \frac{L_{channel}}{t_2 - t_1} \tag{2.25}$$

where u_{av} is the average velocity of the electroosmotic pumping in the microchannel, $L_{channel}$ is the channel length where the solution is replaced, and t_1 and t_2 are the start and end times of the replacement process found from the current-time plot. Under the assumption that the EDL thickness is very small compared to the channel characteristic length the zeta potential could be found from the H-S equation. While it is a qualitative approach of monitoring the current change, quantitative values of the zeta potential are found with very good accuracy. The current-monitoring method offers the simplicity in both the hardware setup and in performing the experiments. Moreover the technique allows the zeta potential to be found from one measurement.

Certain conditions apply to the current-monitoring technique to estimate the zeta potential of microchannels, such as the experiment must be performed with the same solution but with a slightly different conductivity (5 % conductivity difference), the pH of the tested solutions must be identical since ζ is pH dependent, and the solution temperature must be stable [52].

The first application of the current-monitoring technique was presented by Huang *et al.* [47] to measure the average velocity of 20mM phosphate buffer in a fused silica capillary. Soon after, several researchers applied the current-monitoring technique to

measure zeta potential in silica and glass capillaries, glass microchannels and polymer microchannels [4, 46, 41, 42, 47, 48, 49, 50, 51, 52]. Sinton *et al.* [51] used both the current-monitoring technique and a fluorescent flow field visualization method to find the electroosmotic mobility of Polyimide coated silica capillaries and the results of both techniques were comparable.

Other researchers used the current-monitoring technique to find different characteristics of electroosmotic flow and the zeta potential in microchannels. Venditti *et al.* [52] examined the temperature effects on the zeta potential for PDMS/PDMS and PDMS/glass microchannels for different solutions. The reported results show that for some solutions the zeta potential has strong temperature dependence. Pittman *et al.* [46] used both the current-monitoring and a periodic photobleaching technique of a neutral fluorophore in glass microchannels to find the electroosmotic mobility.

On the other hand, previous current-monitoring experiments did not address several issues that may affect the current-monitoring results [46, 52, 49]. In particular, issues such as undesired pressure driven flow and electrolysis were not considered [46, 52, 49]. Undesired pressure driven flow arises when there is liquid level or meniscus shape (Laplace pressure) differences between the reservoirs, which may induce pressure driven flow in the microchannel. Under these circumstances, the flow in the microchannel is due to both the electroosmotic and pressure driven flow. Since the current-monitoring technique is based on measuring the average velocity of the flow, pressure driven flow introduces significant error. Furthermore, undesired pressure driven flow is limiting the throughput and stability of microfluidic chips using electroosmotic flow as a pumping technique [16, 60, 61].

Solution electrolysis at the electrodes is another major problem that affects the operation of microfluidic chips using electroosmotic flow [40, 41]. The electrolysis process depletes water-based solution due to passing of current and creates additional H^+ ions at the anode and OH^- at the cathode, and the solution change to a gas state. Also, electrolysis causes changes in the pH and electrical conductivity of the solution. The formed ions cause perturbations in the zeta potential, electric field, and EDL thickness as well as a steady rise in the background current. Convection of the electrolyzed solution within the microchannel creates a heterogeneous mixture of high and low conductivity regions that affect the stability of electroosmotic flow. Also, zeta potential by nature is a function of the solution pH [44, 45]; therefore, changes in pH will cause unsteady electroosmotic flow conditions.

From present experience, other important issues have to be addressed when using the current-monitoring technique with channels in chip format. The nature of the tech-

nique requires continuous interaction with the hardware and experimental setup, i.e. solution removal in the reservoirs is usually performed manually and the electrodes are repositioned during this procedure. Moreover, the complete solution removal from the reservoirs was not confirmed. In the case where there is some solution residual at the reservoir, it will cause solution mixing between the new and the old solutions. If a large mixing region exists it is difficult to determine the average velocity from the current-time relationship. Thus, the accuracy of finding the electroosmotic velocity with the current-monitoring technique is affected. In general, it was hard to get repeatable data with the current technique in straight channel designs.

2.4 Microchannel Materials

Microfluidic applications require channel materials with certain properties, such as bio-compatible, chemical inherent, and optically transparent. In the first era of microfluidics glass and silicon were the main materials used to manufacture microchips. These chips had the appropriate properties for the numerous applications [1, 3]. However, the manufacturing process of glass and silicon chips involves special techniques that require a clean environment and dangerous chemicals which were expensive and time consuming. Thus, the search for other types of materials was an exploratory area that received interest. Polymeric based materials present an alternative to glass and silicon since different manufacturing processes could be used to make the chips, such as lithography techniques [62, 63], micro machining, and injection molding.

PMMA (polymethyl accurlate), SU-8 polyethylene, and PDMS (polydimethylsilcone) [62, 63, 50, 64, 65], are polymeric based materials that have been used as channel substrates in microfluidics applications. One widely used polymeric material for microchip fabrication is polydimethylsilcone (PDMS). PDMS is an amorphous hydrophobic polymer [62, 63] where low molecular weight species diffuse inside the bulk material [66]. The surface has a negative surface charge when it comes into contact with a polar solution. The chemical structure of PDMS is $(C_2H_6OSi)n$ shown in figure 2.4. Commercially, PDMS is available in a viscous liquid form and cure after adding a curing-agent. PDMS properties, such as optically transparent, bio-compatible, and supporting electroosmotic flow, suited different applications in microfluidics. In addition, PDMS has some flexibility which has been utilized to make active valving and pumping elements [31, 67]. On the other hand, PDMS is not suitable for all microfluidic applications [68]. Problems such as sample adsorption and non-compatibility with some chemical solvents limit its use in some biological sample analysis and chemical synthesis [68, 46, 18].

Moreover the zeta potential of native PDMS is lower than glass. For these reasons different treatments have been used to improve the surface properties of the PDMS [68, 46, 18].

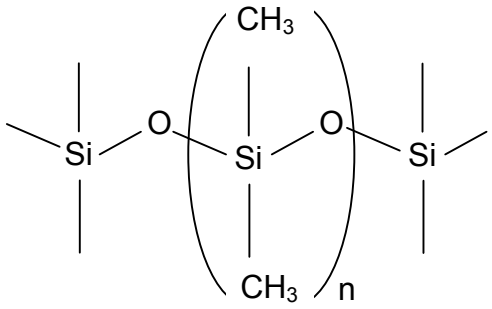

Figure 2.4: The basic structure of PDMS.

A common one-step treatment used to alter the surface properties of PDMS into a hydrophilic state and increase the zeta potential is the plasma treatment. Figure 2.5 presents a schematic of the concept for the plasma treatment and hydrophobic regeneration on the surface of PDMS. The general physics of the plasma treatments can be explained in a simple manner where plasma, an ionized gas, is induced at low pressure with a radio frequency electric field through magnetic induction process [69, 70] . The plasma at high energy state breaks the $Si-CH_3$ bond and forms $Si-O^-$ bond. The formed $Si-O^-$ reacts to form $Si-OH$ groups. The $Si-OH$ groups are better than the previous $Si-CH_3$ in terms of surface charges and hydrophilic nature. Unfortunately, the plasma treatment is not stable with time due to the diffusion of hydrophobic uncured LMW PDMS (LMW: low molecular weight PDMS) to the surface of the PDMS. The phenomenon of regaining the hydrophobic nature of PDMS is favorable in some electrical insulation applications, and for this reason PDMS has been widely used as an insulator [66, 70, 71]. However, this phenomenon is hindering the performance of PDMS in microfluidics chips utilizing electroosmotic pumping techniques. In these applications higher wall surface charges and the hydrophilic properties are desired [66].

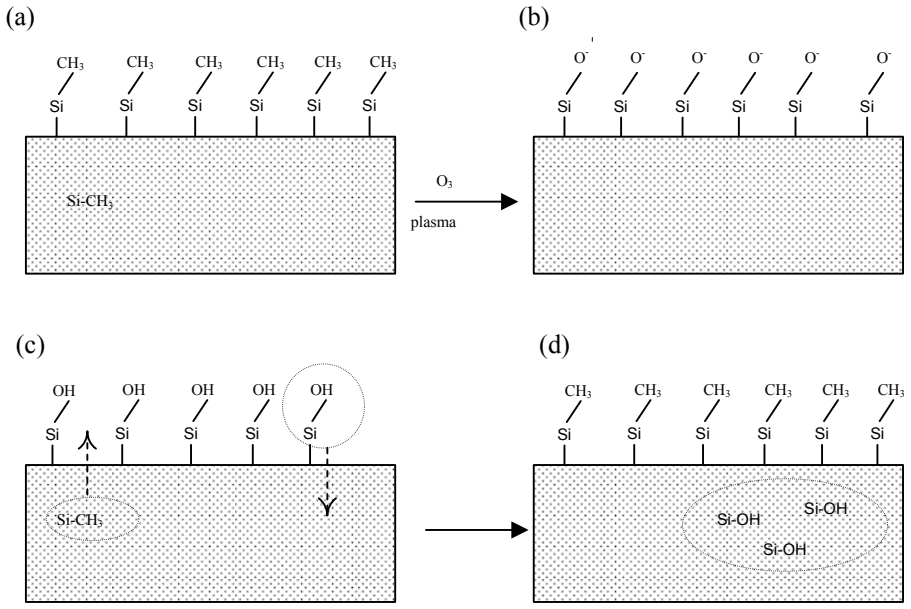

Figure 2.5: Plasma treatment and the hydrophobic regeneration of PDMS.

One approach used to preserve the hydrophilic state of the plasma treated PDMS is to store it in a hydrated environment with deionized water or other aqueous solutions [66, 70]. This is because the formed $Si-OH$ groups prefer environments with higher dielectric constant ($\varepsilon_{water} \approx 80, \varepsilon_{water} \approx 2.6, \varepsilon_{water} \approx 1$) which will keep the $Si-OH$ on the surface of the PDMS. This approach is impractical for long storage time periods and chip transportation. For this reason simple and reliable treatment protocols are needed for preserving the artificial hydrophilic and surface charge properties of the PDMS.

2.4.1 PDMS Treatments

The area of treating PDMS attracted researchers from different disciplines, especially researchers in chemistry. The main goal was to perform simple treatment protocols while maintaining the cost and time effectiveness of manufacturing PDMS based microchips. There are several approaches to modify and improve the surface properties of the PDMS for microfluidics applications which has been examined in the literature [18, 72, 73, 74, 75, 76, 77, 78]. Chemical based surface treatments, such as prepolymer additives, reducing the diffusion effects of the LMW PDMS, and grafting monomers with the desired properties on the surface of the PDMS are commonly used. A review of the surface treatments for microfluidics applications is presented by Liu and Lee [79].

The addition of prepolymer additive to PDMS was investigated by Luo *et al.* [78]. In their work acrylic acid (AA), and undecylenic acid (UDA) where separately mixed with PDMS samples before the curing process. The additives were expected to merge in the PDMS matrix without affecting curing process. In their treatment the PDMS channels were naturally bonded to the substrate. The additives increased the electroosmotic mobility of the PDMS microchannels. Also, it was found that this approach affects the physical properties of the PDMS. On the other hand, the treatment did not show an improvement in the hydrophobic nature of the PDMS [78].

In order to improve the stability of the hydrophilic state for the plasma treated PDMS, researchers approached the problem from two main directions, which are: reduce or prevent the diffusion of the LMW to the surface of PDMS [71, 75], or create stable chemical groups with the desired properties on the surface of the PDMS [72, 73, 74, 76].

The reduction of the concentration of LMW in the PDMS prevents or at least reduces the regaining of the hydrophobic groups on the surface of the plasma treated PDMS. The reduction of the LMW concentration could be achieved by either thermal aging [75] or extraction of LMW PDMS [71]. In the thermal aging approach, the LMW concentration is reduced due to the improvement in the cross linking of PDMS [75]. Eddington *et al.* [75] studied results of thermal aging on plasma treated PDMS samples with contact angle measurements. The work showed improvement and stability of the hydrophilic properties of thermally aged PDMS. Also, it was found that the longer the aging process the better stability of hydrophilic properties for plasma treated PDMS. On the other hand, thermal aging is a time consuming process and it is not desirable for fast chip manufacturing.

The second approach for reducing the concentration of LMW is to perform chemical extraction of the LMW from the cured PDMS [71]. This technique involves application of different chemical solvents to remove the non-cured LMW PDMS from PDMS bulk material. Consequently, the stability of the plasma treated PDMS improves since the LMW concentration is reduced. Vickers *et al.* [71] performed a three stage extraction process to PDMS microchannels. It was found that the process reduces the weight of the PDMS by 5 %. This reduction is due to the removal of LMW from the PDMS. The plasma treated and extracted PDMS showed stable hydrophilic properties compared to native PDMS. The reason for this improvement in the stability is that the SiO_2 compound was stable on the surface of the PDMS for long periods of time. The stability of SiO_2 was confirmed with X-ray photoelectron spectroscopy analysis. Moreover, the extraction process showed improvement in the electroosmotic mobility of the microchannel compared to native PDMS [71].

Another approach that does not deal with changing the concentration of LMW in PDMS is to change the surface chemistry by grafting monomers that have the desired chemical groups, such as $-OH$ and $-CN$, on the surface of the PDMS [73, 74, 76, 79, 80, 81, 82]. Different chemical compounds were used in the literature such as HEMA (2-hydroxy ethyl methacrylate) and acrylonitrile, Acrylic Acid (AA), PEG Poly(ethylene glycol), which could be grafted on the surface of the PDMS [73, 74, 76, 79, 80, 81, 82].

He *et al.* [80] used an plasma induced grafting of acrylonitrile to form chemically stable groups on the surface of PDMS. Results showed improved stability in the hydrophilic properties of PDMS with dry storage conditions. Wang *et al.* [81] used APTES (aminopropyl triethylsilane) to treat the surface after plasma exposure and the results showed stable electroosmotic mobility with time. Hu *et al.* [76] used a UV approach to modify the surface of the PDMS with different monomers, which were Acrylic Acid (AA), PEG Poly(ethylene glycol), and MATC (2-methacryloxy ethyltrimethylammonium chloride) to improve the electrophoretic separation sample. Also, the electroosmotic mobility proved to be stable with time compared to the non-grafted channels.

A chemical monomer that can be successfully polymerized on the surface of PDMS with simple approaches is HEMA (Hydroxyethyl methacrylate). HEMA can be permanently polymerized on the surface of PDMS by either plasma or a heat induced approaches [73, 74, 82]. Bodas and Khan-Malek [73, 74] showed that HEMA could be grafted on the surface of the PDMS with the aid of oxygen plasma treatment. After the HEMA was grafted on the surface of PDMS, stable and hydrophilic chemical groups, $Si-OH$, were permanently formed. Their results were supported by both the contact angle and ATR-FTIR analysis. On the other hand, the plasma induced grafting approach has some drawbacks and limitations to be facilitated in microchannel manufacturing. For instance, long plasma exposure time will cause mechanical aberration of the surface of the PDMS, which will create undesired surface roughness. Moreover it is hard to uniformly spin coat HEMA on in the microchannels with precise thickness.

The other approach was to graft the HEMA with a heat induced approach [82]. Choi and Yang [82] used a heat induced approach to graft the HEMA on the surface of the PDMS. Figure 2.6 presents a schematic of the principle of the heat induced HEMA grafting [82]. This is done by first forming active locations on the PDMS surface so that HEMA will attach to it. The surface activation was achieved with the aid of air plasma treatment. Afterwards, with the support of heat, HEMA will break the $Si-OH$ bond and will be grafted to surface of the PDMS. Results of the heat induced HEMA grafting showed the presence of stable OH groups with the ATR-FTIR analysis [82]. Moreover, improvement in the electroosmotic mobility of HEMA treated PDMS microchannels was reported [82].

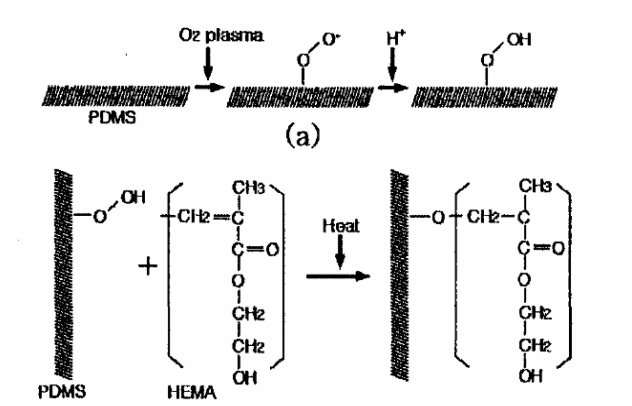

Figure 2.6: Basic concept of heat induced HEMA grafting [82].

2.4.2 Surface Characterization

The area of surface characterization of materials is a well established field [83, 84]. In the literature, different experimental characterization methods have been used analyze the surface chemistry of PDMS specimens. Contact angle, XPS, and ATR-FTIR are some examples for such techniques [71, 73, 75, 82]. In this work and for applicability purposes two surface characterization methods are used to analyze the effects of the treatments on the PDMS surface. The techniques are: the contact angle and ATR-FTIR analysis. These techniques were chosen for valid reasons. Examining the nature of the hydrophilic properties of PDMS sample is done with contact angle measurements. The ATR-FTIR is used for finding the chemical changes on the surface of PDMS after the treatments. A brief discussion on the theory of the contact angle and the ATR-FTIR analysis is presented in Appendix A. For further information on the contact angle refer to [1, 85]. Suggested readings about the ATR-FTIR analysis include [83, 84].

Chapter 3

Experimental Setup and Channel Manufacturing

Experimental studies, qualitative and quantitative, are powerful tools used to validate new theories, examine certain phenomena, or perform parametric studies. In this work different experimental techniques were adapted to perform parametric studies related to microfluidics applications. Figure 3.1 presents a flow chart that summarizes the processes of the performed studies and the integration process between them.

Chemicals used in this work can be divided into different categories according to their function. Figure 3.1 presents the process of using the chemicals for different applications and their integration in the overall study.

The sample manufacturing is briefly discussed in this chapter. The samples are sorted into: profiled and non-profiled samples. The profiled samples are used to manufacture the samples in channel format and are studied with the current-monitoring technique (chapters) and the dry storage analysis. The non-profiled samples are used in the contact angle and ATR-FTIR analysis (chapter 6).

The experimental setups used in this work are briefly discussed. The methodology for using the current-monitoring system is postponed to chapter 4 since it is directly related to the goals of the chapter. The measurement for the contact angle and the ATR-FTIR are discussed in this chapter.

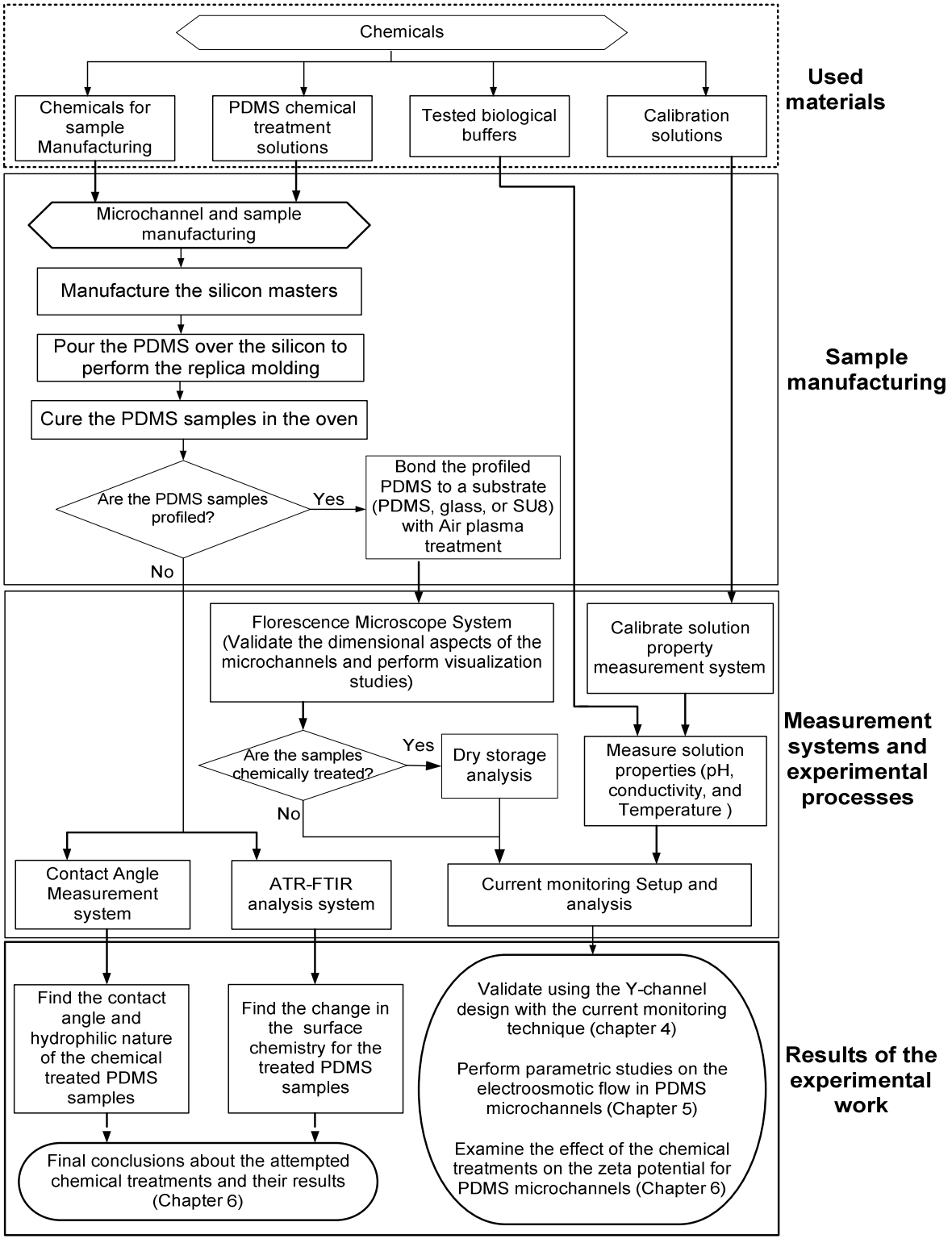

Figure 3.1: Flow chart of the experimental studies.

3.1 Chemicals and Reagents

The chemicals used in this work can be organized into four main categories: sample manufacturing, solutions used in the surface treatment of PDMS, electrode calibration buffers, and solutions that were tested with the current-monitoring technique. Information about the different categories of chemicals are discussed next.

3.1.1 Chemicals used for Manufacturing the Microchannels

Samples in microchannel format were used in the current-monitoring studies (chapters 4 and 5), dry storage analysis (chapter 6), and for examining the effects of chemical surface treatments on the PDMS (chapter 6). The studied microchannels were PDMS based, since they are suitable to numerous microfluidic applications. The manufacturing of the microchannels and samples was done with a soft lithography and replica molding of PDMS [62, 63]. The chemicals used in the manufacturing processes are listed below:

- SU8 (MicroChem Corp.): a polymeric resin used for creating solid profiles of the microchannels on silicon or glass substrates. SU8 is a photoresist that crosslinks when exposed to UV light. The photoresist comes in different grades that correspond to the viscosity of the photoresist, which was correlated to the maximum height of the SU8 hardened profiles [86].
- SU8 developer (Microchem Corp.): used to remove the uncrosslinked SU8 after the UV exposure and postexposure bake [86].
- TCMS (Trimethlylchlorosilane): is a toxic solution used to coat the hardened SU8 profiles before the replica molding of the PDMS elastomer.
- PDMS Base (polydiemthylsilicone) Sylgard 184 silicone elastomer base (Dow Corning, San Diego, CA).
- PDMS curing agent (polydiemthylsilicone) Sylgard 184 curing agent (Dow Corning, San Diego, CA).

3.1.2 Chemicals used for the PDMS Surface Treatment

The main goals of the attempted chemical treatments are to improve the hydrophilic properties and enhance the zeta potential of PDMS based microchannels. In this work

three main chemically based treatments were chosen for applicability and their reported results. The treatments were: prepolymer additive, extraction of PDMS, and HEMA grafting. The following chemicals were used:

- Acrylic acid (Fisher Scientific) was used in the prepolymer additive scheme.
- Triethylamine (Fisher Scientific) used in the PDMS extraction approach.
- Ethyl acetate (Fisher Scientific) used in the PDMS extraction approach.
- Acetone used in the extraction approach scheme.
- HEMA (2-hydroxyethyl methacrylate) (Sigma Aldrich) was used in the monomer grafting methods.

3.1.3 Calibration Solutions

The precise measurement of the solutions pH and conductivity is important for the accurate interpretation of the current-monitoring outcomes. High accuracy electrodes were used for measuring the solution properties. For the purpose of calibrating the pH and conductivity electrodes three conductivity buffers were purchased from VWR for each electrode. The conductivity buffers were of values 100 $\mu S/cm$, 1400 $\mu S/cm$, and 10,000 $\mu S/cm$, which cover the conductivity range of solutions used. The pH calibration buffers were pH 4, pH 7, and pH 10.

3.1.4 Solutions Tested with the Current-Monitoring Technique

One of the goals of this work was to estimate the electrostatic properties of biological buffers that have not been reported in the literature. Some of the buffers are known as Good's buffers, in reference to criteria proposed by Good *et al.* [87]. Other buffers are commonly used in the biological analysis community for DNA, RNA and protein analysis. The solutions were:

- 1X TAE-pH 8.08 (40 mM Tris base, 20 mM Acetic acid, and 1mM EDTA).
- 1X TBE-pH 8.24 (89 mM Tris, 89 mM boric acid, and 2 mM EDTA).
- 1X PBS-pH 6.71 (10mM Disodium hydrogen phosphate Na_2HPO_4, 1.75mM Monopotassium phosphate KH_2PO_4, 13.7mM Sodium chloride NaCl, and 2.65mM KCl Potassium chloride).

- 1X MOPS-pH 7 (3-(N-morpholino)propanesulfonic acid)
- HEPES-pH 8.81 (4-(2-hydroxyethyl)-1-piperazineethanesulfonic acid)
- Tris-HCl-pH 7.78 (tris base adjusted with HCl)
- 1X TE-pH 8 (10 mM Tris, and 1 mM EDTA)
- KCl (50 mM , 10 mM, and 1 mM)
- L-15EX-pH 7

Some buffers came as batches of the high concentrated solutions, such as 10X MOPS and10X PBS. The high concentrated buffers were diluted from the concentration of 10X to 1X with ultrapure[1] water (1 to 9 ratio, buffer to water). Other buffers were prepared in the lab such as 1X TBE and HEPES. The pH of the buffers was measured during the solution preparation with the pH electrode, and if needed, titration was performed. All solutions were filtered through a 0.2 μm filter before using them in the actual current-monitoring experiments.

3.2 Sample Manufacturing

In this work, only PDMS based microchannels were studied because of there vast applicability in microfluidics [62, 63]. The manufacturing technique is known as soft lithography technique. The process goes through two main steps:

- First manufacture the appropriate masters that has the channel profiles.
- Second, replica mold of the microchannels and non-profiled samples with PDMS elastomer [62, 63].

A simple description of the procedure for manufacturing the channels masters is presented in Appendix B Section B.2.

The samples are into two main formats: microchannel and non-profiled formats. The microchannel formats are used in the: current-monitoring studies (chapters 4, 5), the dry

[1]Ultrapure water is a commonly used term for high filtered de-ionized water. The extra filtering step removes impurities and particles from the water. Also, it the total organic carbon and the water electrical conductivity are controlled. The electrical conductivity of ultrapure is less than 10 $\mu S/m$

storage analysis (chapter 6), and the PDMS chemical surface treatment studies (chapter 6). The non-profiled PDMS samples are used in the contact angle and ATR-FTIR analysis (chapter 6).

Air plasma treatment is used to alter the surface properties of PDMS and help the bond the channel to the substrate. The system used is the PDC-001 plasma-cleaner (Harrick Plasma, Ithaca, NY). The common plasma treatment protocol is 29.6 W for 40 s, unless otherwise specified. Figure 3.2 shows a photograph of the plasma treatment system and a typical PDMS chip.

Figure 3.2: Plasma treatment system and a typical bonded chip.

3.3 Experimental Setups

In this work the different experimental setups were used to perform numerous studies. The following systems were used: solution property measurement devises, the current-monitoring setup, the ATR-FTIR system, contact angle system, and the fluorescence microscopy system. Information about each of these systems will be provided next.

3.3.1 Solution Property Measurement

The three important solution properties that have a direct effect on the electroosmotic flow in microchannels are the temperature, the solution pH, and the conductivity. Conventional electrodes can not be used for measuring the solution properties in the chip due to the space and volume limitations at the reservoirs. Hence, small electrodes with high accuracy were needed. The temperature was measured with a high accuracy K-type (chromel-alumel) thermocouple. The pH and conductivity were measured with the

MI-915 and MI-4154 electrodes (Microelectrodes Inc Bedford, USA). The electrodes were connected to an Orion 5 Star meter (Thermo Electron Corporation) for outputting the readings. The electrodes were frequently calibrated prior current-monitoring experiments, each with appropriate buffers. A three point calibration procedure was done for the each electrode. After the calibration the conductivity electrode was kept in a bottle with ultra pure water, while the pH electrode was preserved in an active buffer of pH7.

3.3.2 Current-Monitoring System

The basic concept of the current-monitoring technique is to record the electrical current while performing electroosmotic pumping in microchannels. Thus, an electrical voltage supply and a current measurement system are needed. A schematic of the connections between the components of the current-monitoring system is presented in figure 3.3. The main components of the current-monitoring system used in this work and the operation of each element are listed as follows:

- DC power supply (Spellman SL10*10 B.3.1).
- Current measurement system.
- Electrical switch.
- Chip holder.
- Data recording and monitoring system.
- AC - Fan.

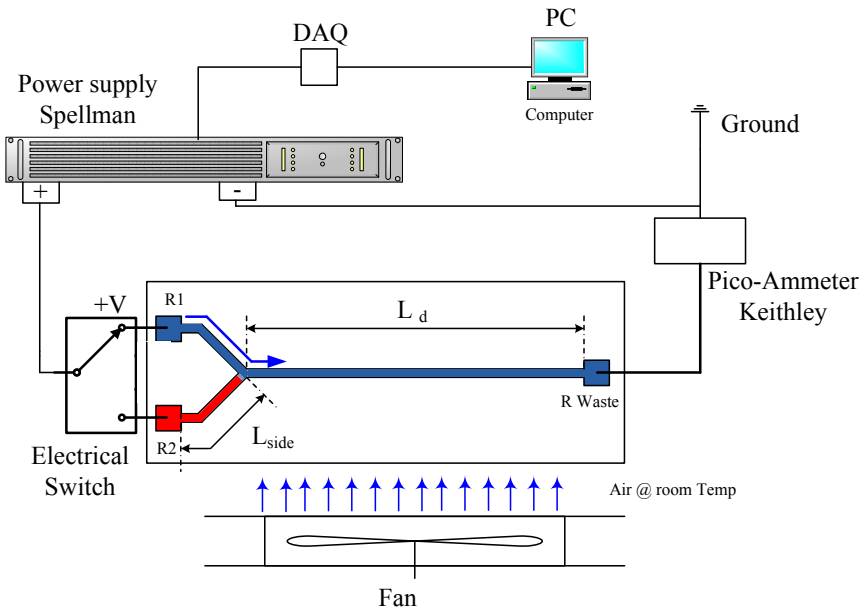

Figure 3.3: Schematic of the current-monitoring experimental setup.

.

The electrical switch and the chip holder were in-house assembled components as shown in figure 3.4. The main function of the AC fan was to keep the chip assembly at room temperature during experiments. The electrical current measurement system will be discussed next. For more information about the current-monitoring main components and specifications refer to Appendix B, Section B.3

In the first stage of current-monitoring experiments the current recorded from the Spellman was sufficient for measuring electrical currents above 2 μA with an accepted accuracy in distinguishing important points of the current-time plot. However, the electrical current exported from the Spellman showed severe noise. In addition, preliminary results of the surface conductance during electroosmotic flow were negative, which contradicts with the physics of the electroosmotic flow. For this reason a high accuracy Pico-Ammeter (Keithley 6485) was integrated in the current-monitoring system. This was done to assure accurate electrical current measurement. Figure 3.4 presents a typical current-time plot recorded during an actual current-monitoring experiment with both the Spellman power supply and the Keithley pico-ammeter.

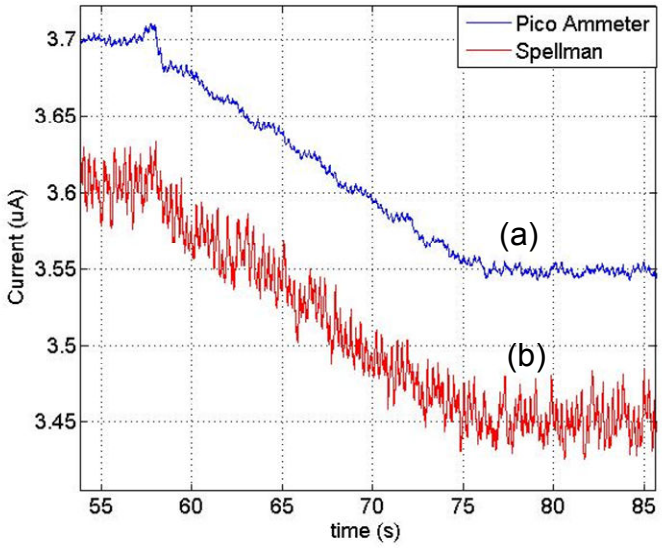

Figure 3.4: Electrical current comparison. (a) Keithley Pico-Ammeter, and (b) Spellman power supply.

.

As shown in figure 3.4, it is apparent that both current-time plots from the Spellman power supply and the Pico-Ammeter were giving close trends in distinguishing important points of current changes. On the other hand, the Spellman is underestimating the actual current by about 3 % compared to the Pico-Ammeter. Moreover, the signal from the Spellman is noisy. Given that the accuracy of the electrical current measurement from the pico-ammeter is higher than the accuracy of measuring the current from the Spellman, it is believed that the current recorded from the pico-ammeter is closer to the real time electrical current during electroosmotic pumping. This supports using the Pico-Ammeter in the current-monitoring experiments.

Note: to integrate the Pico-Ammeter to the current-monitoring setup a surge protection circuit must be used. Refer to Keithley Low Level Measurements Handbook [88].

3.3.3 ATR-FTIR System

The ATR-FTIR analysis is a non intrusive technique used to find the presence of different chemical groups in samples [83]. The ATR-FTIR analysis was adapted to study the chemical groups present in the PDMS samples since the samples were around 2 mm thick. The ATR was also used to examine the chemical surface treatments for the PDMS, as will be presented in chapter 6.

In the present study the TENSOR 27 (Bruker Optics Ltd., Milton, ON, Canada) is used to analyze the treated and non-treated PDMS samples. The TENSOR 27 is capable of finding the IR spectrum ranging from 400-4000 cm^{-1}. To obtain the infra red reflectance signal an ATR MVP-SplitPea accessory with a hemispherical shaped silicon crystal (Harrick Scientific Inc, Pleasantville, NY) was used. The crystal has a refractive index of 3.4. For an organic sample with a refractive index of 1.5 the penetration depth of the IR signal is 0.41 μm at a wave number of 2000 cm^{-1}. The control of the TENSOR 27 ATR-FTIR system was achieved with OPUS program (Bruker Optics Ltd., Milton,ON) which was the interface between the TENSOR 27 and the PC. Figure 3.5 presets the system used for the ATR-FTIR analysis.

The size of the PDMS samples that were tested with the ATR-FTIR system are 3 cm $\times$ 3 cm in order to provide adequate clamping on the silicon crystal. At least three samples for each treatment were prepared for ATR analysis. For each sample, at least three locations are measured. Each measurement covered the range 400 - 4000 cm^{-1} with a 4 cm^{-1} step, and 32 scans were obtained in a single measurement. The measurement startes by obtaining the background spectra for the surroundings. Then the PDMS sample is clamped over the silicon crystal with a torque of 8 $cN \cdot m$, and the measurement is performed. After each measurement the silicon crystal is wiped with acetone for cleaning purposes. The results of the ATR-FTIR analysis will be disscussed in chapter 6.

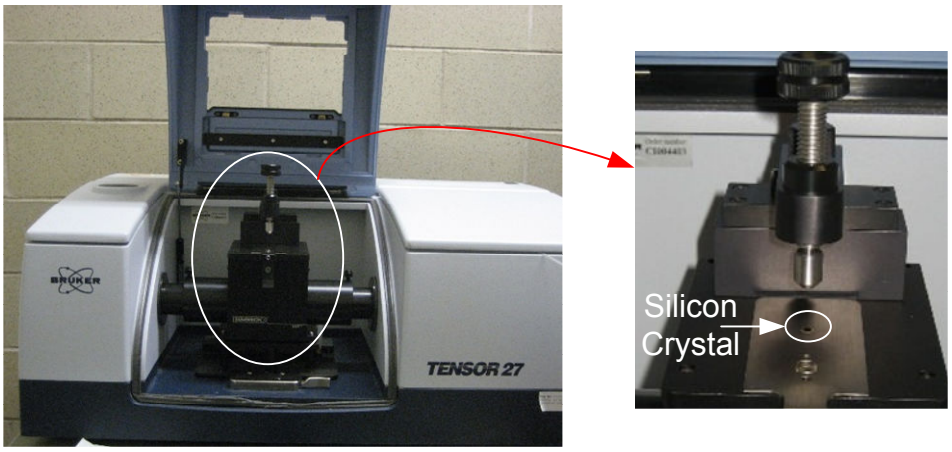

Figure 3.5: Bruker (TENSOR 27) FTIR system. Enlarged figure is the ATR MVP-SplitPea accessory.

3.3.4 Contact Angle System

Contact angle measurement of small solution droplets on solid surfaces gives important information about the nature of the surface. The contact angle measurement was chosen to examine the surface properties of the PDMS used in the channel and sample manufacturing before and after different treatments. The studies covered the effects of the plasma treatment on PDMS. Also, the chemical treatment effects on the properties of PDMS were examined, as will be discussed in chapter 6.

The contact angle measurements are performed with a prearranged system on a vibration free table. The system includes a CCD camera (CHOU model 4915-20001) which was connected to an acquisition and analysis system. PDMS samples with size 1.5 cm $\times$ 1.5 cm were used in the contact angle measurements. The sample was positioned on a sample holder in front of the camera optics. Ultrapure water droplet was put on the sample and the monitoring system was used to assure that the droplet is symmetric. A series of images was taken with the camera. In a typical measurement 30 images were recorded for a one point. The final result was the average of the 30 images. Moreover, for each sample at least two points of contact angle measurements were performed. The program used to analyze the images was ADSA (Axisymmetric drop-shape analyses) software. Figure 3.6 presents a photographic image of the system used for the contact angle measurements.

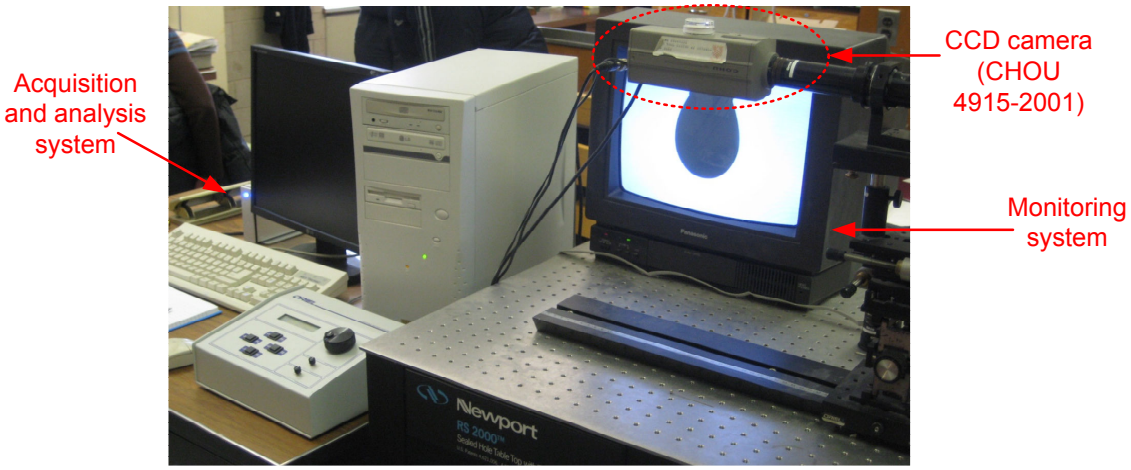

Figure 3.6: Contact angle measurement system.

3.3.5 Fluorescence Microscopy System

A fluorescence microscopy system was used for different applications and sample imaging. An inverted microscope (GX71, Olympus) with numerous dry objectives was used in various studies. The main properties of the objectives are listed in table 3.1.

Table 3.1: Microscope objectives specifications.

Objective name	Magnification	Working distance (mm)	Numerical Aperture (NA)
UMPlanFl-BD 5x	5x	12	0.15
UMPlanFl-BD 10x	10x	6.5	0.3
UMPlanFl-BD 20x	20x	3	0.46
LMPlanFl-BD 50x	50x	10.6	0.5
LMPlanFl-BD 100x	100x	3.3	0.8

The choice of the microscope objective depends on the size of the area of interest in the sample. If the area of interest is small high magnification objectives were used, and vise versa. Figure 3.7 presents a schematic of the sample view and the observed area of interest from the microscope objective. Light illumination was performed with a halogen lamp mounted on the back of the microscope. The microscope was also equipped with an Olympus filter cube (BSWM) for the purpose of fluorescence imaging. This filter is ideal for the imaging the commonly used fluorescent dye (Invitrogen Corp).

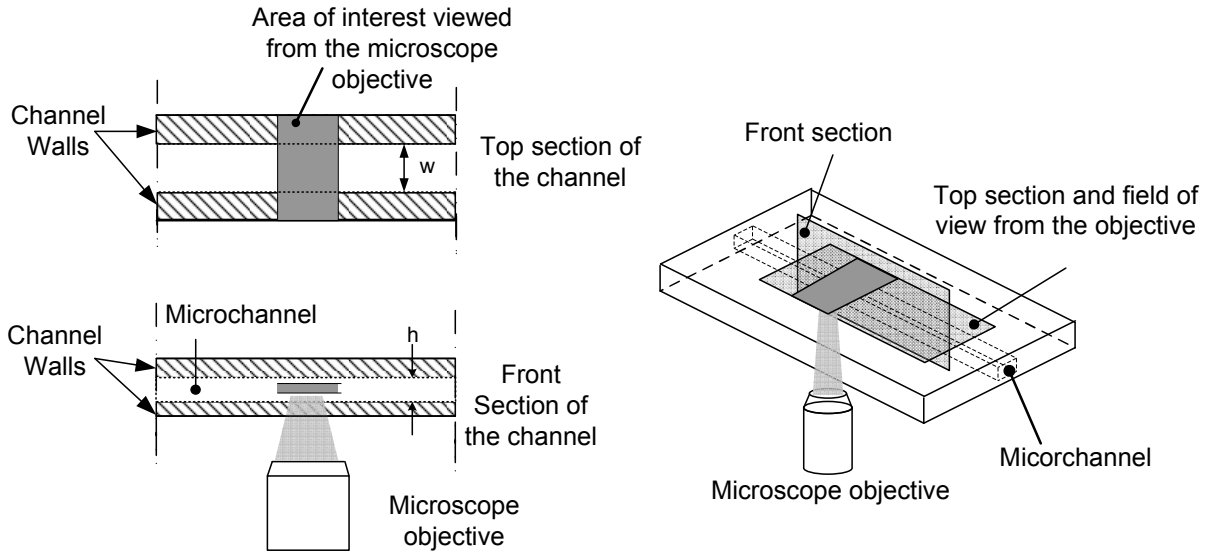

Figure 3.7: Schematic of the area of interest in microchannel observed from the microscope objective.

The imaging of the viewed samples was performed with a CoolSNAP ES CCD camera (1392x1040 pixels, Photometrics) which was coupled to the microscope system. The image capturing and analysis was carried out with the Image-pro Plus software (Media Cybernetics). Figure 3.8 presents a photographic image of the microscopy system.

The microscope was frequently used for the verification of both the master and the chip that will be tested in the current-monitoring experiments to assure the absence of defects. Also the system has been used for flow visualization of electroosmotic pumping in the Y-channel design as will be presented in chapter 4.

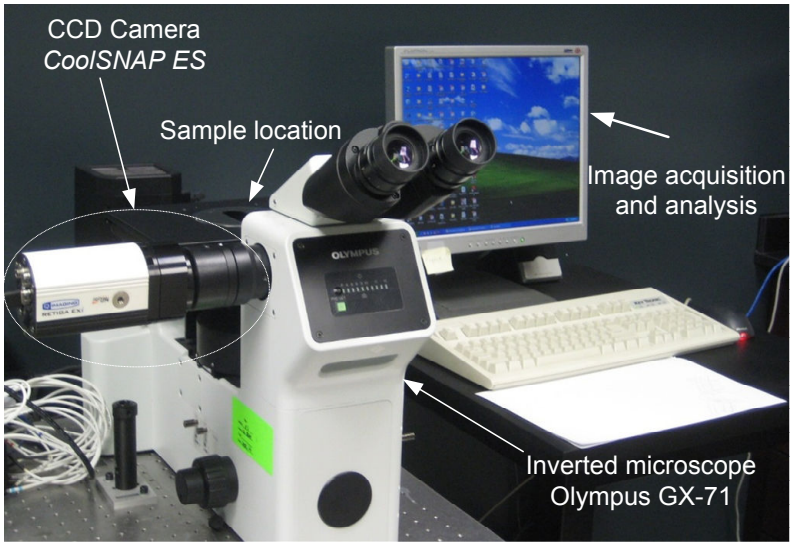

Figure 3.8: Fluorescence microscopy system.

3.4 Final Remarks

In this chapter general information about the chemical used, sample manufacturing process, and experimental setups were presented. A descriptive overview of the microchannel manufacturing process is discussed in Appendix B.2. The processes of chemically treating the PDMS samples will be presented in chapter 6, since it is directly related to the goals of the chapter.

The experimental setups were generally overviewed. The procedures in performing the measurements with each experimental system will be presented in the related chapters. Studies with the current-monitoring system will be discussed in chapters 4 and 5. The ATR-FTIR and contact angle systems were used in the characterization of the chemical treatments, as will be presented in chapter 6. An overview of the uncertainty parameters of the current-monitoring system is presented in Appendix C. Also, an overview of the error propagation is discussed in Appendix C.

Chapter 4

A New Channel Design for the Current-Monitoring Technique

In this chapter a new Y-channel design[1] will be presented, analyzed and validated for studying the electrostatic properties of the microchannel along with the current-monitoring technique. Errors from the undesired pressure driven flow and electrolysis were addressed and reduced in the new channel design.

4.1 Introduction

Electroosmotic flow utilizes the presence of the EDL to create a flow within microchannels. By applying an electric field tangentially to the EDL the mobile ions in the EDL will move to an appropriate electrode, and with viscous effects the moving ions with in the EDL will drag the solution in the region out of the EDL [4, 11, 26]. Figure 4.1 presents a schematic of an electroosmotic flow with the driving body force inside a microchannel. As discussed in chapter 2, for a thin EDL compared to the channel characteristic length the average velocity in the microchannel is approximated with the slip velocity, which is found from the Helmholtz-Smoluchowski equation 4.1:

$$u_{slip} = -\frac{\varepsilon_o \cdot \varepsilon_r \cdot E}{\mu} \cdot \zeta = \mu_{emo} \cdot E \tag{4.1}$$

where u_{slip} is the slip velocity at the shear layer of the EDL, E is the electrical field, ε_r the solution relative permittivity, ε_o the vacuum permittivity, ζ is the zeta potential, and

[1] The introduction of the Y-channel design was done in the IMECE2007 conference, in Seattle 2007 [89]. The first paper discussing the Y-channel is published in the proceedings of the conference [89].

μ is the viscosity of the solution. Another commonly used term is the electroosmotic mobility μ_{emo} of the microchannel which groups the solution properties with the zeta potential into one value.

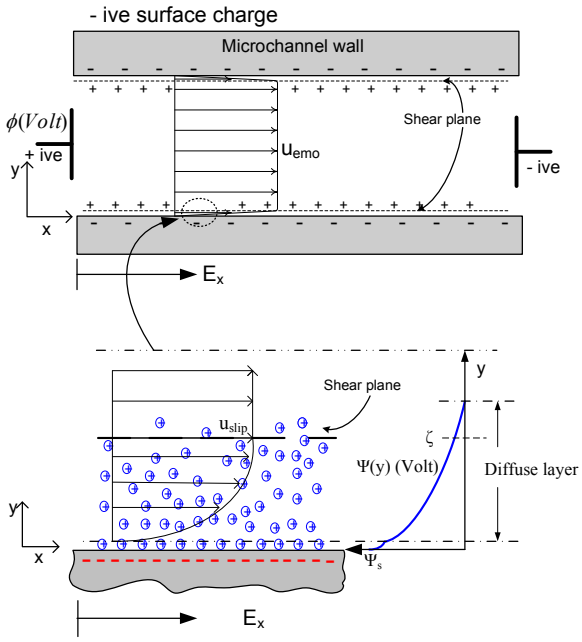

Figure 4.1: Schematic of electroosmotic flow in a microchannel.

Electroosmotic flow has been widely used in several microfluidic applications because the ease of implementation in the microchips, fast response time, ease of control through complex channel geometry, and most important is the plug like velocity profile [4, 11, 51]. The significance of the plug like profile comes from that it does not allow sample dispersion, thus increasing the accuracy of analyte detection. The most important factor that defines the electroosmotic flow in microchannels is the zeta potential. This property is unique for each solution wall pairing, thus it is important to accurately measure its value.

The current-monitoring technique is the most widely adopted method for finding the zeta potential of microchannels due to its simplicity of the hardware, ease of interrupting the results and accuracy [4, 46, 41, 42, 47, 48, 49, 50, 51, 52]. In this method the average electroosmotic velocity is measured by qualitatively monitoring the current change as the test solution is replaced by the same solution but with a slightly different concentration (i.e. lower conductivity) in a straight microchannel. It is important that the concentration difference be small ($\approx$5% concentration difference) or inaccuracies will occur due to variations in zeta potential between the two solutions. By knowing the time needed for

solution replacement in the microchannel and the channel length the solution average velocity inside the microchannels could be estimated:

$$u_{av} = \frac{L}{\triangle\ t} \tag{4.2}$$

where L is the channel length where the solution is being replaced, and $\triangle\ t$ is the time needed for the full solution replacement within the microchannel (ie. from one reservoir to the second reservoir). The full replacement is identified by reaching a steady electrical current value, which indicates that only a specific solution is pumped in the microchannel. Afterwards the zeta potential is inferred from the Helmholtz-Smoluchowski slip velocity 4.1 for a thin EDL compared to the channel characteristic length. A simple schematic of the principle of the current-monitoring technique with a typical current-time plot reported from the literature is presented in figure 4.2.

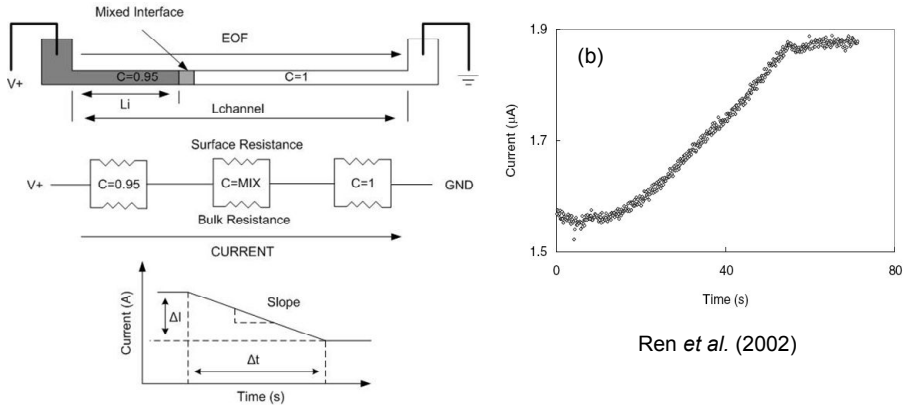

Figure 4.2: Schematic of the principle for the current-monitoring technique and a typical outcome [19, 48].

As discussed in chapter 2, previous current-monitoring experiments did not address several problems that have an affect on the current-monitoring results. Issues such as undesired pressure driven flow and electrolysis were not discussed nor were the prevented. Also, other problems were encountered when using the current-monitoring technique with microchannels in chip format, such manual removal of the solution at the reservoirs and positioning the electrodes. The nature of the technique requires continuous interaction with the hardware and experimental setup. The solution removal at the reservoirs was done manually with no assurance of emptying the reservoirs. Moreover, the current-monitoring experiment must be repeated several times to obtain consistent results

for identical experimental conditions. This process was time consuming and the results were not reliable.

In this work a Y-channel design was presented to study the electrostatic properties of PDMS based microchannels with the current-monitoring technique. The main aspects of the design will be discussed in the next sections.

4.2 Y-Channel Design

In the Y-channel design, two side channels are connected to a displacement channel, as schematically shown in figure 4.3. The basic concept of the design is to fill the two source reservoirs, R1 and R2, with the high and low concentration solutions, 100% and 95 % concentrations. The solution pumping is alternated between the two source reservoirs. This is achieved with an electrical switch that is connected to the electrodes touching the solutions at the source reservoirs. The current is monitored while the pumping process is performed from the reservoirs and replacement is occurring in the displacement channel. This design offers the ease of repeating the experiments several times by only changing the direction of the applied electric field, thus; performing more measurements without the need of manually removing the solutions from the reservoirs.

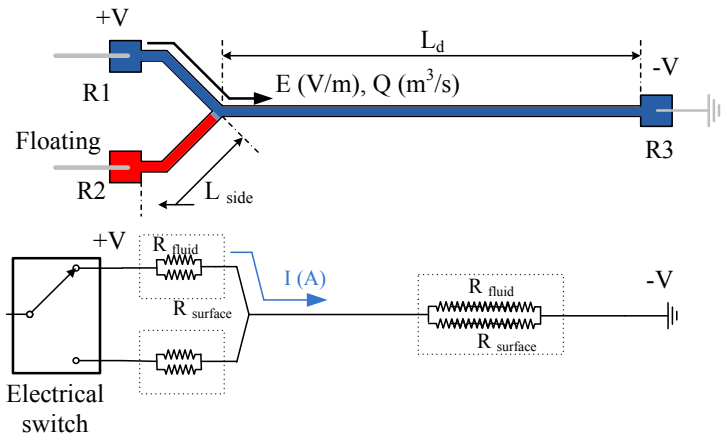

Figure 4.3: Schematic of the proposed Y-channel design.

The operation principle of the Y-channel design is as follows. First an electric field is applied between the high concentration (R1) solution and the third reservoir (R1 $\rightarrow$ R3), while leaving R2 floating, which will pump the high concentration solution in the displacement channel. The electrical current is monitored during the process and full

solution replacement inside the displacement channel is indicated by reaching a steady current value. Afterwards, the electric field direction is applied to the other reservoir with the electrical switch, and the electric field is applied from R2 to R3 while leaving R1 floating. The low concentration solution is pumped inside the displacement (L_d) microchannel, casing a change in the current due to difference in the solution conductivity. The current is monitored while the low conductivity solution was being replaced inside the displacement microchannel. Likewise, full replacement was indicated when the current reach a plateau.

Figure 4.4 presents the expected current-time plot from the Y-channel design during the two pumping scenarios, and the current-time plot for a straight channel design with the same geometrical aspects (same cross-section area and $L_{channel} = L_d + L_{side}$).

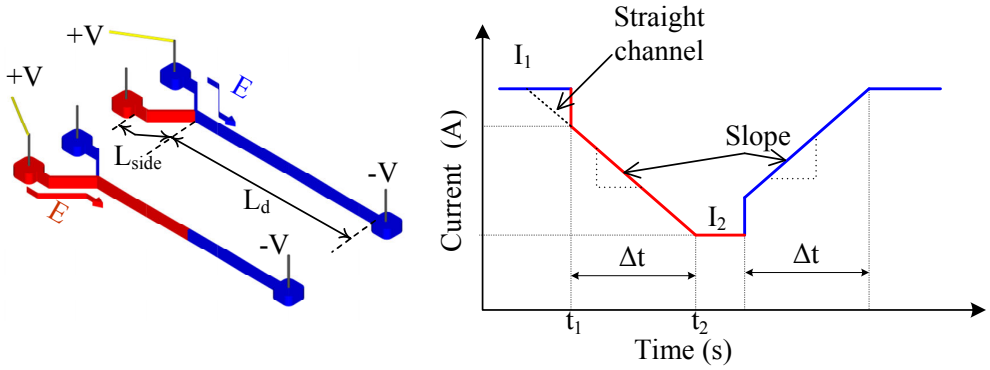

Figure 4.4: Expected current trend during the replacement from the Y-channel design. The red line represents pumping the low concentration solution (R2 $\rightarrow$ R3), the blue line represents pumping the high concentration solution (R1 $\rightarrow$ R3), and the dashed line is the expected current from the straight channel design.

Notice, in both cases, the slope of the current-time relationship is the same. The current-time trend from the Y-channel design is similar to a straight channel design partially filled with the solution being replaced. The average velocity of the solution during the replacement in the Y-channel design can be calculated as:

$$u_{av} = \frac{L_d}{\triangle\ t} \tag{4.3}$$

where L_d is the length of the displacement channel and $\triangle\ t$ is the time needed for the full replacement of the solution inside the channel. By comparing the current draw from the

Y-channel to the straight channel designs there are some noticeable differences. In the Y-channel and immediately after switching there is a sudden change in the current, either drop or increase. This is due to the fact that the side channel is already filled with the solution that has a different conductivity from the solution which is in the displacement channel at the time of the switch. The magnitude of the sudden current change is influenced by the solution electrical resistance from the side channel to the total electrical resistance between the reservoirs. If the cross-sectional area of the side channel is similar to the displacement channel, which is the case in these designs, the relation reduces to be a geometrical ratio of side channel length to total length between the reservoirs ($L_{side}/L_{channel}$, where $L_{channel} = L_d + L_{side}$).

4.2.1 Undesired Pressure Driven Flow

In devices utilizing electroosmotic flow, undesired pressure driven flow limits the throughput and stability of the device operations conditions [16, 61]. In the presence of both pressure driven and electroosmotic flows the velocity in the microchannel will be the superposition of the two components.

The accuracy of the current-monitoring technique in finding the zeta potential of microchannel is affected by the pressure driven flow since it finds the average velocity of the of the pumping without distinguishing the either velocity component. However, if the pressure driven flow can not be eliminated and its magnitude and direction are known, the electroosmotic velocity could be found by accounting for the average velocity of the pressure driven flow.

There are two main contributors for the pressure driven flow in current-monitoring technique for channels that must be addressed: solution height differences between the reservoirs and Laplace (meniscus shape differences) pressure effects. In order to perform accurate current-monitoring measurements pressure driven flow must be eliminated.

An effective approach for reducing the effects of the undesired pressure driven flow is to increase the hydrodynamic resistance of the microchannel. The hydrodynamic resistance for a microchannel can be approximated by equation 4.4:

$$R_{hyd} = \frac{12 \cdot \mu}{w \cdot h^3} \tag{4.4}$$

where L is the channel length, μ is the solution viscosity, w is the channel width, and h is the channel height. In order to effectively increase the hydrodynamic resistance the denominator must be reduced. This could be done by either decreasing the channel width or height. Changing the channel height is more effective since its effect is powered by

three ($R_{hyd} \propto 1/h^3$). On the other hand the channel height must not be in the same order as the scale of the EDL thickness so that the approximation of the Helmholtz-Smoluchowski equation 4.1 is still valid.

As presented in chapter 2, the thickness of the EDL is in the same order of the Debye length scale. And it is known that for very dilute solutions the thickness of the EDL is very high. i.e. for ultra pure water the thickness of the EDL is around 300 nm [11]. Hence, the characteristic length of the channel dimensions must not interfere with the thickness of the EDL, in order for the approximation of equation 4.4 to be valid.

Figure 4.5 presents the effect of changing the channel height on the velocity ratio of pressure driven flow to electroosmotic flow, ($u_{pressure}/u_{electroosmotic}$), in a situation where the pressure difference between the reservoirs is around 100 Pa and the solution has a very low electroosmotic velocity, 166 $\mu m/s$[2].

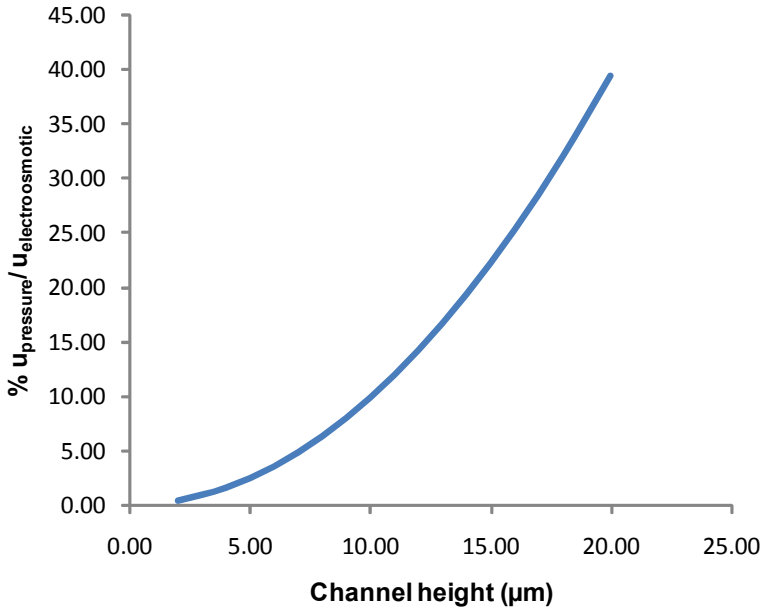

Figure 4.5: Channel height affect on the velocity ratio ($u_{pressure}/u_{electroosmotic}$). The analysis was performed for a pressure difference of 100 Pa between the reservoirs and an average electroosmotic velocity of 166 $\mu m/s$.

The analysis presented in figure 4.5 was performed to prove the concept of the effect of changing the channel height height on the velocity ratio ($u_{pressure}/u_{electroosmotic}$). The

[2]This average velocity is equivalent to pumping a solution with very low electroosmotic velocity, such as 1X PBS buffer. The example presented in figure 4.5 is performed for an applied electric field of E_x =10 kV/m and a solution having an electroosmotic mobility of $\mu_{emo} = 1.66 \times 10^{-8} m^2/V \cdot s$.

values of the electroosmotic velocity and the induced pressure difference between the reservoirs were chosen to be severe situations. In most cases the electroosmotic velocity in microchannels is higher than 166 $\mu m/s$. Also, this pressure difference was equivalent to solution height differences of 1 cm between the reservoirs, which was not allowed in the real experimental conditions.

As shown in figure 4.5, the velocity ratio is below 10 % when the channel height is between 5 - 10 μm. Thus, the error from the undesired pressure driven flow is significantly reduced and it is within the uncertainty of the measurements from a typical experimental setup, as presented in Appendix C. Moreover, this range of channel heights does not violate the approximation of the average velocity with Helmholtz-Smoluchowski equation.

4.2.2 Solution Electrolysis Effects

Electrolysis of the background electrolyte, at reservoirs, has severe effects on applications where the solutions must maintain a certain pH value, such as DNA electrophoreses. Thus, it must be eliminated or significantly reduced. This motivated researchers in the chemistry discipline to study solution electrolysis experimentally and numerically in order to overcome these problems [40, 41, 90, 91].

The major problems associated with electrolysis in electroosmotic pumping are as follows:

- Changing the solution properties [40, 41, 90, 91].
- Creating bubbles around the electrodes that are used to implement the electric fields [3].
- Depleting the solutions at the reservoirs [19].

One important issue with electrolysis that affects the stability of electroosmotic pumping is the formation of bubbles around the electrodes. The formed bubbles increases the electrical resistance during electroosmotic pumping since they will form an insulating layer around the electrode. These bubbles create an unsteady electroosmotic pumping conditions. This trend has been observed in preliminary current-monitoring experiments with the Y-channel design for 10 and 9.5 mM KCl. Figure 4.6 shows the effect of bubbles formation on the current-time plot during long term electroosmotic pumping.

[3] This was observed in preliminary current-monitoring experiments performed in the lab.

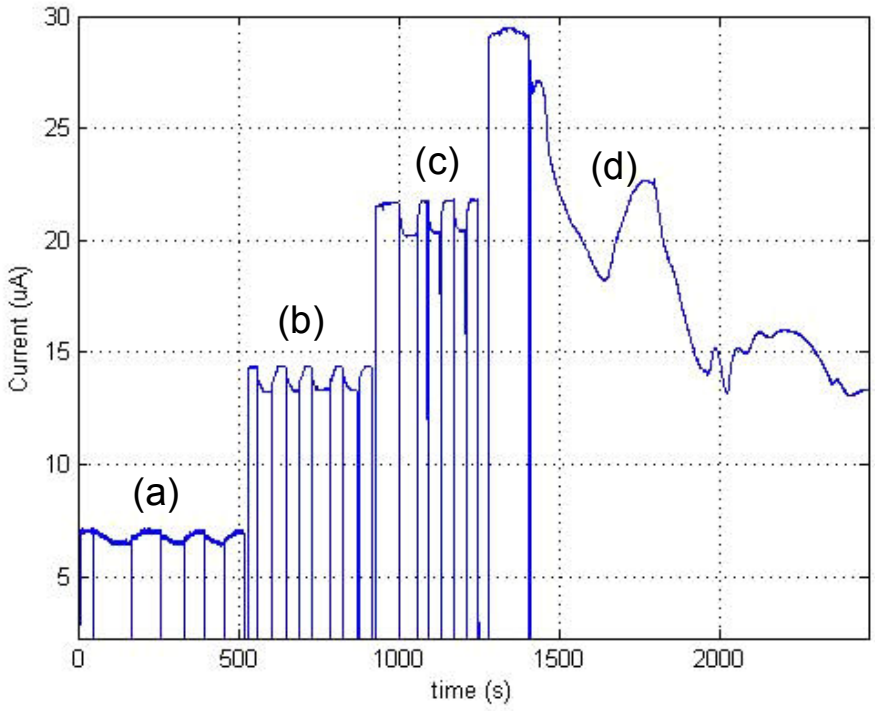

Figure 4.6: current-monitoring experiment for 10 mM KCl and 9.5 mM KCl. The experiment was performed for four different applied voltage differences between the reservoirs, (a)-250 V, (b)-500 V, (c)- 750, and (d)- 1000 Volts during which the solutions were kept in the reservoirs.

From the current-plot shown in figure 4.6, there is a clear and repeatable trend for the solution replacements in regions (a), (b), and (c). In these regions, the replacement between the 9.5 mM KCl and 10 mM KCl was occurring and clearly identified. On the other hand, the forth region (d) there was neither a clear trend nor stable solution replacement as indicated in the current-time plot. Bubbles were observed on the electrodes during this experiment, which affected the stable pumping conditions of the solutions since the applied electric field was fluctuating due to the change of electrical resistance. Also, the solution pH changed at the source reservoirs from 6.83 to 3.5 during the experiment. Fluctuations in the recorded current were attributed to the forming of bubbles around the electrodes and to the unstable changes of the solution pH at the reservoirs.

Another problem that electrolysis has on the current-monitoring technique is its effects in changing the solution conductivity. This is due to the formation of free ions during electrolysis that contributes to an increase in the local solution conductivity which is being pumped in the microchannel. In the current-monitoring experiment this unpredictable change in current creates a chance of not accurately finding the end of solution

replacement during the electroosmotic pumping. This problem has severe effects on solutions that have low or no buffering capabilities, such as electrolytes and buffers with high electrical conductivity. Figure 4.7 presents the electrolysis effects in changing the solution conductivity during a current-monitoring experiment for 1XPBS buffer.

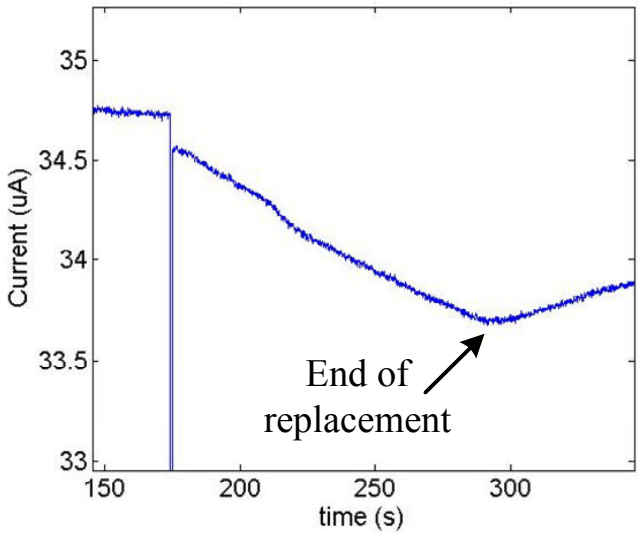

Figure 4.7: current-monitoring experiment for 1X PBS.

In this experiment the channel was filled with 1X PBS, the 100 % solution, and it was replaced with 95 % 1X PBS solution, as it is clear from 4.7. After the replacement has ended there was an increase in the recorded current. To have a better understanding on the nature of solution property changes during this experiment, table 4.1 presents pH and conductivity properties before and after the experiment.

Table 4.1: Solution property change during current-monitoring experiment presented in figure 4.7 with 1X PBS.

	pH		Conductivity λ_b $(\mu S/cm)$		
	pH_1	pH_2	λ_{b1}	λ_{b2}	$\%\triangle\lambda_b$
Reservoir 1 1XPBS (100 %)	6.7	6.62	11,260	11,490	2.04%
Reservoir 2 1XPBS (95 %)	6.67	6.60	10,830	11,100	2.49 %
Reservoir 3 1XPBS (100 %)	6.67	6.99	11,180	11,820	5.72 %

As observed in table 4.1, the solution property changes during this experiment are caused by electrolysis since the temperature at the reservoirs did not change. In this experiment the electric field was applied to the solutions in the reservoirs for 14 minutes, which increased the undesired electrolysis effects. This trend, showing the effect of pH changes on conductivity, was also observed by Rodriguez and Chandrasekhar [41]. Thus, to perform accurate current-monitoring experiments, certain precautions and remedies must be done to reduce the effects of electrolysis.

As seen previously, electrolysis as a phenomenon associated with electroosmotic pumping could not be eliminated. Hence, it is the toughest obstacle confronting electroosmotic pumping in microchips. Reducing the effects of electrolysis is important for the long run of electroosmotic pumps. Also, for accurate interpretation of current-monitoring experimental outcomes, electrolysis must be significantly reduced.

Figure 4.8 presents a schematic of the different phenomena occurring during solution electrolysis that have an effect on the current-monitoring technique.

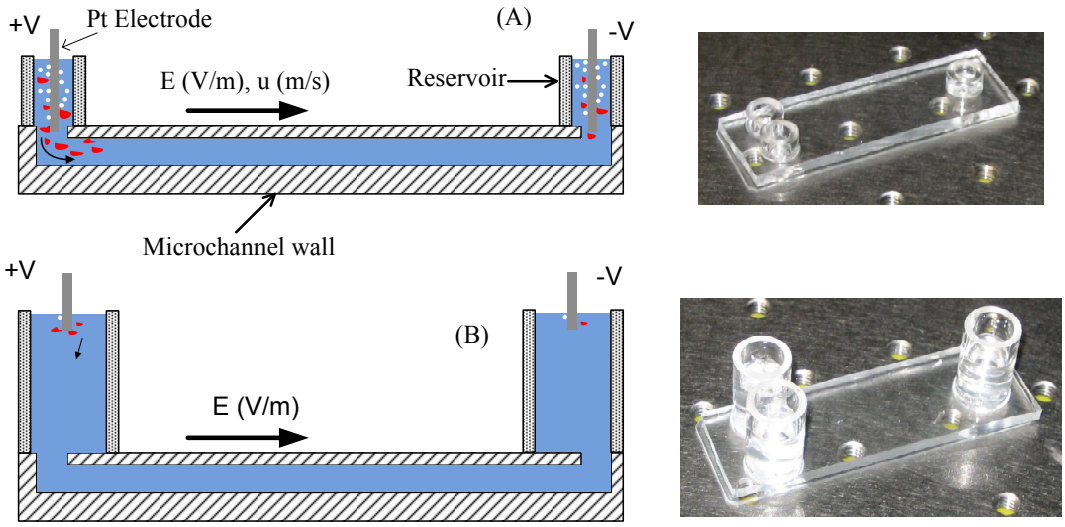

Figure 4.8: The electrolysis phenomena and its effects on the solutions at the reservoirs during electroosmotic pumping. White dots represent the bubble formation around the electrode and red regions represent electrolyzed solution parcels. (a) First Y-channel design and (b) final Y-channel design.

As shown in figure 4.8, the two major phenomena associated with electrolysis that have an affect on the current-monitoring technique are the bubble formation at the electrodes and the diffusion of the parcels of electrolyzed solution in the channel. These two phenomena could be significantly reduced by using large volumes of solution at the reservoirs which will absorb small electrolysis changes around the electrodes. Another remedy was to position the electrodes far away from the entrance of the channel. This will allow more time for performing the experiment before parcels of electrolyzed solution enters the microchannel. Macka *et al.* [40] found that to reduce the effects of electrolysis in capillary electrophoresis application the electrodes should be positioned 1 mm above and 1 mm away from the capillary entrance [40]. This will give more time before the electrolyzed solution reaches the microchannel.

In the present work large extended reservoirs, as shown in figure 4.8, were used for the current-monitoring experiments. The electrodes were positioned 1.5 cm above the entrance of the channel.

Another important safety measure that has an influence in reducing and delaying electrolysis was to reduce the current draw during electroosmotic pumping. This was done by increasing the electrical resistance of the channel/solution configuration. In a

microchannel, the electrical resistance of the solution is found from equation 4.5:

$$R_{electrical} = \frac{L}{\lambda_b \cdot A_c} \tag{4.5}$$

where L is the channel length, λ_b is the solution bulk conductivity, and A_c is the cross sectional area of the microchannel. By using a shallow channel the cross section area will be reduced. This will reduce the effects of electrolysis, as it will also reduce the undesired pressure effects, as disused in the previous section.

Nevertheless, to insure that the electrolysis effects were reduced in the current-monitoring technique several precautions were taken during the current-monitoring experiments: performing the experiment at low currents, shortening experiment times for non-buffered solutions, replacing the solutions after each stage of the experiments if needed, and the platinum electrodes were touching the tip of the solutions in the reservoirs.

4.3 Experimental Setup and Procedure

The main Y-channel design aspects and the experimental procedure will be presented next.

4.3.1 Y-Channel Designs Aspects

Based on the forgoing discussions, the major aspects of the Y-channel design were decided. First, the side channel to the displacement channel lengths was chosen to be 1:4. This ratio will provide more time for the solution to be displaced in the microchannel, which makes it easer to locate the start and end of the solution replacement. Channel heights were chosen to be in the range of 5 - 10 μm, which will significantly reduce the effects of undesired pressure driven flow and electrolysis. To assimilate the variety of solutions that will be studied numerous masters with different dimensions of Y-channel designs were manufactured in the same approach presented in chapter 3. A summary of the Y-channel designs is presented in table 4.2:

Table 4.2: Dimensions of the fabricated masters for the Y- channel designs.

Master No.	Avg. Width (μm)	Avg. Height (μm)
Y-500-2	483.83	9.06
Y-500-3	490.00	7.11
Y-200-1	192.83	10.37
Y-200-2	192.50	5.82
Y-200-3	192.25	7.00
Y-100-1	94.75	5.76
Y-100-2	94.12	7.32

4.3.2 Experimental Procedure

An appropriate Y-channel design is chosen for the solution that will be studied in the current-monitoring experiment. This is done by finding the expected channel cross sectional area from equation 4.6, and under an applied voltage 750 V and a current 2 - 10 μA, and using the equation:

$$A_{c\_exp} = \frac{I \cdot L_{channel}}{V \cdot \lambda_b} \tag{4.6}$$

where A_{c_exp} is the channel cross-sectional area of the channel, $L_{channel}$ is the total length of the channel, I is the current, V is the voltage, and λ_b is the solution conductivity. The current was chosen in this range because of the accuracy of current measurement system. The electrical current renge condition (2 - 10 μA) was applied when recording the electrical current from the Spellman power supply. However, if the Pico-Ammeter was used the electrical currents could be recorded with smaller values, refer to figure 3.4.

Prior to performing the current-monitoring experiment a branch symmetry validation was done for each Y-channel chip. The validation was a two step procedure. First a check with the microscope was done to assure that there were no obvious dimensional defects in the channels. The second step of the symmetry validation was done by filling both reservoirs R1 and R2 with the same solution and alternate the pumping source between the reservoirs with the same applied electrical field while monitoring the current for each pumping scenario. If both branches were symmetrical the current draw during pumping will be identical regardless of the source reservoir. After the symmetrical validation was confirmed, new solutions were introduced into the reservoirs. The first reservoir contains a 100 % solution, while R2 contains the same solution but diluted to 95 %. The solution

properties such as the temperature, pH and conductivity were measured at the start and end of the experiments.

The experiment starts by applying an electric field between R1 and R3 and pumping the high concentration solution in the microchannel. The current was monitored until reaching a steady current value, which indicates that the full solution replacement in the displacement channel was achieved. Afterwards, the electric field is switched to the other reservoir, R2 and R3 and pumping the low concentration solution. The current will change during the replacement and the full replacement in the displacement channel was identified when the current reaches a steady value. These first two switches were done to prime the chip for the actual measurements. This was done to assure that the residual solutions from the symmetry check were removed. The switching procedure was repeated several times by alternating the direction of the applied electric field between R1 and R2 and getting accurate solution replacement. In a typical experiment several switches between the reservoirs were performed for a certain electric field, furthermore different electrical fields were also tested. The solution properties were measured after each set of switches to assure that the electrolysis effects were minimal and if needed the solutions were replaced. It was found that electrolytes and some high conductive buffers, such as 10 mM KCl and 1XPBS, needed to be replaced before starting other measurements with different electrical fields.

The study of dynamic solution displacement during switching at the Y-intersection was performed with fluorescent dye visualization. The visualization was done by filling the first reservoir (R1) with 1X TAE buffer dyed with 10 mM florescent dye while the second reservoir (R2) was filled with 1X TAE (non-dyed). A set of images showing the fluid flow when alternating the pumping source between the reservoirs, R1 and R2, are presented in the figure 4.9.

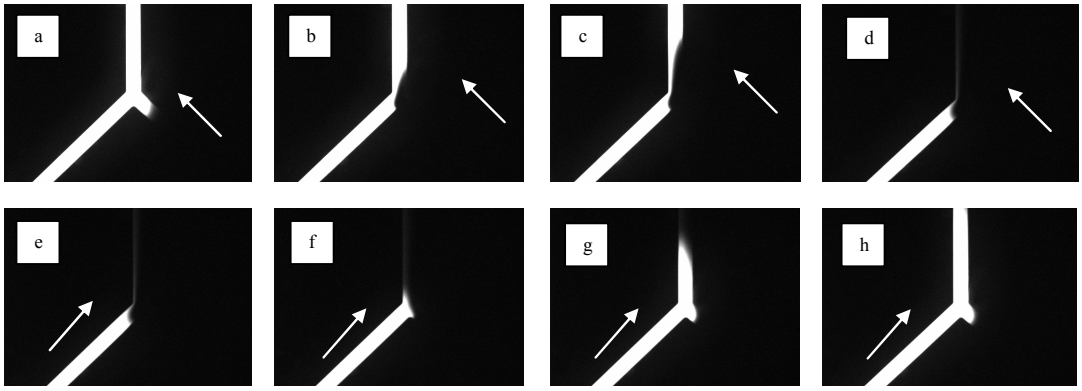

Figure 4.9: Florescent dye imaging at the Y-connection. R1 contains a dyed solution and R2 non dyed solution. (a-d) the electric field is applied between R2 and R3, and (e-g) the electric field is applied between R1 and R3. The arrow indicates the direction of electric field.

At first the dyed solution was filing the displacement channel, as show in figure 4.9 (a). In figure 4.9 the electric field is applied to the second reservoir and the non-dyed solution starts its replacement in the displacement channel, this scenario is sequenced in figures 4.9(a $\rightarrow$ d). The other pumping scenario is presented in figure 4.9(e $\rightarrow$ h).

It is clear that the switching and solution replacement process at the Y-intersection is smooth for any electric field direction and there was no back flow. It is also observed that there is large diffusion between the two solutions in the side channels. The diffusion of the dyed solution to other branch (clearly observed in figure a), is due to the large concentration difference between the dyed and non-dyed solutions (100% to 0 % of dye). In real time current-monitoring experiments the concentration difference is around 5%, this will reduce the effects of solution diffusion between branches.

Figure 4.10 presents a typical current-time plot from current-monitoring experiments with the Y-channel design and a straight channel design using the same solution.

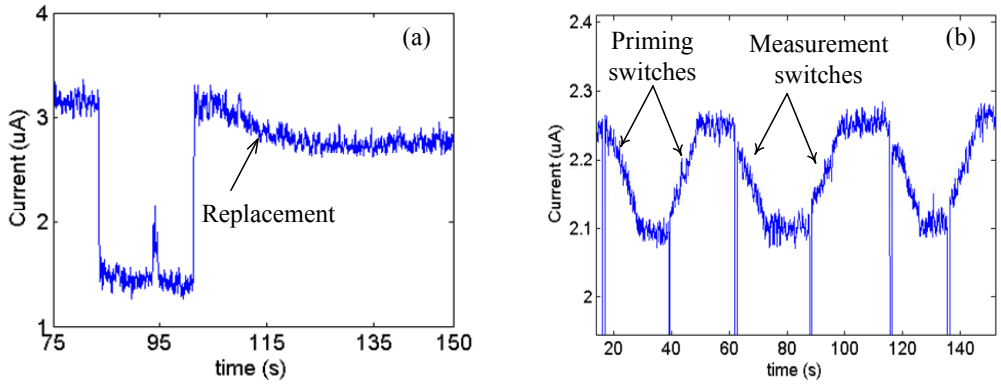

Figure 4.10: Results of a current-monitoring experiment for 1 mM KCl , (a) -straight channel design, and (b)- Y-channel design.

As clearly shown in figure 4.10(a), in the straight channel design it is hard to accurately locate the end of solution replacement, since there is a gradual current change. Also, the time needed for removing the solution from the source reservoir was around 20 s, (the region from t = 81 - 100 s in figure 4.10(a)). From figure 4.10(b), the results from the Y-channel design for the same solution has a better trend. Locating the start and end of solution replacement in the displacement channel between the two pumping scenarios was easier since the current-time plot was sharp. Note that the lines with a negative slope correspond to the low conductivity solution replacement, or applying the electric field between R2 and R3, and vise versa. Furthermore, the number of replacements with the Y-channel design was more than with the straight channel design. To get more replacements with the straight channel design the experiment must be stopped and the solution at reservoir needs to be manually removed, without assurance of getting good results. Thus, the Y-channel design has advantages over the straight channel design since it gives a better current trend and it is more time effective in performing the experiments.

4.3.3 Data Analysis

An in house Matlab program [92] was written to analyze the experimental outcomes of the current-monitoring technique. The program imports the experimental results and performs the calculation of the different parameters that could be obtained from the current-time plot. The zeta potential, the electroosmotic mobility and the surface conductance were the main variables calculated in the program. The first step of the analysis was to input the experimental conditions, such as number of analyzed replacements, solution temperature, the solution conductivity and the solution pH. This was implemented in the

program with a graphical user interface (GUI), as shown in figure 4.11(a). Afterwards, another GUI will open that allows locating the important points in the current-time plot, as clearly shown in figure 4.11(b). This GUI is repeated with the same number of displacements that was chosen for analysis. After finishing all the sets of replacements and performing the analysis a final GUI appears with the results of each individual set, such as the zeta potential and the electroosmotic mobility, which allows the user to chose individual experimental sets of interest and average their results in the output file.

Uncertainty analysis of the parameters calculated from the current-monitoring outcomes was employed in the program. The uncertainty analysis is similar to the procedure presented in Beckwith *et al.* [93], also discussed in Appendix C. The uncertainty was calculated with a confidence level of 90 %. A final result file was that written that summarizes the important results of the chosen individual sets and the average of the chosen sets.

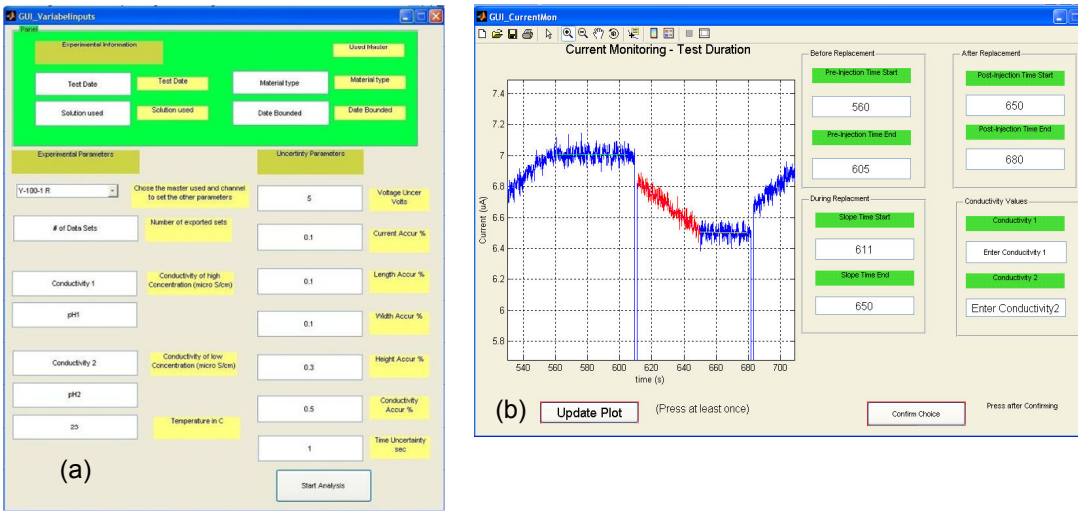

Figure 4.11: GUI's of the Matlab analysis program. (a)- GUI of the experimental parameters and conditions, and (b)- GUI for choosing the important points of interest for a certain replacement.

4.4 Results and Discussion

In this section the results of the current-monitoring experiments with the Y-channel will be presented. The main goal of this section is to validate the use of the Y-channel design with the current-monitoring technique in studying the different electrostatic properties of microchannels. The criteria chosen for the validation process are as follows: first to

compare the consistency of results of a single solution with different Y-channel designs. Secondly, find the effect of the change of solution concentration on the zeta potential value for a certain solution. Finally, compare the values of the zeta potential found from the Y-channel design with results in the literature from the straight channel design.

4.4.1 Consistency of the Results from the Y-channel Design

One important property of the zeta potential is that for a certain solution/wall pairing the zeta potential value is constant [4, 11, 45]. This property was chosen as a criterion to validate using the Y-channel design with the current-monitoring technique. The 1XTBE buffer was chosen for these experiments and the experiments were performed with different Y-channel designs for PDMS/glass chips. Table 4.4 presents the results of each individual experiment.

Table 4.3: The effect of changing the channel dimensions on the zeta potential for 1X TBE buffer and PDMS/glass chip.

Solution	Chip format	Master Name	Zeta potential ζ (mV)
1X TBE	PDMS/glass	Y-100-2	-48.01 $\pm$ 3.77 %
1X TBE	PDMS/glass	Y-200-1	- 49.90 $\pm$ 2.65 %
1X TBE	PDMS/glass	Y-200-3	-48.91 $\pm$ 3.76 %
1X TBE	PDMS/glass	Y-500-2	-51.48 $\pm$ 1.78 %
1X TBE	PDMS/glass	Y-500-3	-48.16 $\pm$ 3.76 %

As presented in table 4.4, the zeta potential value for 1X TBE buffer was not affected by the channel dimensions for different Y-channel designs. Differences in the zeta potential were within the uncertainty of the experimental measurements, as briefly discussed in Appendix C. This validates the consistency of finding the the zeta potential with the Y-channel design.

4.4.2 Effects of Changing the Solution Concentration on the Zeta Potential

It is known that the solution concentration directly affects the zeta potential value where the higher the concentration the lower the zeta potential [11, 44, 45]. This is due to

the fact that with higher concentrations more ions are available to counteract the surface charge and reduce the thickness of EDL, as discussed in chapter 2. Three different concentrations of KCl were chosen to examine the effects of changing solution concentration on the zeta potential with the Y-channel design. Figure 4.12 presents the results of the current experiments for the KCl concentrations with the Y-channel design.

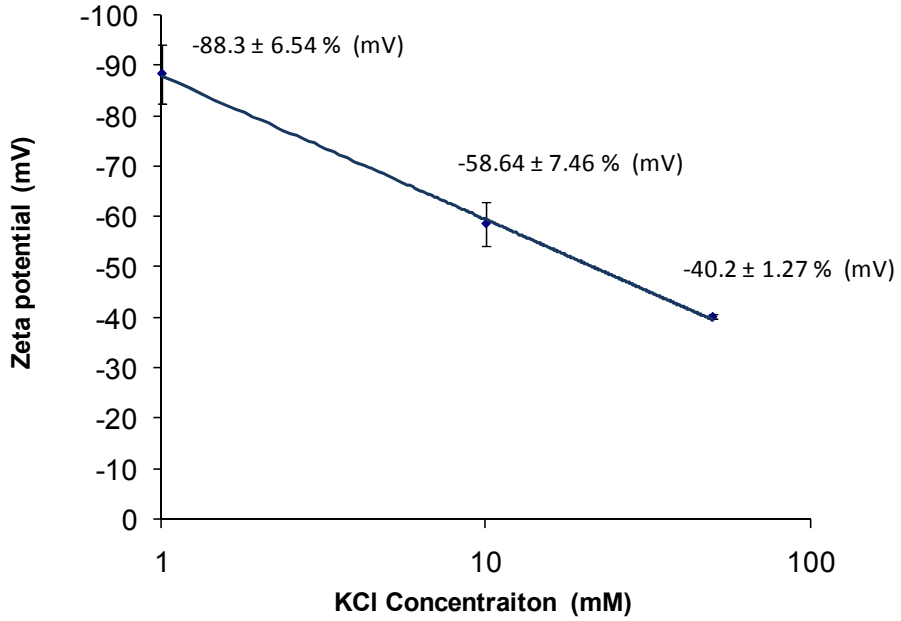

Figure 4.12: Solution concentration effect on the zeta potential.

It is clear from figure 4.12, that the zeta potential decreases as the solution concentration increases. This reduction in the zeta potential vlaue could be approximated with a logarithmic relation, which was similar to trends of the zeta potential with solution concentration reported by researchers in the literature [11, 44, 45], thus validating this finding from the Y-channel design.

4.4.3 Comparing to Results in the Literature

The most important criterion that validates the use of the Y-channel design in studying the electrostatic properties of microchannels is to compare the results from the Y-channel design with the results of straight channel design reported in the literature. Finding results in the literature presented difficulties, since most of the published results of identical solutions were hard to find, especially when the results lack the information of solution

properties. Moreover the channel manufacturing technique, the accuracy of the experimental setup, and plasma treatment protocol are several reasons that can cause disagreement. The most important factor that affects the results is the plasma treatment protocol and the waiting period prior to performing the current-monitoring experiments.

Table 4.4 presents a comparison of zeta potential values for straight channel designs with the current-monitoring technique found in the literature and Y-channel design. The total length calculation method, equation 4.3 is used in the results comparison process.

Table 4.4: The zeta potential values for different solutions for the Y-channel and straight channel results found in the literature. $^{(*)}$ is from experiments performed in the lab with a straight channel design.

Solution	Channel format	Zeta potential, $\zeta(mV)$ Straight Channel	Zeta potential, $\zeta(mV)$ Y-Channel
50 mM $NaHCO_3/Na_2CO_3$	P/G	-59.12$^{(*)}$	-56.79
1 mM KCl	P/G	-88.32 [52]	-83.64$\pm$ 6.54 %
	P/P	77.80 [58]	-82.65 $\pm$ 7.10 %
10 mM KCl	P/G	-54.84 [52]	-56.10 $\pm$ 7.46 %
	P/P	-37.57 [52]	-52.39 $\pm$ 5.11 %
1X TE	P/G	-68.13 [52]	-66.09 $\pm$ 5.67 %
1X TBE	P/G	-48.05 [52]	-44.01$\pm$ 3.77 %

From table 4.4, it is clear that the zeta potential results from the Y-channel design were in good agreement with zeta potential values found in the literature. The small discrepancies between the results were within the uncertainty of the measurements.

4.5 Conclusions

In this chapter a new Y-channel design was presented and validated for studying the electrostatic properties of microchannels with the current-monitoring technique. Errors from the solution electrolysis and undesired pressure driven flow were discussed and extensively reduced.

As presented through this chapter, the Y-channel design has several advantages over the conventional straight channel with the current-monitoring technique. First, the time effectiveness in performing the experiments with the Y-channel design was better compared to the straight channel design, since the solution replacements could be alternated without the need to remove the solutions from the reservoirs. Also the current-time plots from the Y-channel design showed sharp trends which made it easier and more accurate to distinguish the important points during solution replacement from the current-monitoring technique.

Current-monitoring results from the Y-channel design were validated with several criteria and it was proven to be consistent. This justifies using the Y-channel to study the electrostatic properties of microchannels.

Chapter 5

Applications of the Y-channel Design in Different Electroosmotic Studies

In the previous chapter the Y-channel design was applied for analyzing the electrostatic properties of microchannels with the current-monitoring technique. This chapter is devoted for studying electroosmotic flow in PDMS based microchannels with the current-monitoring technique. At first, a new analysis approach for interpolating the outcomes of the current-monitoring technique will be presented. This new method is called the current-slope method which has several advantages over the traditional slope method. Afterwards, different parametric studies on electroosmotic flow in PDMS based microchannels will be further examined. Studies will be sequenced as follows: first, the zeta potential values of different biological buffers that have not been previously reported will be found. Second, the effects of the chip substrate material on the average zeta potential of the PDMS based microchannels will be presented. Third, temperature effects on zeta potential will also be examined. Finally,to analyze the phenomena of the surface conductance during electroosmotic flow in micorchannels.

5.1 Current-Slope Method

In the previous work, which used the current-monitoring technique and a straight channel design for zeta potential measurements, locating the start and end of a solution displacement was a significant source of error. As discussed in chapter 4, the zeta potential is found after estimating the average velocity in the microchannel during electroosmotic pumping with equation 5.1:

$$u_{av} = \frac{L_{channel}}{\triangle t} \tag{5.1}$$

where $L_{channel}$ is the channel length in which the solution displacement occurs, and $\triangle t$ is the time needed for the displacement. The zeta potential is found from the H-S equation 2.21 by using the calculated average velocity. Thus, if the value of $\triangle t$ could not be accurately found, the calculated average velocity will not represent the actual electroosmotic pumping in the microchannel. This cases an error that propagates to the calculation of the zeta potential. The inability to accurately determine the start and end times of the solution displacement is due to the fact that the current trend is not sharp and there is a gradual current change. This gradual current change is due to the presence of a solution dispersion region (see figure 4.10 a). In some cases, small current fluctuations and gradual transitions due to diffusive mixing of the two solutions at the interface causes difficulties in determining the start and end of the displacement process. To address this problem, Ren *et al.* [48] developed an alternative analysis technique where the zeta potential is determined from the slope of the current-time plot. The slope analysis approach is performed by finding the slope for a linear region of the current-time plot, which represents the actual linear difference of the pumping process between the two different solutions. This approach reduces the errors associated with locating the start and end of the solution replacement.

The major assumption for slope approach proposed by Ren *et al.* [48] is that the solution conductivity in pumping process is similar to the bulk conductivity at the reservoirs, thus representing the actual current during electroosmotic pumping [48]. Also, the solution conductivity difference will be similar to the current difference during the experiment. The analysis of the slope method neglects the effects of the surface conductance and the surface current during electroomostic pumping. The slope analysis is found by [48]:

$$\mu_{emo} = \frac{slope \cdot L_{channel}}{E^2 \cdot (\triangle \lambda_b \cdot A_c)} \tag{5.2}$$

where μ_{emo} is the electroosmotic mobility, $slope$ is the slope of the current-time plot (A/s), $L_{channel}$ is the total channel length, $\triangle \lambda_b$ is the difference in the conductivities between the solutions, A_c is the cross sectional area of the microchannel.

The major issue with the slope approach presented by Ren *et al.* [48] is that the solution conductivity value is taken to be identical as the bulk conductivity measurement. The assumption of constant conductivity value has several issues. First, the solution conductivity varies rapidly with the change of temperature $(\sim 2\%^oC)$[1] , and the actual

[1]This conductivity change with temperature was obtained by experiments performed in the lab on the solutions used in the current-monitoring experiments. The relation may differ for other solutions.

temperature inside the microchannel could not be accurately measured nor could the solution conductivity. Hence, there is some ambiguity in the real time solution conductivity. Other means of measuring the conductivity inside the microchannel could be done by planting conductivity electrodes downstream of the microchannel [94], which is hard and may affect the electroosmotic flow. Second, the analysis ignored the changes in the surface conductance phenomena due to solution changes.

Another major issue with the present experimental setup is that the accuracy of the conductivity measurements with the conductivity electrode was in the range of 0.5 - 2 %, and the solution conductivity difference is within 5 % . Thus the uncertainty in calculating the conductivity difference is fairly high ($\triangle\lambda_b$ has an uncertainty of 39 % for an electrode with 1 % accuracy).

Also, in the preliminary current-monitoring experiments two unexpected outcomes were observed that showed disadvantages of using the slope method. First, the slope method was not in good agreement with the total length method in finding the average velocity in microchannels. Second, the conductivity ratio was not similar to the current ratio ($\lambda_{b1}/\lambda_{b2} \neq I_1/I_2$), where the current ratio was higher than the conductivity ratio. These issues motivated the search for an improved slope approach to find the velocity, especially for the case where the start and end of the replacement was not clearly identified.

To reduce the effects of errors associated with the conductivity measurement, the actual current values measured at the plateaus of the current-time plot were used instead of the solution conductivity difference. By using this approach errors from the bulk conductivity measurement and any changes in surface current were eliminated. In addition, measuring the current is at least an order of magnitude more accurate than measuring the solution conductivity. The proposed current-slope analysis is presented as:

$$\mu_{emo} = \frac{slope \cdot (L_d + L_{side})}{E \cdot (I_2 - I_1)} \tag{5.3}$$

where I_1 and I_2 were the steady state currents before and after the solution replacement. Figure 5.1 presents a typical current-time outcome from a Y-channel design with the current-monitoring technique. Also, the important regions of the solution displacement during the current-monitoring experiment are highlighted in figure 5.1.

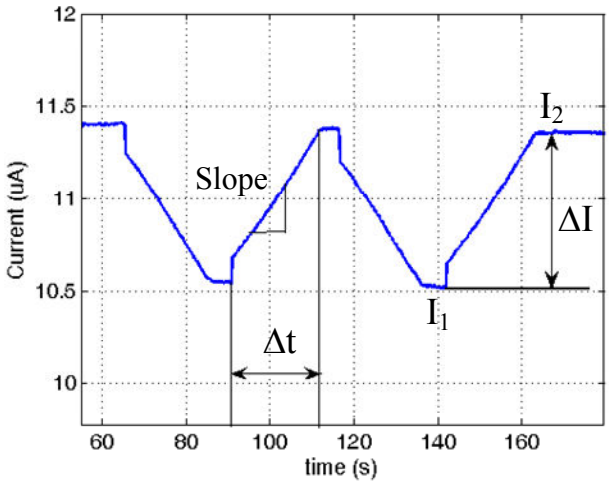

Figure 5.1: A typical outcome of the current-monitoring experiment with the Y-channel design.

5.2 Zeta Potential Results for Different Biological Buffers

Introducing new solutions in microfluidic applications is a common practice. Thus, the knowledge of the zeta potential for these solutions is important if electroosmotic flow is used as a pumping method.

In this work different biological buffers commonly used for numerous applications [19, 91, 95] were studied with the current-monitoring technique and the Y-channel deign. The procedure of performing current-monitoring experiments with the Y-channel design was discussed in chapter 4. For each tested solution, different Y-channel designs were used with different channel dimensions. The average results of all the experiments are presented in figure 5.2. At least 35 measurements were performed for each solution, except the 1XPBS, 1XTE, 25 mM Tris-HCl, and the L-15ex where 20 measurements were performed.

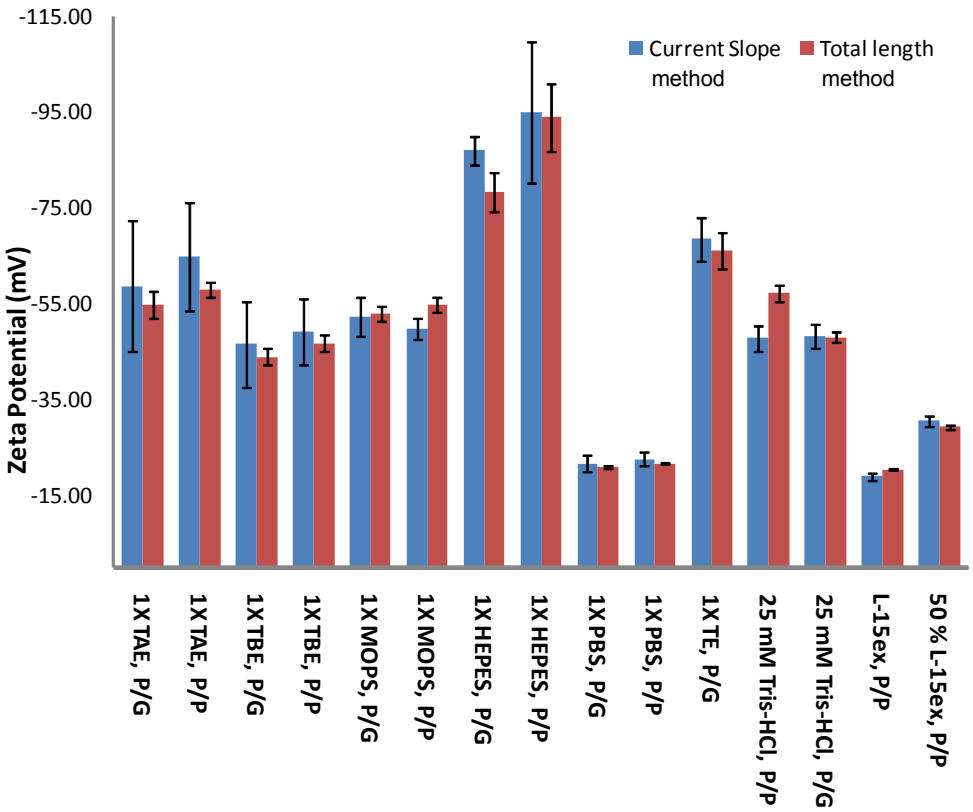

Figure 5.2: The Zeta Potential of different biological buffers.

Figure 5.2 indicates that the modified current-slope method is in good agreement with the total length method, this validates using the modified current-slope method for analyzing the outcomes of the current-monitoring technique. This comparison between the two methods is accurately achieved with the Y-channel design since the current-time plot is sharp and linear, and the start and end of replacement were clearly identified in most of the experiments, as observed in figure 5.1. From the results presented in figure 5.2 it was observed the HEPES buffer, which is a Good's buffer [88], showed the largest zeta potential compared to all other buffers $\sim$ -95 mV. It was observed while performing current-monitoring experiments that the 1X TBE buffer showed the highest resistance to electrolysis during electroosmotic pumping.

5.3 Effect of Changing the Chip Substrate Material

For hybrid microchannels made of different materials it was reported in the literature that each portion of the channel contributes to the overall zeta potential of the microchannel

[96]. This overall zeta potential, for a hybrid microchannel, is calculated with a weighted average approximation [96]. In PDMS based microchannels, glass slides and PDMS are the most commonly used substrates. Therefore, for a hybrid PDMS microchannel, i.e. PDMS/glass, it is a reasonable conclusion that the average zeta potential of this hybrid channel is a weighted average of both portions of channel wall [96]. This trend was observed in the literature when using hybrid PDMS microchannels where the PDMS/glass microchannels has a higher zeta potential compared to the PDMS/PDMS [52].

In a typical hybrid PDMS/glass Y-channel design used in the current-monitoring experiments the glass portion of the microchannel was about 50% of the channel, as shown in figure 5.3. It was expected that this high portion of glass will contribute to the overall zeta potential of the microchannel giving the PDMS/glass a higher zeta potential value compared to the PDMS/PDMS.

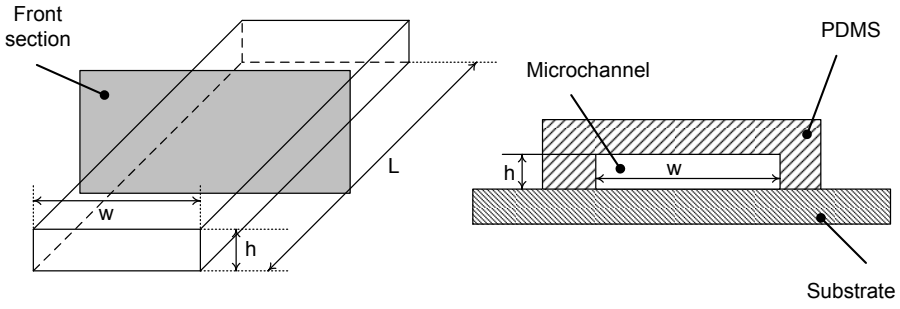

Figure 5.3: Schematic of a hybrid microchannel.

From the zeta potential results shown in figure 5.2, the average zeta potential of the PDMS/PDMS and PDMS/glass for any tested solution gave similar values, if not identical. Small differences in the zeta potential values between the PDMS/PDMS and PDMS/glass lie within the uncertainty of the measurements, as shown by the error bars. This does not conflict the above discussion about the weighted average calculation of the zeta potential, but gives more insight into the dosage of plasma treatment for PDMS microchannels. As a conclusion from figure 5.2, the plasma treatment dosage was capable of creating artificial silanol, $SiOH$, groups on the surface of PDMS with concentrations similar to SiO^- concentration on the surface of glass. In other words the surface charge of the air plasma treated PDMS is similar to the surface charge of the glass. This finding of the close values for the zeta potential in plasma treated PDMS/glass and PDMS/PDMS microchannels was observed by other researchers working with electroosmotic [49].

This finding motivated further examination for other PDMS microchannel substrate

material. SU8 photo resist, which was used to manufacture the channel profiles on silicon wafers, has been recently used to fabricate microchannels [50]. The SU8-microchannels showed an electroosmotic mobility higher than other polymeric microchannels [50]. For this reason, SU8 was used as a substrate for PDMS microchannels in order to observe the effects on the zeta potential of microchannel. SU8 was coated on microscope glass slides with different thicknesses similar to the procedure for making the adhesion layer on the silicon wafer, as presented in chapter 3. The glass slides coated with SU8 were bonded to PDMS microchannels with the aid of plasma treatment, similar to the protocol used in bonding the Y-channel chips. Results of the zeta potentials for PDMS/SU8 chips are presented in table 5.1.

Table 5.1: Results of PDMS/SU8 microchannels with different solutions and different Y-channel designs.

Design used	Solution	Chip Type (Substrate thickness)	Zeta potential (mV)
Y-100-2L	Tris-HCl (25 mM)	PDMS/SU8 (5 μm)	-49.65 $\pm$ 3.00 %
Y-100-2 M	Tris-HCl (25 mM)	PDMS/SU8 (1 μm)	-54.13 $\pm$ 3.21 %
Y-100-2 M	1X TBE	PDMS/SU8 (5 μm)	-46.80 $\pm$ 2.92 %
Y-500-2 M	1X TBE	PDMS/SU8 (5 μm)	-45.50 $\pm$ 2.36 %

From the results presented in table 5.1 and by comparing them to the results presented in figure 5.2 it is observed that the zeta potential for microchannels with SU8 as a substrate is similar to the zeta potential of PDMS/PDMS and PDMS/glass microchannels. As a final conclusion for plasma treated PDMS based microchannels with glass, PDMS or SU8 substrates, the overall zeta potential of the channel is similar, and the weighted average analysis for the zeta potential is not applicable.

5.4 Temperature Effects on the Zeta Potential

It is known that the temperature changes during electroosmotic pumping affect the velocity inside the microchannel, since it affects solution properties (the viscosity and the dielectric constant). Moreover, it has been recently found that the zeta potential is also temperature dependent for certain solutions with different relations [52]. Venditti *et al.* [52] used the current-monitoring technique to investigate the effect of temperature

changes on the zeta potential and it was found that for some solutions showed a strong temperature dependence of the zeta potential, such as 10 mM KCl, and 1X TBE. The zeta potential of other solutions was not affected with temperature changes, such as 1 mM KCl and 1XTAE. The major problem in their approach was that the solution concentration changes during the experiments were not prevented. Therefore, results may not represent the actual solution conditions at the start of the experiment. Also, for some solutions the pH is a temperature dependent property. To properly examine temperature effects on the zeta potential, the solution pH must remain constant with respect to temperature.

Considering the problems associated with the experimental setup and approach presented by Venditti *et al.* [52] to examine the temperature effect on the zeta potential, improvements on the current-monitoring experimental setup has been done. First, to assure uniform temperature distribution the chip holder with the chip were put into a UV incubator with controllable temperature. The incubator uses heat convection as the heat transfer mechanism for changing and controlling the temperature inside the chamber. In a typical experiment the chip was left for 45 minutes at a certain temperature before performing current-monitoring experiments to assure uniform temperature conditions in the chip and at the reservoirs. This was also confirmed by measuring the solution temperatures at the reservoirs with a thermocouple.

To prevent the changes in the solution concentration at the reservoirs during the experiment, a layer of mineral oil was placed over the top of the solutions at the reservoirs as shown in figure 5.4. This layer of mineral oil will prevent the solution evaporation at the reservoirs during the experiment.

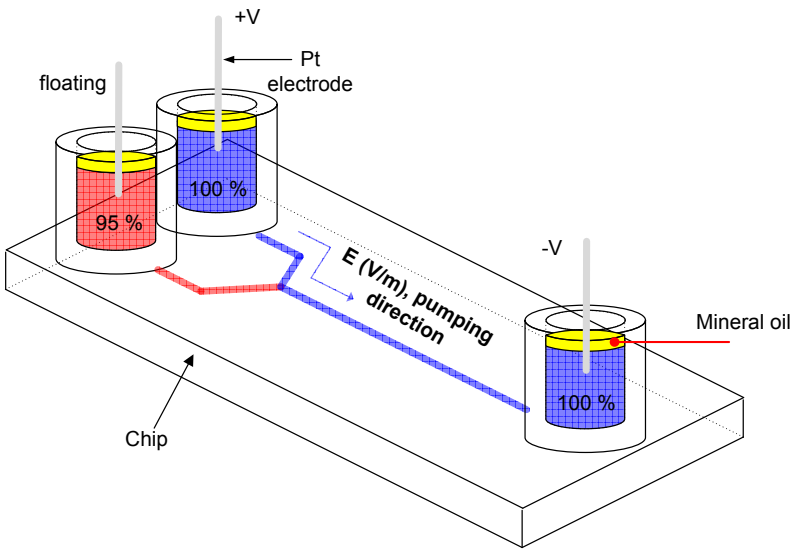

Figure 5.4: A schematic for the approach used to study the temperature affect on the zeta potential. Mineral oil was used to prevent solution evaporation from the reservoirs.

In the analysis of the experimental outcomes, the viscosity and dielectric constant were corrected to be temperature dependent. The solutions were assumed to have properties identical to those of water, since they were water based solutions. The correction of the viscosity and dielectric constant was done following [52]:

$$\varepsilon_r = 305.7 \cdot \exp\left(\frac{-T}{219}\right) \tag{5.4}$$

$$\mu = 2.761 \times 10^{-6} \cdot \exp\left(\frac{1,713}{T}\right) \tag{5.5}$$

where ε_r is the relative permittivity of the solution, μ is the solution viscosity, and T is the absolute solution temperature. This correction was incorporated in the Matlab analysis algorithm. Table 5.2 presents the effects of the temperature effects on the zeta potential for different solutions.

Table 5.2: Temperature effects on the zeta potential for different solutions.

Solution	Chip Type	Temperature (^oC)	Zeta potential (mV)
1X TBE	PDMS/glass	30	-26.12 $\pm$ 1.4%
	PDMS/glass	50	-33.52 $\pm$ 2.4 %
L15ex 10%FBS	PDMS/glass	24.3	-10.2 $\pm$ 0.65 %
	PDMS/glass	45	-14 $\pm$ 0.91 %

From table 5.2, it can be noticed that the zeta potential of the 1X TBE and the L15ex 10%FBS have increased with the temperature, hence improving the electroosmotic pumping in the microchannel. This tendency was also observed by Venditte *et al.* [52] for some solutions, as discussed earlier. Thus, improving the electroosmotic pumping of solutions can be archived with increasing the temperature [52].

5.5 Surface Conductance

In previous current-monitoring work with microchannels, the surface conductance was mostly ignored, since it was assumed that the surface conductance will not change with the solution replacement in the microchannels [47, 48, 49, 52]. Also, it was assumed that the surface current is negligible compared to the current carried from the bulk solution conductivity [47, 48, 49, 52]. In the present work, the surface current was found to be 10 $\sim$ 15 % of the total current. Thus, the surface conductance could not be neglected.

As presented in chapter 2, the surface conductance is the phenomenon related to the current flow within the EDL, making it a function of factors that affect the EDL thickness, such as solution concentration and wall surface charge density. Thus, accurate measurement of surface conductance is important to have full characterization of electroosmotic pumping in microchannels. The streaming potential technique is the most adopted method for finding the surface conductance of different materials [4, 11, 26]. Recently, the current-monitoring method was used to find the surface conductance [42]. The results show that it was affected by the channel dimensions [42].

For steady electroosmotic pumping of one solution in a microchannel, the electrical current draw has two main components which are the current from the bulk solution conductivity and the current carried within the EDL [11]. Equation 5.6 represents both

components of the electrical current during electroosmotic pumping:

$$I_{total} = I_{bulk\_cond} + I_{surf\_cond} = \lambda_b \cdot A_c \cdot E + \lambda_s \cdot P \cdot E \tag{5.6}$$

where λ_b (S/m) is the solution bulk conductivity, A_c (m^2) is the cross sectional area of the microchannel, λ_s (S) is the surface conductance, P (m) is the perimeter, and E (V/m) is the applied electrical field. By knowing the bulk conductivity of the solution the surface conductance was found from equation 5.7 :

$$\lambda_s = \frac{I_{measured}}{P \cdot E} - \frac{\lambda_b \cdot A_c}{P} \tag{5.7}$$

where $I_{measured}$ is the steady recorded current of the electroosmotic flow for a solution in the microchannel. In the present work, the surface conductance was found with the current-monitoring experimental setup and with adding a high accuracy Pico-Ammeter (Keithley 6485) for high precision electrical current measurement.

The effects of two main parameters the electric field and the channel substrate material on the surface conductance were examined in this work. The experiments were performed by pumping one solution and monitoring the current, similar to the channel symmetry validation process (chapter 4).

A typical result of the effect of changing the electric field on the surface conductance is presented in figure 5.5 for 1X TAE solution in a PDMS/PDMS microchannel.

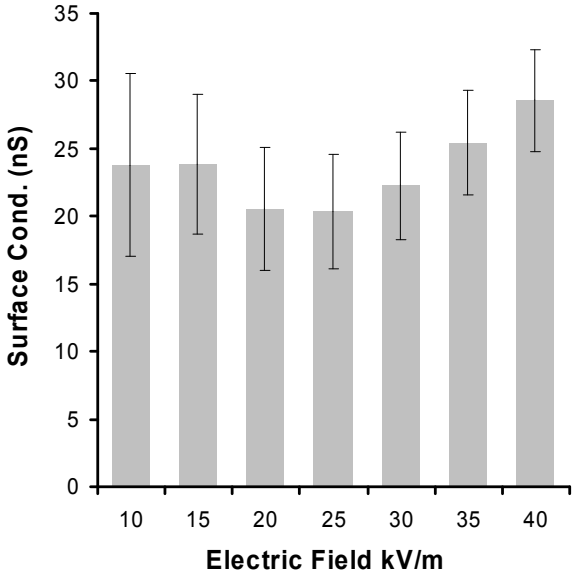

Figure 5.5: The effect of changing the electric field on the surface conductance for 1X TAE in a PDMS/PDMS microchannel.

As presented in the figure 5.5, it is observed that the surface conductance has small variations with changing the applied electrical field. At most of the applied electric fields, the fluctuations in the surface conductance are within the uncertainty of the surface conductance measurement. This trend, the small changes in the surface conductance, was observed in a number of experiments used to find the surface conductance. Thus, the surface conductance of microchannels will not change with applied electric field, which was also observed in the literature [42].

It was observed that the experimental uncertainties associated with calculating the surface conductance from the steady current values are high compared to other electrostatic properties found with the current-monitoring technique, such as the zeta potential. This is due to the nature of the surface conductance calculation (equation 5.7) where the equation used for finding the surface conductance has a subtraction operation. The propagation of uncertainty for parameters found from the subtraction operation has the highest uncertainty compared to other mathematical operations [93]. Unfortunately, this is the only equation that can be used for finding the surface conductance from steady electroosmotic pumping [11, 42].

Another observation, which had a big influence on the calculation of surface conductance, was the effect of the solution conductivity changes on the surface conductance results. During electroosmotic pumping the solution conductivity could change because of the temperature change or solution electrolysis. Hence, the conductivity value used in the analysis could be misleading in calculating the surface conductance. In a typical electroosmotic pumping experiment electrolysis might change the conductivity by about 2%, especially in the case of using electrolytes.

Figure 5.6 presents the changes in the calculated surface conductance when changing the solution bulk conductivity for a 10 mM KCl in a PDMS/PDMS microchannel. The experiment was performed in 7 min and the solution electrical conductivity at the reservoirs changed from 1301 $\mu S/cm$ at the start of the experiment to 1315 $\mu S/cm$ at the end [2]. The change in solution conductivity ($\approx$1 %), caused a change of 15 % in the calculated surface conductance for each applied electric field.

[2] In figure 5.6 the electric field is chosen as the x-axis to be consistent with the previous figure 5.5. The change in the applied electric field (20 kV/m - 40 kV/m) also correspond to an increase in time, where at the start of the experiments the electric field was and 20 kV/m it was increased with time until reaching 40 kV/m after 6 min.

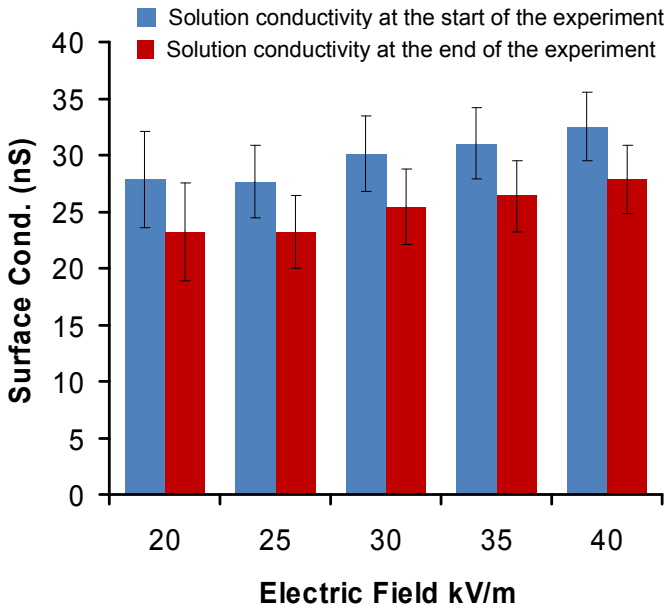

Figure 5.6: Effects of changing the solution conductivity value on the calculated surface conductance vs. electric field.

The reason for this change in the surface conductance with respect to the solution conductivity value (observed in figure 5.6) , is that any minute change of the solution conductivity during electroosmotic pumping will affect both terms of equation 5.7, hence affecting the calculated surface conductance. For the first term, the recorded current will change according to the change of solution conductivity, which leads to over estimation of the surface conductance with increasing the time, as clearly shown in blue bars of figure 5.6. The second term of equation 5.7 suffers more from solution conductivity changes since the conductivity term appears directly. The contribution of the second term is higher than the first term in changing the results of the surface conductance. Thus, if using the value of the solution conductivity at the start of the experiment it will lead to an overestimation of the surface conductance. By performing simple comparison between the surface conductance calculated with the solution conductivity at the start of the experiment (blue bar figure 5.6) at 20 kV/m and surface conductance calculated at 40 kV/m calculated with the solution conductivity at the end of the experiment (red bar figure 5.6), both these results are close.

In order to reduce the effects of solution conductivity changes on the surface conductance several measures were taken. First the time for performing the experiments was shortened in order to reduce the electrolysis effects. Second, the temperature of the solu-

tion at the reservoirs were maintained constant with the aid of a fan, but with no assurance of maintaining constant temperature inside the channel. In addition to be consistent in the analysis, surface conductance calculations were performed using the conductivity at the end of the experiment since it was the closest value to the actual value of the pumped solution. The average results of the surface conductance analysis for different solutions and different channel formats are presented in figure 5.7.

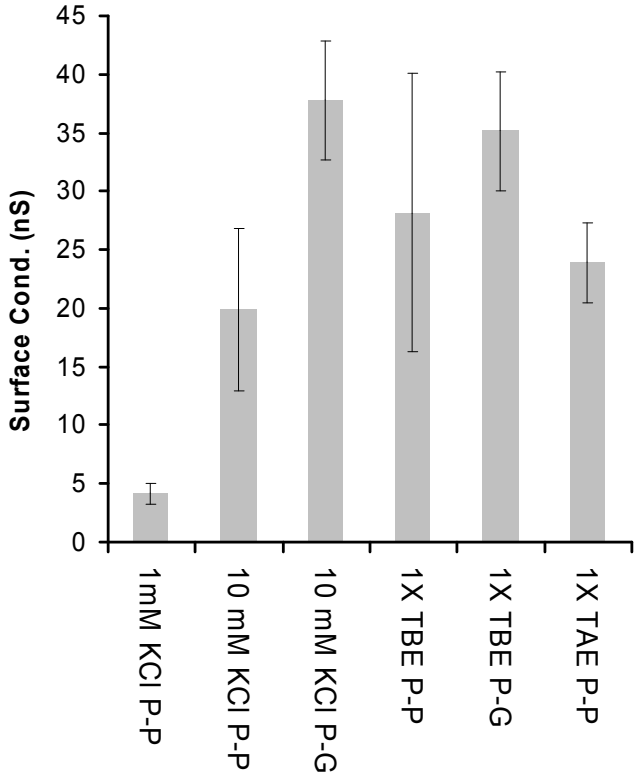

Figure 5.7: Surface conductance of different solutions for P-P (PDMS/PDMS) and P-G (PDMS/glass) microchannels. (Each surface conductance value is an average of 20 measurements, and error bars represent the standard deviation of the results).

From figure 5.7, it is clear that the average surface conductance differs for different solutions. These differences are associated with the differences of the EDL properties among different solutions. The surface conductance from the 10 mM KCl is higher than the surface conductance of the 1 mM KCl. This is due to the fact that the 10 mM KCl has more ions within the EDL which will carry more current (2) [11].

Another unexpected finding is that channel substrate has an effect on the calculated surface conductance in microchannels with electroosmotic pumping. Form figure 5.7 it

is observed that the PDMS/glass microchannels gave higher surface conductance compared to the PDMS/PDMS microchannels. The glass portion of the microchannel was around 50% of the surface area of the microchannel. The high surface conductance of PDMS/glass compared to PDMS/PDMS microchannels leads to the speculation that the current carried within the EDL of the glass portion is higher than the current carried in the EDL of the plasma treated PDMS. Also, this indicates that the EDL of the glass portion differs from EDL of the PDMS portion. On the other hand, the overall zeta potential of the microchannels is not affected by such material changes, as seen previously in figure 5.2. There is no clear explanation for these contradicting findings and more investigation is recommended with other techniques, such as the streaming potential.

5.6 Conclusions

This chapter covered several studies of electroosmotic pumping in PDMS microchannels using the current-monitoring technique. A modified current-slope approach to analyze the current-monitoring outcomes was presented and validated.

The zeta potential of different biological buffers was found in PDMS based microchannels with the Y-channel design. The effect of the chip substrate on the average zeta potential was examined. It was found that for PDMS based microchannels with air plasma treatment, the type of channel substrate does not have an affect on the average zeta potential of the microchannel.

The temperature effect on the zeta potential was examined with a modified approach, compared to the work presented by Venditti *et al.* [52]. Results for the tested solutions show that the zeta potential, was affected by temperature change and will increase with an increase of temperature. The surface conductance of the PDMS based microchannels were studied with the current-monitoring technique. It was found that the surface current (the current carried within the EDL) during electroosmotic pumping was around $10 \sim 15$ % of the total current draw, thus the surface conductance could not be neglected.

Chapter 6

PDMS Surface Treatment

PDMS (polydimethylsilicone) is widely used for manufacturing microfluidic chips because of its favorable properties, as previously discussed in chapter 2. But in the case of using electrokinetic driven flow, PDMS has poor electrostatic properties compared to glass and silica microchannels. Moreover PDMS is hydrophobic in nature. Hence, improving the PDMS properties by the means of different treatments is very desirable, and as such has received great interest for microfluidic applications. One popular and yet simple treatment is the plasma treatment. Plasma treatment is a one step procedure that alters the surface properties of PDMS to a hydrophilic state and increasing the zeta potential. Unfortunately plasma treatment in not long-lasting and the PDMS regains its hydrophobic properties with time due to the diffusion of the non cured low molecular weight PDMS (LMW) from the bulk material to the treated surface. Different treatments have been carried out and examined by researchers to modify and preserve the hydrophilic properties of the PDMS such as the incorporation of a prepolymer additive, reducing the diffusion of the LMW, and grafting monomers with preferred properties [70, 71, 73, 74, 75].

In this chapter several protocols for treating PDMS were chosen. The treatments that were analyzed were the prepolymer doping of PDMS with acrylic acid (AA), extraction of the PDMS and different HEMA grafting protocols. The aim of these treatments was to improve the electrostatic properties (the zeta potential), and enhance the stability of the hydrophilic state of the plasma treated PDMS. The treatments were chosen according to two main criteria: their claimed results from the literature, and their applicability to the microfluidics lab for PDMS microchannels. Unlike other studies [70, 71, 73, 74, 75], where a maximum of two methods were used to examine the effects of PDMS treatments, this study used four methods to examine the PDMS treatment protocols. The main protocols employed for the analysis of the PDMS treated samples included the

current-monitoring technique, static contact angle measurements, dry storage analysis, and ATR-FTIR. The first step required the current-monitoring and dry storage experiments to be performed for all the treatment protocols. The second stage was contact angle measurements for each protocol. Finally, the ATR-FTIR technique was used to find the effective chemical groups responsible for the observed improvements.

6.1 Sample Preparation

The samples that were tested are in two formats: microchannel format and non-profiled PDMS slabs. The preparation of the microchannels is done according to the procedure detailed in Appendix B, section B.2. The non-profiled PDMS slabs were manufactured using the following procedure. Briefly, the PDMS base elastomer and curing agent were mixed in a 10:1 ratio and the mixture was degassed for 30 minutes. The mixture was poured onto a flat silicon wafer and degassed for a further 25 minutes. The mixture was cured over a hotplate at 150 ^oC for 20 minutes. Cured samples were cleaned with acetone and dried in a vacuum oven at 40^oC and -25 psi for 2 hrs. All PDMS samples were plasma treated for 40 s using a power setting of 29.6 W.

The samples that were manufactured in the channel format were tested using the current-monitoring technique and dry storage analysis, and the non profiled samples were tested using contact angle and the ATR-FTIR analysis. The procedures used for the sample preparation of each chemical treatment will be presented next.

6.1.1 Prepolymer Additive

Acrylic acid (AA) is a simple carboxylic acid with a double bond. It was reported by Luo *et al.* [78] that doping the PDMS with AA gives an improvement to electroomostic mobility of PDMS microchannels [78]. The procedure of treating PDMS required the addition of AA to the PDMS mixture, base and curing agent, before the curing process. Two AA weight percentages were tested, which were 0.5 % and 1 % of AA to the weight of PDMS. The curing process of the PDMS mixture was carried out using the same procedure as presented previously in Appendix B (section B.2). Prior to bonding the chip to the substrate the channel and the substrate, for the specimens to be tested with the current-monitoring technique, were plasma treated. The channels were left for two days prior to performing the current-monitoring tests.

6.1.2 PDMS Extraction Process

In the PDMS extraction process, the procedure was carried out in a similar way to the protocol presented by Vickers *et al.* [71], which requires PDMS samples to be put into three chemical baths for 2 hrs respectively. First, the PDMS samples were put in a triethylamine bath at room temperature for 2 hrs. During this stage the PDMS swelled and changed its shape and size. Secondly, the samples were put into an ethyl acetate bath for 2 hrs at room temperature. Finally the samples were left in an acetone bath for 2 hrs at room temperature. After the acetone bath, the PDMS returned to its original shape. The samples were then dried in the oven at 60 C for 4 hrs. It was noted that after the extraction the PDMS samples showed a decrease of around 3 % in weight compared to the initial weight. This reduction in the weight indicated that the concentration of the LMW PDMS reduced during the treatment.

6.1.3 HEMA Grafting

HEMA (2-hydroxyethyl methacrylate) with a purity of 98% was purchased from Sigma Aldrich. HEMA was chosen since it has stable OH groups in its structure. If it is successfully grafted the OH groups will remain on the surface of the PDMS. There are two main approaches to graft HEMA on PDMS including plasma induced grafting, and heat induced grafting [73, 74, 82]. Details on both of these approaches will now be given.

Plasma Induced HEMA grafting

In the plasma induced grafting approach, the procedure was similar to the protocol presented by Bodas and Maklek [73, 74], but with the modification of a different plasma treatment and different power. Bodas and Maklek [73, 74] used an oxygen plasma treatment wherein this work used air plasma cleaner for the treatments. The treatment methodology requires that first the PDMS samples and substrates, which were glass slides coated with PDMS, were plasma treated for 100 s at a power of 29.6 W. The plasma treatment was performed to create active locations on the surface of the PDMS for which the HEMA could bond. Then a thin layer of HEMA was spun coated on the plasma treated surfaces at 1600 rpm for 30 s. Afterwards, another stage of plasma treatment was performed on the samples for 10 minutes. The reason for the large plasma treatment times was to achieve the same power range of the treatment performed by Bodas and Maklek [73, 74]. After the final plasma treatment the PDMS was either bonded to the substrate forming a microchannel chip, or left for the ATR-FTIR analysis.

Heat Induced HEMA grafting

The process of the heat induced HEMA grafting was motivated by the work presented by Choi and Yang [82]. The principle of the heat induced HEMA grafting was presented in chapter 2 and figure 2.6. The main steps of the HEMA heat grafting principle are as follows:

- Create active locations on the PDMS surface for the HEMA to be chemically attached.
- Introduce the HEMA to the activated PDMS surface.
- Graft the HEMA with the aid of heat.
- Removing the residual HEMA which has not been grafted on the surface of the PDMS.

The activation of the PDMS surface is done by changing the chemical structure of the PDMS to have more reactive chemical groups. The surface of the PDMS was archived with plasma treatment where the chemical $Si - CH_3$ was broken to a more reactive chemical group $Si - OH$. The first attempts for the heat induced HEMA grafting were not successful and several heat grafting protocols were examined. The attempted protocols are named as heat protocol 1, heat protocol 2, heat protocol 3, and heat protocol 4. The integration of the treatments was done in several steps until achieving the final protocol. The main difference between the protocols was grafting the HEMA either after or before bonding the chip. This was only for samples in channel format. Table 6.1 presents summarizes the steps for the different heat induced HEMA grafting protocols.

The HEMA grafting attempts were carried out on cured PDMS. No prior pretreatments were done to the PDMS samples, except for one approach where the PDMS samples were extracted before the HEMA polymerization protocol.

The heat bath process is important since it will aid the polymerization rate of HEMA on the PDMS surface. There are two approaches for the thermal grafting which are putting the samples in the oven at the desired degree, or putting the samples in a bath of HEMA to assure the temperature uniformity around the chip.

Table 6.1: The heat induced HEMA grafitng protocols. Sample type: 1 - profiled PDMS, 2 - PDMS substrate, 3 - microscope glass slide, and 4 - non-profiled PDMS slabs. $^{(*)}$ This step is for the samples that are tested with the current-monitoring and dry storage analysis. DI water (deionized water).

	Heat protocol 1	Heat protocol 2	Heat protocol 3	Heat protocol 4
Sample type	1 and 3	1 and 3	1, 2, 3 and 4	1, 2, 3 and 4
Pretreatment	No			PDMS extraction
Surface activation	Air plasma treatment 100 s 29.6 W	Air plasma treatment 40 s @ 29.6 W		
Bonding to the substrate $^{(*)}$	Yes		No	
HEMA treating	Infuse the HEMA in the channel		Immerse the plasma treated sample in a HEMA bath	
Heat grafting protocol	40 ^oC for 4 hrs in the oven	Immerse the chip in a HEMA bath for 6 hrs at 60 ^oC	Immerse in a HEMA bath for 6 hrs at 55 ^oC	Immerse in a HEMA bath for 6 hrs at 55 ^oC
Removal of the HEMA Residual	Infuse DI water at room temp for 1 hrs	A DI water bath at 40 ^oC for 2 hrs		
Drying	6 hrs at 45 ^oC in the oven			
Plasma treatment	No		Air plasma treatment 40 s 29.6 W	
Bonding to the substrate $^{(*)}$	No		Yes	

6.2 Experimental Methods

Several techniques were used to analyze the chemically treated PDMS samples. Figure 6.1 presents the flow chart of the characterization process of the surface treatments. The analysis of the studied surface treatments required the employment of several methods. First, the current-monitoring experiments and dry storage analysis were performed for all of the chemically treated PDMS microchannels. Afterwards, the treatments that gave good results were tested using contact angle analysis (discussed in chapter 3, section 3.3.4) to determine the nature of the surface properties of the treatments. Finally, the ATR-FTIR analysis (discussed in chapter 3, section 3.3.3) was performed on the successful treatments to define the chemical groups responsible for the improvements.

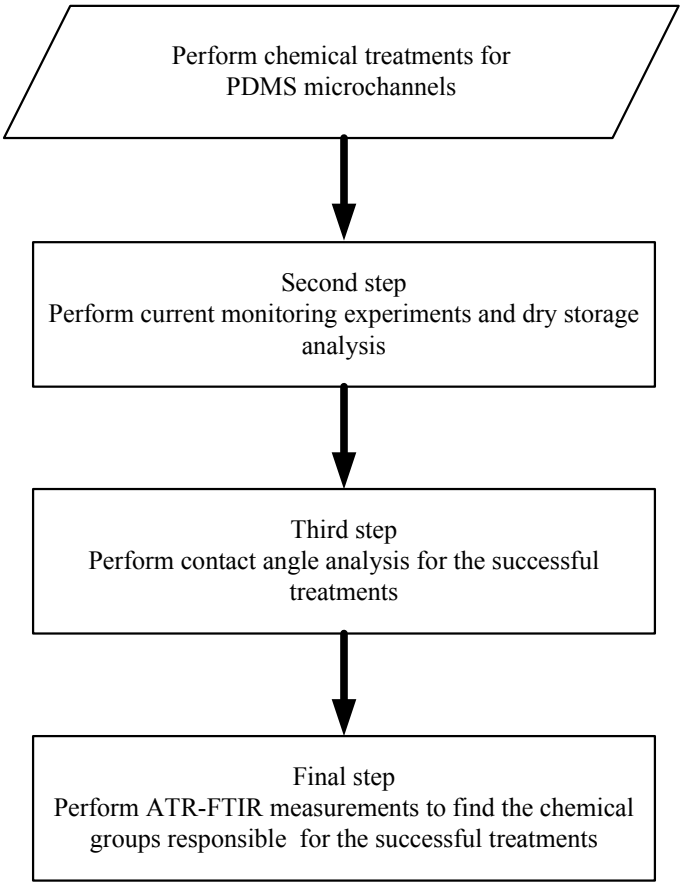

Figure 6.1: Flow chart for the characterization process of the surface treatments.

The current-monitoring experiments were performed with the Y-channel design using the same procedure as presented previously in chapters 4 and 5. The 1X TBE buffer

was chosen as the main solution for the current-monitoring experiments, since it demonstrated the greatest stability against electrolysis during the current-monitoring technique and gave reproducible results.

The dry storage analysis were performed by bonding the microchannels and then dry storing them for two days, unless otherwise specified, without filling them with water. After the waiting period, water was introduced into the reservoirs to fill the channels by capillary action; if the channel is hydrophilic, water will flow in the microchannel, but if the PDMS channel regains its hydrophobic properties water will not flow.

The ATR-FTIR analysis were done with the approach presented in section 3.3.3. The expected chemical groups for the PDMS and chemically treated samples are presented in table 6.2.

Table 6.2: Infrared frequencies and the assigned chemical compounds [85]

Peak location, wave number (cm^{-1})	Chemical Group (type of vibration)
3250 - 3400	$-OH$ (stretch)
2850 - 2990	CH_3 (antisym. and sym. stretching)
1250 - 1280	$Si-CH_3$ (sym CH_3 deformation)
1000 - 1100	$Si-O-Si$ (antisym. stretching)
790 - 810	CH_3 (plane swing)

6.3 Results and Discussion

6.3.1 Regular PDMS

The results of native and plasma treated PDMS were first obtained. This was done to give a reference point for future comparison. Results of the current-monitoring experiments are presented in chapter 4 and 5. It is known that native PDMS has a hydrophobic nature with a contact angle greater than 90^o , but with plasma treatment the surface becomes hydrophilic. However, the plasma treated PDMS regains it natural hydrophobic state with time in dry storage conditions. This phenomenon was examined with the contact angle measurements and the change of the contact angle with time for plasma treated PDMS is presented in figure 6.2.

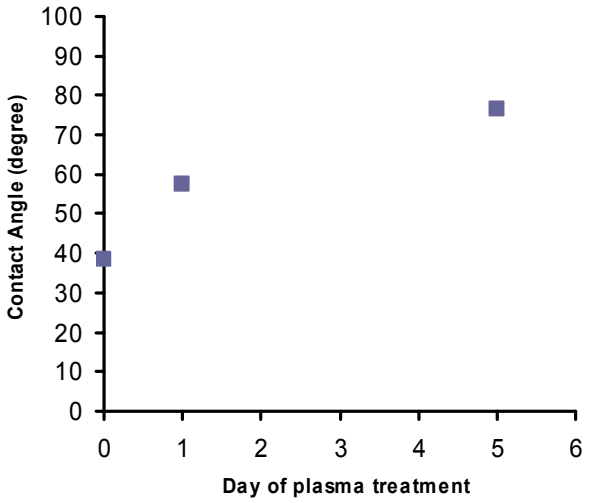

Figure 6.2: Contact angle change with time for plasma treated PDMS.

From figure 6.2, the plasma treatment changed the hydrophobic properties of the PDMS to a hydrophilic state. This is clear since the contact angle for samples prepared on the same day, the experiment on day 0, gave a contact angle around 40^o. The plasma treated PDMS regains its hydrophobic state with time as shown in figure 6.2, where the contact angle increases as time passes by.

The results of the ATR-FTIR analysis of native and plasma treated PDMS are presented in figure 6.3. In this analysis, the same sample was tested with the ATR-FTIR before and after the plasma treatment on the same day. From the transmittance spectra presented in figure 6.3, the chemical compounds of the pure PDMS were identified for both tested cases. The peaks numbered 1-4 in figure 6.3 correspond to the following chemical groups: (1) CH_3, (2) $Si-O-Si$, (3) $Si-CH_3$, and (4) CH_3. The region confined between the two dashed lines is the region that indicates the presence of the OH^- groups. From examining figure 6.3, it is observed that the plasma treatment was not successful in creating large concentrations of OH^- groups on the surface of the PDMS. This implies that the plasma treatment did not alter the surface of the PDMS, and the surface remained hydrophobic, since there were no peaks for the OH^- groups. However, simple contact angle observations of ultrapure water on the surface of the samples confirmed that the surface was in fact hydrophilic. Moreover, the contact angle analysis of similar plasma treated PDMS samples showed hydrophilic properties as shown in figure 6.2.

The plasma treatment dosage might have changed the surface chemistry of the PDMS but at low concentrations that were not detectable with ATR-FTIR. As discussed in chapter 3, the ATR-FTIR signal exceeds the surface of the sample and penetrates to the bulk

material. For the silicon crystal used in the ATR accessory (MVP-SplitPea) and for PDMS samples, the IR beam will penetrate the surface of the PDMS with 0.41 μm at the region 3500 - 3000 cm^{-1}, which is the region for the OH groups. Thus, the OH groups can be present on the surface of the PDMS but with very low concentrations.

Researchers found that in order to obtain detectable OH^- groups for plasma treated PDMS using ATR-FTIR, long exposure periods must be used [70]. However, long exposure times damage the surface of the PDMS, making it unsuitable for microchannel fabrication since it will introduce undesirable surface roughness. In the case of electroosmotic pumping, the surface roughness affects the uniformity of the applied electrical field and the shape of the EDL; hence the use of the Helmholtz-Smoluchowski equation in estimating the zeta potential of the microchannel might not be appropriate.

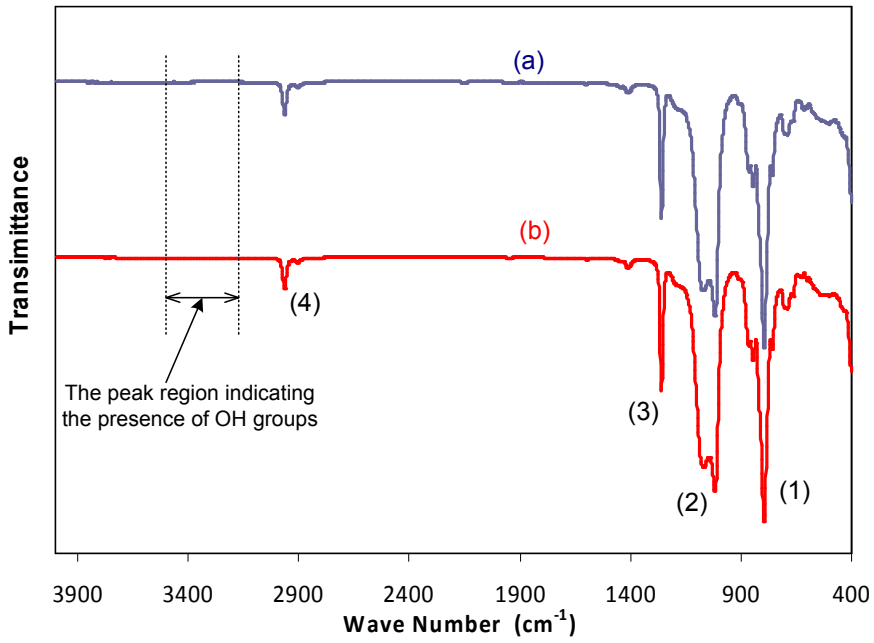

Figure 6.3: IR transmittance spectra of PDMS samples. (a) native PDMS, and (b) plasma treated PDMS.

A quantitative estimation of the concentration of chemical compounds was done using Beer's law (equation A.6), which relates the concentration of the chemical compound in the sample with the absorbed infrared beam, as discussed in Appendix A. By using the area ratio of the peaks at 1265/1030 (CH_3 and SiO_2), the analysis showed that the plasma treated PDMS specimen had an increase in the concentration of the SiO_2 with around 3 % compared to the non-plasma treated PDMS. This increase in the SiO_2 groups

indicates that the plasma treatment was capable of altering the properties of the PDMS but very small concentration.

6.3.2 Prepolymer Additive

PDMS doped with AA gave unfamiliar results. After the addition of AA, the PDMS became less transparent. Also, the PDMS became spongy where it was observed by hand and eye examinations. For both of the concentrations used, the PDMS doped with 1% of AA showed the largest change compared to the 0.5% level. The surface properties of the AA doped PDMS were found to be hydrophobic by means of contact angle observations.

The plasma treatment was performed for a duration of 40 s, similar to the protocol used for bonding channels. For PDMS doped with 1 % AA, it was hard to bond the channel to the substrate after the plasma treatment, and deformations in the channel geometry were observed. Figure 6.4 presents the Y-intersection for PDMS doped with 1% and 0.5 % AA on the basis of PDMS mixture weight. These deformations, clearly shown in figure 6.3 (a) are for the sample doped with 1% AA. Moreover, the PDMS microchannels doped with 1 % AA collapse after plasma treatment and bonding to the substrate, and therefore attempts of the current-monitoring experiments were unsuccessful. For these reasons, the PDMS treatment with 1 % AA was abandoned.

PDMS doped with 0.5 % AA was easier to bond and showed a more uniform cross section. The results of the current-monitoring experiments showed that the doping did not improve the zeta potential of microchannels. The zeta potential was found to be -47 mV for 1X TBE buffer and -41 mV for 10 mM KCl, which was close to the values of the non AA doped PDMS. This result does not contradict the findings of Luo *et al.* [78] since in their work they did not perform plasma treatment to the PDMS microchannels.

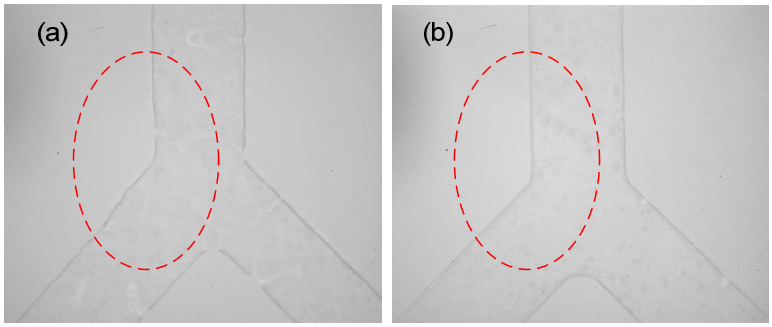

Figure 6.4: Y-intersection of PDMS microchannels predoped with AA, (a) predoped with 1% AA, and (b) predoped with 0.5% AA.

ATR-FTIR analysis was performed on AA doped PDMS with and without plasma treatment. Samples for the ATR-FTIR analysis were prepared in the same way as presented in the sample preparation. The reason for this analysis was to determine if adding the AA will improve the plasma treatment of PDMS and increase the presence of OH groups after the plasma treatment. The results are presented in the figure 6.5.

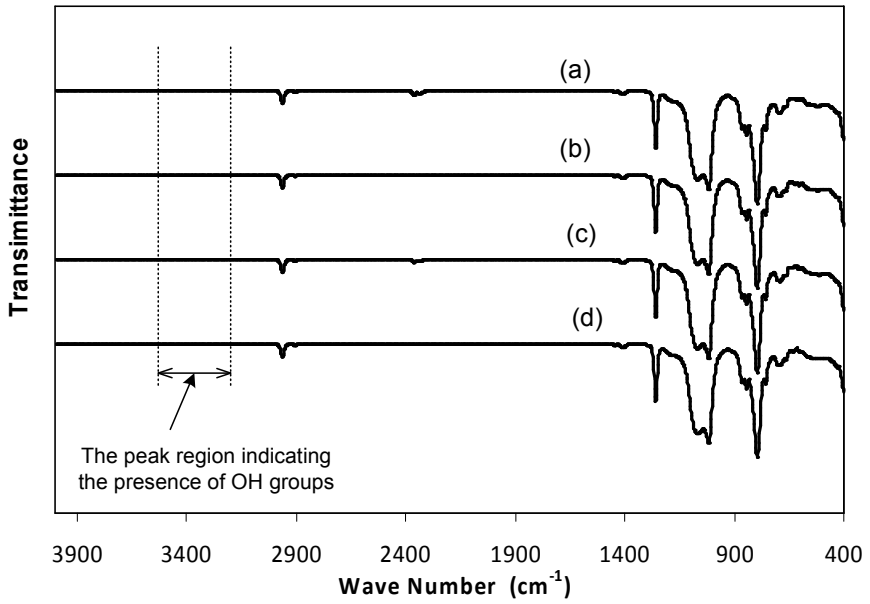

Figure 6.5: IR transmittance spectra of the different predoped PDMS samples. (a) PDMS doped with 0.5 % AA, (b) plasma treated PDMS doped with 0.5 % AA, (c) PDMS doped with 1 % AA, and (d) plasma treated PDMS doped with 1 % AA.

As shown in figure 6.5, the prepolymer additive with and without the plasma treatment did not change the surface properties or the chemical structure of the PDMS. The same peak locations of the native PDMS (figure 6.3) are present in figure 6.5 with no new peaks for other chemical groups. For the PDMS doped with 0.5 % AA (6.5 a & b) the plasma treatment did not change the overall chemical structure of PDMS nor were the presence of the OH group. Similar conclusion is reached for the PDMS doped with 1% AA (figure 6.5 c & d).

6.3.3 PDMS Extraction

Motivated by the finding of Vickers *et al.* [71] in which the electroosmotic mobility of the microchannels was improved after the extraction process, the current-monitoring

experiments were performed with the Y-channel extracted PDMS. The results showed that the average zeta potential of the extracted and plasma treated PDMS was -47 mV for 1X TBE buffer, which is close to the native (non extracted) PDMS. This finding does not contradict the work presented by Vickers *et al.* [71] since their work compared native PDMS with extracted PDMS. While they published results of plasma treated and extracted PDMS, the work did not include any results of the plasma treated PDMS.

The dry storage analysis of the plasma treated and extracted PDMS samples showed that the channels preserve their hydrophilic nature even after three days of dry storage.

The change of the contact angle with time for the plasma treated and extracted PDMS is presented in figure 6.6. The extracted PDMS gave stable hydrophilic properties with time since the contact angle was lower than 90^o, as observed in figure 6.6. This trend supports the findings of the dry storage analysis. The slight variability in the contact angle measurements with time, especially between day 1 and day 3, has several explanations. The time effects must studied on the same plasma treated PDMS sample. However, in this work the time effect was examined by making a batch of extracted PDMS samples and performing the plasma treatment on different days. Hence, the effects of the uncontrollable differences between the plasma treatments may vary slightly between samples. Unfortunately, the accessibility of the contact angle measurement system could not be guaranteed. Secondly, other sources of errors between measurements were not controlled, such as the cleanness of the PDMS surfaces, the presence of impurities, the asymmetry of the water droplet, and the temperature.

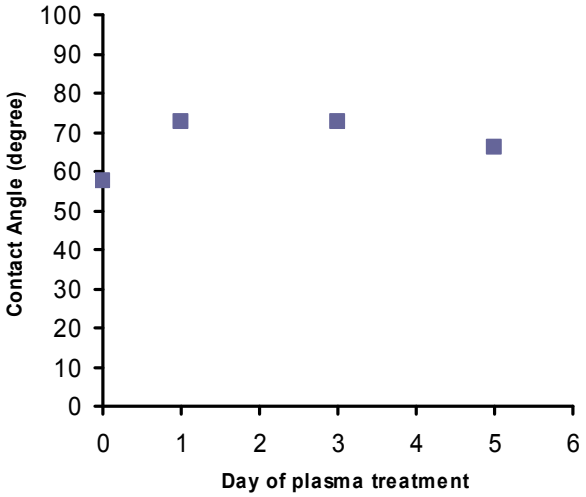

Figure 6.6: Contact angle change with time for plasma treated extracted PDMS.

Figure 6.7 presents the infrared transmittance spectrum results for extracted PDMS

with and without plasma treatment. The chemical groups that were found from the ATR-FTIR analysis were identical to the native non-extracted PDMS. Moreover, plasma treatment did not change the surface chemistry of the PDMS.

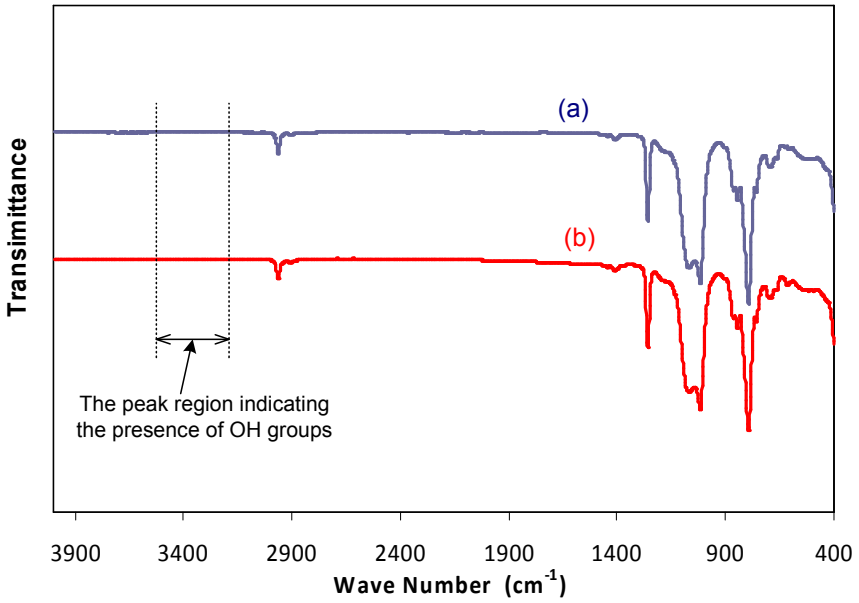

Figure 6.7: IR transmittance spectra of extracted PDMS. (a) extracted PDMS, and (b) plasma treated extracted PDMS.

6.3.4 HEMA Grafting

The current-monitoring experiments and dry storage analysis gave the first indication on how successful the HEMA grafting treatments were. A summary of the current-monitoring and dry storage results for the different HEMA treatment protocols are presented in table 6.3. A first observation of table 6.3 shows that the different HEMA grafting treatments vary in their outcomes. Results of the dry storage analysis for the different HEMA treatments were dissimilar. The three approaches that showed very good hydrophilic were the plasma induced HEMA grafting and the HEMA heat protocols 3 and 4. The HEMA heat protocol 1 showed some hydrophilic properties. However, the HEMA heat protocol 1 did not show any hydrophilic properties from the dry storage analysis. Moreover, the current-monitoring experiments were successful for all the HEMA treatments except the HEMA heat protocol 2.

Table 6.3: Results of the current-monitoring exepriments and the dry storage analysis for different HEMA grafting protocols. P/P is the PDMS/PDMS microchannel, and P/g is the PDMS/glass microchannel.

The HEMA treatment	Dry storage analysis	Zeta potential value used solution (ζmV)
Plasma induced HEMA grafting	Showed hydrophilic properties	1XTBE, P/P, (-35) 1XTBE, P/g, (-46)
HEMA heat protocol 1	Showed some hydrophilic properties	1XTBE (-35)
HEMA heat protocol 2	No flow, and didn't show hydrophilic properties	-
HEMA heat protocol 3	Showed good hydrophilic properties	1XTBE (-55)
HEMA heat protocol 4	Showed good hydrophilic properties	1XTBE, P/P, (-30) 1XTBE, P/g, (-50) 10mM KCl,P/P, (-48) 10 mM KCl, P/g, (-49)

For the HEMA heat protocol 1, it was hard to fill the channels and additional pressure was needed. This indicates that for this approach, the hydrophobic properties of PDMS were regained. This also indicates that this protocol failed in grafting HEMA on the PDMS surface. The current-monitoring experiments showed that the zeta potential was lower than the plasma treated PDMS.

Samples treated according to the HEMA heat protocol 2 showed poor hydrophilic properties by dry storage analysis. Moreover, current-monitoring experiments for chips treated with this approach failed. This was because the treatment was not uniform. As observed using the microscope, some locations in the treated microchannels allowed the flow of water while other locations repelled water. This indicated that this approach of heat induced HEMA grafting after the bonding of the microchannel was unsuccessful and it was giving heterogeneous wall surface properties.

As presented in table 6.3, plasma induced HEMA grafting, the HEMA heat protocol 3 and HEMA heat protocol 4 were successful in performing HEMA grafting since they showed good results in the dry storage analysis. However the current-monitoring exper-

iments that were performed on these protocols did not show an improvement in the zeta potential. These approaches were chosen for further analysis to understand the reason for their success in the dry storage analysis.

Figure 6.8 presents the contact angle change with time for the HEMA heat protocols 3 and 4.

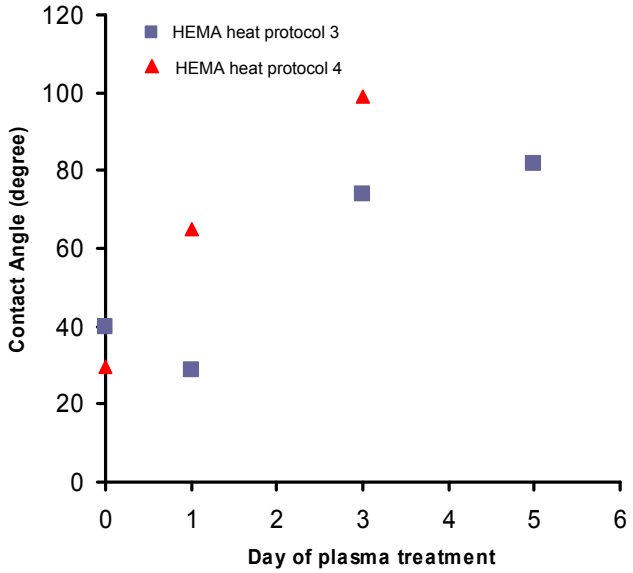

Figure 6.8: Contact angle change with time for HEMA treated heat protocols. (a) HEMA heat protocol 3, and (b) HEMA heat protocol 4.

From figure 6.8 it is shown that the PDMS treated with HEMA heat protocols 3 and 4 showed hydrophilic properties with time. This confirms the finding from the dry storage analysis (table 6.3). The HEMA heat protocol 4 showed a change to a hydrophobic state at the third day after dry storing conditions. This conclusion was reached since the contact angle was around 90^o. Compared to the HEMA heat protocol 4, the HEMA heat protocol 3 is more stable in the hydrophilic properties (figure 6.8 (a)) and the process involved in performing this treatment is better, since no extraction of PDMS is needed. The plasma induced HEMA grafting protocols showed hydrophilic properties for up to 5 days of dry storing. This was confirmed by means of qualitative contact angle observations of ultra pure water.

The discussed findings show that the surface of PDMS treated with the above protocols maintained their hydrophilic properties with time periods up to 5 days. This is beneficial for microchips since maintaining the hydrophilic properties is important for long term chip storage and transportations applications. On the other hand the zeta potential

values for the PDMS treated with the above protocols did not show any improvement compared to PDMS treated with plasma alone (table 6.3).

As a result, the plasma induced HEMA grafting and the HEMA heat protocol 3 were chosen for ATR-FTIR analysis. For each measurement by ATR-FTIR at least two samples were prepared and three locations in each sample were tested. Figure 6.9 presents the transmittance spectra from the ATR-FTIR analyses. From figure 6.9, for plasma induced HEMA grafting (6.9 (a)), the HEMA grafting was evident since the OH^- groups are present between 3200 - 3400 cm^{-1}. Most of the measurements performed on samples treated with the plasma induced HEMA grafting showed this trend of spectra. This indicates that the plasma induced grafting of HEMA creates permanent OH groups on the surface of the PDMS.

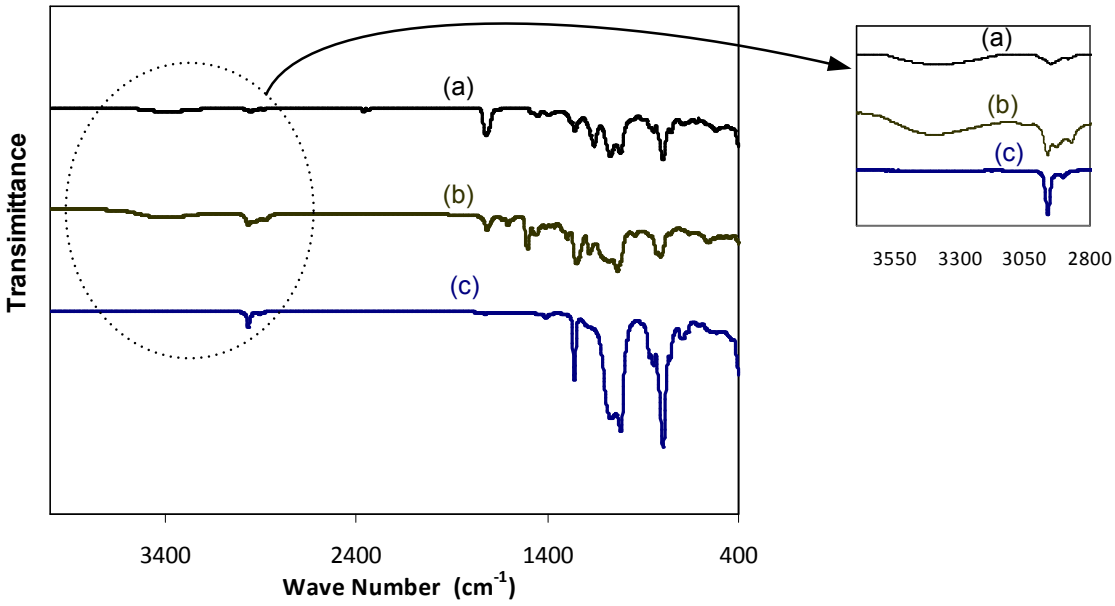

Figure 6.9: IR transmittance spectra of PDMS using different HEMA grafting protocols. The enlarged figure is to magnify the region 2800 - 3200 cm^{-1}. (a) plasma induced HEMA grafting, (b) HEMA heat protocol 3 at point 1, and (c) HEMA heat protocol 3 at point 2.

On the other hand, the plasma induced HEMA grafting had some drawbacks. The zeta potential of the plasma induced protocol did not improve when compared to the regular plasma treated PDMS (table 6.3). Furthermore, this method is not suitable for treating PDMS based microchannels for several reasons. First, the procedure of spin coating the HEMA onto the surface of the PDMS is not applicable to the manufacture of microchannels. The main reason is that the uniformity of the spun coated HEMA

film was not confirmed. Thus other HEMA coating methods must be used. Several approaches for coating the HEMA were attempted, such as manually depositing a thin layer of HEMA on the PDMS or dipping the PDMS in a small jar of HEMA, but with no success. Secondly, the long plasma exposure times needed to perform the HEMA grafting are not applicable since they will create undesired surface roughness on the PDMS.

The ATR-FTIR data of samples treated using the HEMA heat protocol 3 gave sissimilar results at different locations. One location in the sample showed polymerization of the HEMA on the surface. This was identified by the presence of the peak for the OH groups at 3200 - 3400 cm^{-1} . The OH peak is enlarged figure 6.9(b). However, most of the tested locations did not show the presence of the OH groups, with the samples giving a similar transmittance spectrum as the native PDMS (figure 6.3). This is shown in figure 6.9 (c). Note that both the 6.9 (a) and 6.9 (b) infrared spectrum were tested on two different locations for the same sample. Moreover, most of the HEMA heat protocol 3 samples tested with ATR-FTIR did not show the presence of OH groups, which indicates that there the grafting of HEMA was unsuccessful.

If the ATR-FTIR analysis was considered as the only criterion to verify HEMA grafting, the HEMA heat protocol 3 was not successful. However, the contact angle results and dry storage analysis for this treatment showed stability of the hydrophilic properties.

These results of the HEMA heat protocol 3 can be explained by two main discussions. The first is that the HEMA has been chemically polymerized on the surface of the PDMS but at very low concentrations. The concentration of the polymerized was not detectable by ATR-FTIR in most of the locations on the PDMS surface. The ATR-FTIR measurements showing the presence of OH groups support this explanation. The other explanation is that the HEMA did not chemically graft on the surface, but it was adsorbed into the surface of the PDMS. The layer of the adsorbed HEMA created a barrier that prevented diffusion of the LMW PDMS to the surface of plasma treated PDMS. This adsorbed layer will help preserve the hydrophilic groups on the surface of the PDMS. The results of the contact angle and dry storage analysis support this explanation.

6.4 Conclusions

In this chapter several PDMS treatments protocols for improving the surface properties of the PDMS have been examined and evaluated using different experimental techniques.

The results of predoping the PDMS with acrylic acid did not show an improvement in zeta potential values or in the hydrophobic nature of the PDMS. Also, it was found

that predoping the PDMS with 1% of AA/PDMS caused defects in the cross section of microchannel after bonding into the substrate. Thus, this ratio is not recommended for pretreatment.

Extraction of PDMS gave favorable results in terms of stable hydrophilic properties by dry storage analysis and contact angle analysis. However, no improvement in the zeta potential of the plasma treated extracted PDMS was achieved compared to regular plasma treated PDMS.

Several HEMA grafting protocols were examined in this chapter, and the two that showed changes in the properties of the PDMS were the plasma induced HEMA grafting and HEMA heat protocol 3. The stability of the hydrophilic properties for PDMS samples improved with both of these approaches. This was confirmed with the dry storage analysis and the contact angle measurements. However, the zeta potential did not improve with any attempted approach.

It was also observed that the ATR-FTIR analysis of the HEMA heat grafting protocol 3 gave inconsistent results for the same sample. The OH groups were observed to be present in some locations, while not in others. Although these findings are encouraging it is recommended that further investigation should be carried out on the HEMA heat protocol 3 with other surface characterization techniques, such as X-ray photoelectron spectroscopy (XPS) to further understand the effects and allow the development of an improved methodology.

Chapter 7

Final Conclusions and Recommendations

7.1 Conclusions

This work was mainly concerned with studying the surface properties of polymeric microchannel materials. The experimentally based studies focused on the electroosmotic flow characterization and enhancement in PDMS microchannels. The PDMS microchannels were fabricated using a soft lithography technique which is commonly employed in the microfluidic community. Two new contributions presented were: the introduction of a modified Y-channel design to study the electrostatic properties of microchannels using the current-monitoring technique, and the introduction of a modified current-slope approach to analyze the outcome of the current-monitoring experiments. The new channel design was used to perform and examine on different parametric studies of electroosmotic flow in PDMS based microchannels. Also, with the aim of improving the surface properties of PDMS microchannels, different chemical based surface treatments were carried out and thoroughly examined.

Performing the current-monitoring experiments with the Y-channel design was found to be advantageous compared to using the conventional straight channel design. The current trend and the number of measurements that could be performed with the Y-channel design made it the superior option for studying the electrostatic properties of microchannels when compared to the straight channel design. Moreover, the simplicity in performing the experiments and the capability of performing long term studies are additional advantages offered by the new design.

The current-slope analysis approach was presented and validated to analyze the out-

come of the current-monitoring technique. This approach showed good agreement with the total length method, and better results than the slope approach presented previously [48] since it eliminated the different error sources, such as solution conductivity changes and uncertainty in the conductivity measurements. The problems were thoroughly discussed in chapter 5. In situations where it is hard to locate the start and end of the replacement from the current-monitoring outcome, the current-slope method is advised. Both the new channel design and the current-slope approach were enhancements to the current-monitoring technique for examining the electrostatic properties of microchannels.

The zeta potential of different biological buffers used for DNA, RNA and biomedical applications were estimated for plasma treated PDMS based microchannels. The current-monitoring experiments were performed for each test buffer with different microchannel dimensions and designs. The reported zeta potential value was then calculated as the average of at least 35 measurements. An unexpected finding from the current-monitoring experiments was that the chip substrate material did not have an effect on the average zeta potential for plasma treated PDMS microchannels. This finding was confirmed by testing the three channel formats of: PDMS/PDMS, PDMS/glass, and PDMS/SU8. This result should be treated with caution since other plasma treatment protocols may differ, and therefore their outcome might be different.

Some side effects of long term electroosmotic pumping were observed on solutions when using electrolytes and buffers with high electrical conductivity as a pumped medium. Effects such as solution depletion, bubble formation, conductivity changes and pH changes were observed with long periods of electroosmotic pumping. Electrolysis could not be eliminated as it is a phenomenon associated with electrostatic pumping but its effects could be reduced with several precautions. Using large volumes of solutions, and reducing the applied voltage and current draw are important design aspects that need to be taken into consideration. The most important factor that helps to reduce the effects of electrolysis is the proper choice of the pumped solution. In situations where the application requires long periods of electroosmotic pumping, such as cell culture chips [19], it is highly recommended to use buffers that have high resistance to electrolysis. Of the solutions tested in this work, 1XTBE buffer demonstrated the highest electrolysis resistance.

The surface conductance phenomenon of microchannels during electroosmotic pumping was studied using the current-monitoring technique and with the aid of a high precision Pico-ammeter. The surface conductance was not affected by the change of the applied electrical field. The solution concentration affected this phenomenon with a higher concentration resulting in a higher surface conductance. It was also observed that

the surface conductance was affected by changing the channel substrate material. For the same solution, the PDMS/glass showed a higher overall surface conductance than the PDMS/PDMS microchannels. This finding was clearly demonstrated in the surface conductance results using the 10 KCl and 1XTBE buffers. While the zeta potential was not affected with the change of substrate material, this change in surface conductance implied that the flow of ions in the EDL of the glass portion is different to the plasma treated PDMS portion. This finding implies that the EDL shape and the ion distribution of the glass portion differ from the plasma treated PDMS sides. There is no clear explanation for this finding and further investigation is advised using other techniques such as the streaming potential.

One explanation for this end result was the affect of surface roughness. The model used to estimate the surface conductance neglects the effects of surface roughness on the flow of ions within the EDL. However, the contribution of the effects of surface roughness on the surface conductance cannot be ignored. Numerous difficulties have arisen in measuring surface roughness since the nature of the surface roughness is irregular for different samples and no confirmation of the nature of the microscale surface roughness could be found. Moreover, to numerically study the effect of surface roughness on the flow of ions in the EDL, higher order numerical techniques such as molecular dynamics, must be used. This type of modeling and analysis was outside the scope of the work.

Another major goal of the work was to enhance the surface properties of PDMS based microchannels with chemical treatment, a strategy that was thoroughly discussed in chapter 6. As a final conclusion the zeta potential of the treated PDMS microchannels did not improve with any of the attempted surface treatments when compared to the zeta potential of plasma treated PDMS microchannels. On the other hand, the stability of the hydrophilic properties of the microchannels showed an improvement using the extraction and some HEMA grafting protocols. The PDMS extraction process is recommended for chip manufacturing in order to stabilize the hydrophilic properties of PDMS microchannels.

7.2 Recommendations and Future Work

There are two main areas for improvements on the work presented: improving the hardware setup, and performing new studies on both the current-monitoring technique and the surface treatment analysis.

An improvement to the current-monitoring setup could be achieved by automating the experiments. This could be done by using a controllable circuit to perform the switching of the electric fields between the reservoirs.

There are a number of different areas of study that are open as a result of this study. The effects of different plasma treatment protocols, such as oxygen plasma treatment, on the zeta potential of the PDMS microchannels should be examined. At the time of writing this thesis, oxygen plasma accessories were arranged to be integrated to the present plasma treatment system. Moreover, the effect of the chip substrate material on the average zeta potential of PDMS based microchannels with oxygen plasma treatment should be examined to observe if it the same trend as the air plasma treatment will be observed.

It is highly recommended that quantitative studies on the electroosmotic flow in the Y-channel design be performed. This could be achieved using the μ-PIV system. Unfortunately the μ-PIV system was in the process of being installed during the period of writing this chapter. An important location that should be focused upon and quantitatively studied is the Y-intersection during the switching of the electric fields between the reservoirs and the effect of the intersection corner radius on the flow field. The experimental quantitative studies should also be supported with numerical modeling in 2D and 3D using commercial software, such as COMSOL multiphysics.

Although different surface treatments were attempted to improve the different surface electrostatic properties of PDMS based microchannels the results were inconclusive, especially with regards to the HEMA grafting protocols. It is recommended to confirm the speculated findings of the HEMA treatment by examination in conjunction with other surface characterization techniques such as X-ray photoelectron spectroscopy (XPS).

The attempts made to improve the zeta potential of the PDMS based microchannels with chemicals were not realized. The zeta potential threshold was the same value of plasma treated PDMS microchannels. The zeta potentials for the chemical treatments did not overcome the zeta potential of air plasma treated PDMS.

Final recommendations for the surface treatments are to improve the HEMA grafting by performing pre treatment of the PDMS with an initiator before introducing the

HEMA. This will improve the grafting and therefore may improve the zeta potential. One initiator that could be used is the AIBN initiator (Azobisisobutyronitrile).

Appendix A

Surface Characterization

A.1 Contact Angle Analysis

The contact angle is a simple method used to find the surface energy of solid materials by measuring the angle of a pure symmetric droplet of a solution on a horizontal sample. Direct measurement of the angle between the liquid gas interface indicates if the surface is hydrophilic or not. The contact angle is related to the surface energy attained between the surface and the solution particles. This is also related to the surface energy from Young's model [1, 3, 85]. Another name for the method is the sessile static drop. In order to get accurate results from the contact angle measurements two important conditions apply, which are: the solution must not react with tested material, and secondly the pure solution droplet must be symmetric. Figure A.1 presents a schematic of the principle of contact angle.

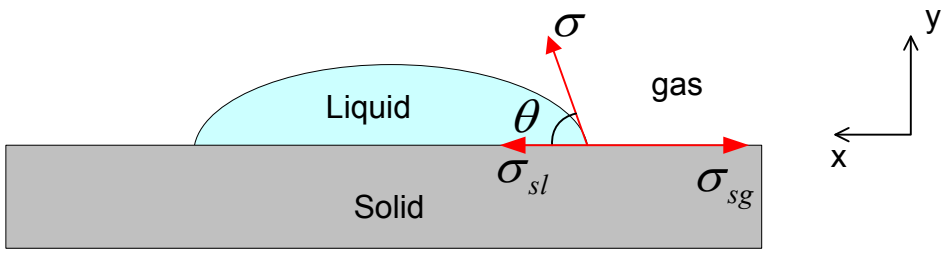

Figure A.1: Basic concept of the contact angle measurement [85].

For static conditions and by performing a force balance in the x-direction, presented

in figure A.1, the relation between the energy of the solid liquid interface is [1, 85]:

$$\sigma \cdot cos\,(\theta) = \sigma_{sg} - \sigma_{sl} \tag{A.1}$$

where σ is the liquid-vapor interfacial energy between the gases liquid, σ_{sg} is the solid-gas interfacial energy, σ_{sl} the solid-liquid interfacial energy, and θ is the angle between the gas liquid interface. In the literature the contact angle has been used to find the nature of plasma and non plasma treated PDMS surfaces. Moreover, the rate of regaining the hydrophobic properties of plasma treated PDMS was examined with the contact angle [70, 73, 75]. Eddington *et al.* [75] studied the effects of thermal aging on stabilizing the hydrophilic properties of plasma treated PDMS and the results show that the aging improved the stability of PDMS. The effect of storing conditions was investigated by Chen *et al.* [70] with the contact angle analysis and it was shown that wet conditions are better for preserving the hydrophilic state of plasma treated PDMS.

A.2 ATR-FTIR Analysis

The basic principle of the Fast Fourier Transform Infrared Spectroscopy (FTIR) is to study the vibration of atoms between molecules under the influence of an electromagnetic wave. Due to the nature of the chemical bonds formed between molecules, atoms vibrate with a certain frequency [83, 84]. A simple model for the vibration could be presented as the vibration of the spring-mass model. The natural frequency of the spring connecting to vibrating masses is calculated from [84]:

$$\omega = \frac{1}{\pi}\sqrt{\frac{k}{2m}} \tag{A.2}$$

where ω is the natural frequency (Hz), k is the spring constant (Nm^{-1}), and m is the mass (kg). If a force is exerted on the spring mass system it will cause it to vibrate. This is a simplification of what happens in the molecular regime where different atoms are attracted together with electromagnetic forces. By applying an electromagnetic wave to the specimen the molecules will vibrate in frequency ranges that correspond to the strength and type of bond between the atoms. The location of the vibration frequencies are fingerprints of different molecules.

The vibrational frequencies of molecules are very high (around $10^{13}s^{-1}$). Another unit that is commonly used to assess the location of the vibration is the frequency divided by the speed of light. This unit is known as the wave number and has a unit of (cm^{-1}).

$$W = \frac{\omega}{C_{light}} \tag{A.3}$$

where W is the wave number (cm^{-1}), and C_{light} is the speed of light $(3 \times 10^8 m/s)$. The FTIR (Fast Fourier Transform Infrared Spectroscopy) analysis is performed by exposing the sample to a mid-spectrum of Infrared beam (IR) and recording the response of the sample in a frequency spectrum. The response of the sample to the IR is measured in either the transmittance or absorbance of the infrared beam in the ordinate and the wave number in the abscissa. This is known as the IR spectrum. Thus, by performing peak assessment the presence of different chemical compounds are distinguished. The IR transmittance and the absorbance are related with the following equation [83]:

$$A_{ab} = -\log\left(T_{tran}\right) \tag{A.4}$$

where A_{ab} is the absorbed infrared beam, and T_{tran} is the transmitted infrared beam from the sample [83].

The FTIR analysis is also a quantitative method for finding the concentration of different molecules in samples. This is achieved with Beer's law which relates the concentration of a certain compound with the absorbance of the IR beam [83]. Equation A.5 presents Beer's law:

$$A_{ab} = l \cdot C \cdot \alpha \tag{A.5}$$

where l is the path length of the IR beam, C is the concentration of the chemical compound, and α is the concentration coefficient. Another quantitative analysis approach is to perform a ratio analysis of different samples at the same frequency location. This indicates the change in the concentration of chemical compounds between different samples. This approach will eliminate experimental errors between the measurements, such as the change of the background noise [83]. Also in the absence of certain values such as the concentration coefficient of the sample the ratio approach is advantageous. Equation A.6 presents the basis of the peak ratio analysis:

$$\frac{A_{ab1}}{A_{ab2}} = \frac{C_1}{C_2} \tag{A.6}$$

where A_{ab1} is the absorbance at peak 1, A_{ab1} is the absorbance at the second peak, C_1 is the concentration of the first compound, and C_2 is the concentration of the second compound. Thus the FTIR analysis is a powerful technique for finding the change of different chemical compounds.

One major limitation for using FTIR analysis is that the thickness of the samples must be in very small (μm) ranges in order that the IR beam passes through the sample [84, 85]. To overcome this limitation another approach has been developed which was to study the reflectance of the infrared beam with the aid of a non-IR absorbing crystal [83, 84].

When an IR beam is guided through a non IR-absorbing crystal with a high refractive index and comes into contact with a sample the beam will be reflected from the sample. Due to the difference of the refractive indices between the sample and the crystal the IR-beam under goes an internal reflectance known as attenuated total reflectance. By recording the reflected IR beam an IR-spectrum is found. This is called as the attenuated total reflectance (ATR-FTIR). The major advantage of this method is that it is not affected with the specimen thickness and any thickness could be used in the analysis [83]. Figure A.2 presents a schematic of the principle of the ATR-FTIR.

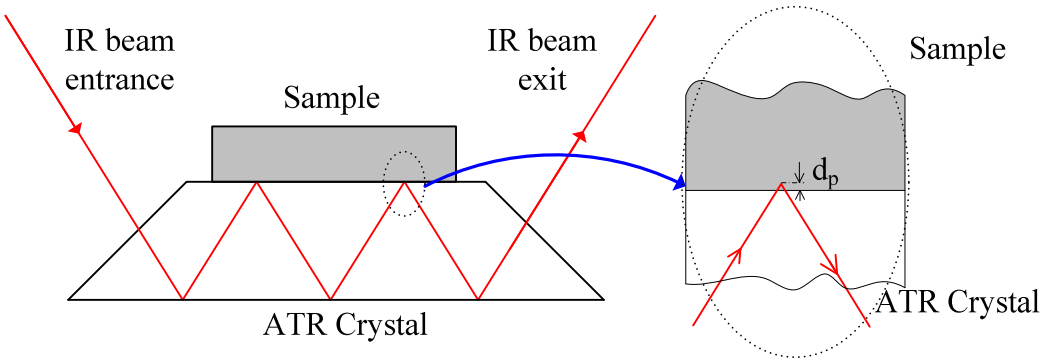

Figure A.2: Basic concept of the ATR-FTIR crystal.

An important property of the ATR analysis is that the reflected beam has a depth of penetration inside the sample [83]. The depth of penetration of the IR beam depends on several factors such as the angle of incidence of IR beam, the refractive indices of the sample and the crystal, and the wave number. In the present work, the ATR-FTIR analysis was chosen to characterize the different surface treatments performed on PDMS samples, especially the treatments that involved the chemical grafting of the HEMA monomer, since the PDMS samples are thick (2 mm).

Appendix B

Experimental Setup (Extra Information)

In this section extra information about chip manufacturing process and the current-monitoring experimental setup is presented.

B.1 Precautions for te PDMS Surface Treatment Chemicals

The chemicals used for the PDMS surface treatment (Section 3.1.2) need special handling and precautions when used. Information in the MSDS must be taken with great care. The HEMA solution has an inhibitor for stabilization purposes. The inhibitor was removed with a column technique to improve the HEMA polymerization.

Note: some treatments require a drying process in the oven. It was observed that the oven will be contaminated afterwards. It is highly recommended that after drying processes that the oven must be cleaned with acetone. Then it should be dried at 140^oC *for 2hrs while closing the chamber door and leaving the ventilating valve open in order to remove all the chemical fumes from the oven.*

B.2 Chip and Sample Manufacturing

A simple description of the procedure for manufacturing the channels masters is presented next, and for a complete view on the protocols used in the microfluidics lab please refer to the master thesis's presented by Sami [97] and Glawdel [19].

Silicon wafers were used as masters for the SU8 channel profiles. The main steps for profiling the wafers with the designs were as follows: first the wafer (Montco Silicon, Spring-City) undergoes a dehydration process at 200 ^oC for 20 minutes over a hotplate. After that the wafer was cooled for 10 minutes. Then an SU8 adhesion layer was spun coated on the wafer with a thickness of 5 μm with SU8-2005. This layer helps the permanent adhesion of the profiles on the wafer. The wafer with the adhesion layer undergoes a soft bake; UV exposure and post bake as recommended by the SU8 manufacturer [86]. Another SU-8 layer with the desired channel thickness was spun coated on the wafer and then soft baked. The choice of the SU-8 grade depends on the desired channel height [19, 86, 97]. A high accuracy transparency mask (CAD/Art Services, Bandon) containing the channel profiles were positioned over the wafer in the vacuum mask aligner (Newport, Stratford). The wafer was UV-exposed with the appropriate dosage [86]. The exposed wafer was post baked and then developed in SU-8 developer, and dried with nitrogen gas. The height and width of the channel profiles were measured with a contact profilometer (Mitutoyo SJ-400). Figure B.1 presents a typical silicon wafer with hardened channel profiles.

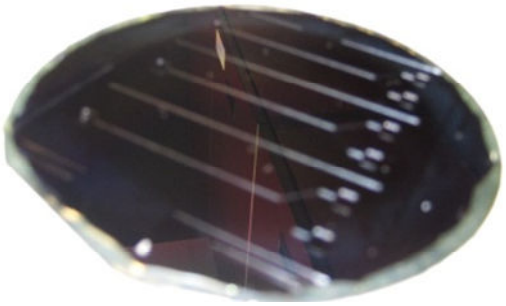

Figure B.1: Silicon wafer with the hardened SU8 profiles.

PDMS microchannels were fabricated by replica molding of the profiled silicon wafer. The PDMS mixture was prepared by mixing Sylgard 184 silicone elastomer base and Sylgard 184 (Dow Corning, San Diego, CA) silicone elastomer curing agent in a 10:1 ratio. The mixture was degassed for 20 minutes in a vacuum oven, poured over the master and baked at 80o C for 2 hr. The cured PDMS was then removed from the master and reservoir holes were punched for fluidic access ports. The PDMS Y-channel molds were then air plasma treated for 40s and a power of 29.6 W (Harrick Plasma, Ithaca, NY) and bonded either to a PDMS coated microscope slide or to a microscope glass slide. The glass slides coated with PDMS were fabricated by spin coating 1mL of PDMS (10:1) at 3000 rpm for 30s on the surface of the glass slide to achieve a thickness of 30 μm PDMS layer. Ultra pure water was introduced in the channels after the process

bonding and glass reservoirs (1.5mL); were attached using liquid PDMS to make a leak-proof attachment. Figure 3.2 shows a photograph of the plasma treatment system and a typical PDMS chip.

The PDMS samples that were tested with the ATR-FTIR and the contact angle were prepared with the same approach discussed above, but were poured and cured over a non-profiled silicon wafer. The details of the treatments will be presented in chapter 6.

B.3 Current-Monitoring System

A schematic of the connections between the components of the current-monitoring system is presented in figure 3.3. The basic concept of the current-monitoring technique is to record the electrical current while performing electroosmotic pumping in microchannels. Thus, an electrical voltage supply and a current measurement system are needed. The process of integrating the different system devices was time consuming and went through several integrations. The main components of the final current-monitoring system used in this work and the operation of each element are listed as follows:

- DC power supply.
- Current measurement system.
- Electrical switch.
- Chip holder.
- Data recording and monitoring system.
- AC - Fan.

Information about the DC power supply and the Data acquisition system is presented next.

B.3.1 DC Power Supply

A Spellman SL10*10 (Spellman, Hauppauge, NY) power supply was used as a voltage source. This model is capable of outputting 10 kV with a maximum current of 1 mA. The system could be manually controlled as voltage based or current based control with the knobs located in the front panel. The output of the system is monitored from the LCD

panels located in the front panel. Moreover the signal was exported via the terminal block located in the back of the system to a data acquisition card. The exported signals range from 0-10 V which is linearly related with the voltage and current of outputted from the Spellman.

B.3.2 Data Acquisition System

The monitored voltage and current, from both the Spellman and the Keithley, were exported through a connector block CB-37F-LP (National Instruments, Austin, TX) to a data acquisition board NI- PCI-6221 DAQ (National Instruments, Austin, TX) which allowed monitoring of the signals in LabView. The acquisition board can monitor a maximum voltage difference of 10 V between its terminals which is in the range for the exported signals from the devises. The terminals were connected in a differential mode to improve the accuracy of the measurement. Figure B.2 presents photographs of the hardware devices used in present current-monitoring system.

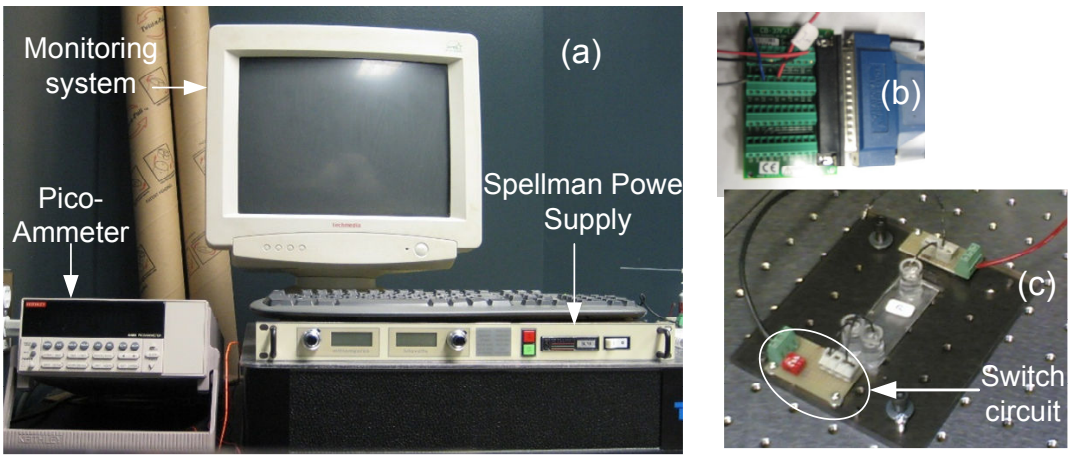

Figure B.2: Photograph of the current-monitoring experimental setup. (A) The DC power supply and monitoring system, (b) the data acquisition connector block, and (c) the chip holder with the electrical switch.

Appendix C

Uncertainty Analysis

Uncertainty analysis of experimental measurements is important since it shows how accurate the measurement was. The choice of the hardware setup and the approach of performing the experiments have an effect on the confidence in the results of the measured parameter. Mainly, there are two main sources of errors in experimental work, which are [93]:

Bias uncertainty: These types of errors come from the limitations and sensitivity of the measurement devices. Bias errors can be calibration errors, certain consistently recurring human errors, errors caused by defective equipment, loading errors, and limitations of system or resolution. These types of errors cannot be eliminated, but assigned a value of the measurement. Most device manufacturers assign a value for the bias uncertainty which could be a constant percentage of the measurement or a certain value with the same unit as the measured variable.

Random uncertainty: The random uncertainty is also known as precision uncertainty. This type of error comes from the procedure of uncontrolled randomness effects on the experimental setup. It can be reduced by taking a large number of samples and averaging them over the results, since these types of errors can be approximated by a normal distribution (Gaussian curve). These types of errors can come from certain human errors, errors caused by external disturbance to the equipment, errors caused by fluctuating experimental conditions, and errors driven from the measuring system-sensitivity.

For a limited number of samples the precision uncertainty is approximated by [93]:

$$P_x \approx t_{\alpha/2,\gamma} \frac{S_x}{\sqrt{n}} \tag{C.1}$$

where P_x is the random uncertainty of the measurement, S_x is the standard deviation of the sample, t is the assigned t-distribution value the corresponds to the confidence level and number of samples, n is the number of samples, α is related to the chosen confidence level ($\alpha = \frac{1-c}{2}$), and $\gamma = n - 1$.

For a dependent variable y, which depends on several independent measured variables $(x_1, x_2, ..., x_n)$, the uncertainty will propagate by [93]:

$$U_y = \sqrt{\left(\frac{\partial y}{\partial x_1} \cdot U_1\right)^2 + \left(\frac{\partial y}{\partial x_2} \cdot U_2\right)^2 + ... + \left(\frac{\partial y}{\partial x_n} \cdot U_n\right)^2} \tag{C.2}$$

where U_y is the uncertainty of the dependent variable y, U_1 is the uncertainty of the independent variable x_1, U_2 is the uncertainty of the independent variable x_2, and U_n is the uncertainty of the independent variable x_n.

The equation presented in C.2 is for finding the propagation of the uncertainty for a certain measurement. It is important to point out that each type of uncertainty is found separately, where the random uncertainties for all the independent variables are summed together in one calculation of equation C.2, and similar approach apply to the bias uncertainty. Afterwards, the total uncertainty of the measurement is found by combining both bias and random uncertainty with:

$$U_y = \sqrt{(B_y)^2 + (P_y)^2} \tag{C.3}$$

where U_y is the total uncertainty of variable y, B_y is the bias uncertainty of y, and P_y is the random (precision) uncertainty for variable y.

The next table presents the independent parameters that contribute to the uncertainty of the experimental measurements that were performed and presented in this thesis:

The bias parameters were taken from the literature provided by the device manufacturers, except for the time where it was given a bias uncertainty of 1 sec. This bias uncertainty for the time was given since the accuracy in locating the start and end of replacement in the current-time plots (is see figure 5.1 may differ between experimental sets and human error in locating the locations. Therefore, this value was chosen as an upper limit of the uncertainty and in most cases the error is lower than this value.

A simple estimation of the uncertainty of a dependent variable calculated in this work will be presented next, where the uncertainty of the velocity is found from various independent parameters. The velocity of the slope approach was found by:

$$u_{slope} = \frac{slope \cdot L_{channel}}{E \cdot \triangle\lambda_b \cdot A_c} \tag{C.4}$$

Thus the uncertainty for the velocity of the slope method will be:

$$U_{u_{slope}} = \sqrt{\left(\frac{\partial u_{slope}}{\partial L} \cdot U_L\right)^2 + \left(\frac{\partial u_{slope}}{\partial E} \cdot U_E\right)^2 + \left(\frac{\partial u_{slope}}{\partial A_c} \cdot U_{A_c}\right)^2 + \left(\frac{\partial u_{slope}}{\partial \triangle\lambda_b} \cdot U_{\triangle\lambda_b}\right)^2} \tag{C.5}$$

In equation C.5 the term that has the largest affect on the uncertainty is the conductivity difference $\triangle\lambda_b$ ($\triangle\lambda_b = \lambda_{b2} - \lambda_{b1}$), since it has a subtraction operation. This uncertainty is calculated by:

$$U_{\triangle\lambda_b} = \sqrt{\left(\frac{\partial \triangle\lambda_b}{\partial \lambda_{b1}} \cdot U_{\lambda_{b1}}\right)^2 + \left(\frac{\partial \triangle\lambda_b}{\partial \lambda_{b2}} \cdot U_{\lambda_{b2}}\right)^2} \tag{C.6}$$

By taking a typical conductivity difference values for a certain current-monitoring experiment with 1XTBE buffer the high and low concentrations were: 980 $\mu S/cm$ and 905 $\mu S/cm$. The uncertainty in finding the conductivity difference will be:

$$U_{\partial\triangle\lambda_b} = \sqrt{\left(\frac{\partial\left(\lambda_{b2} - \lambda_{b1}\right)}{\lambda_{b1}} \cdot U_{\lambda_{b1}}\right)^2 + \left(\frac{\partial\left(\lambda_{b2} - \lambda_{b1}\right)}{\partial \lambda_{b2}} \cdot U_{\lambda_{b2}}\right)^2} \tag{C.7}$$

$$U_{\triangle\lambda_b} = \sqrt{\left((-1) \cdot U_{\lambda_{b1}}\right)^2 + \left((+1) \cdot U_{\lambda_{b2}}\right)^2} \tag{C.8}$$

For a conductivity electrode with 1 % accuracy the uncertainties of the conductivity measurements were:

$$U_{\lambda_{b1}} = 1\%\lambda_{b1}$$

Table C.1: Uncertainty parameters of the experimental setup. (1) STDV is the standard deviation of the recoded signal for a window of interest of the measurement.

Parameter	Unit	Bias Uncertainty	Random Uncertainty
Channel length	(m)	0.1 %	-
Channel width	(m)	0.1 %	-
Channel height	(m)	0.3 %	-
Solution conductivity	$(\mu S/cm)$	0.5 %	-
Current measurement	(A)	0.1 %	STDV(1)
Voltage measurement	(Volt)	5 Volt	STDV(1)
Time	(s)	1 sec	-

and

$$U_{\lambda_{b2}} = 1\%\lambda_{b2}$$

making them for the presented values

$$U_{\lambda_{b1}} = 1\% \cdot (980) = 9.8\mu S/cm$$

and

$$U_{\lambda_{b2}} = 1\% \cdot (905) = 9.05\mu S/cm$$

This makes the total uncertainty of the conductivity difference to be:

$$U_{\triangle\lambda_b} = \sqrt{(9.8)^2 + (9.05)^2} = 13.34\mu S/cm$$

The uncertainty percentage of the conductivity differences to the actual conductivity difference is equal to:

$$\%U_{\triangle\lambda_b} = \frac{13.34}{980 - 905} = 17.78\%$$

This uncertainty value is very high from a certain variable. If the electrode is less accurate than 1 %, the uncertainty will be very high and it will severely affect the confidence in the measurement. Unfortunately this range of accuracy is a typical value for conductivity measurement devices.

For the conductivity measurements used in this work, a three point calibration procedure was performed to the conductivity electrode, which will reduce the uncertainty to a range of 0.5 - 1 % of the actual conductivity measurement.

On the other hand, the current-slope method, which was proposed in chapter 5, was also used to find the velocity with the next equation:

$$u_{current,slope} = \frac{slope \cdot L_{channel}}{\triangle I} \tag{C.9}$$

Thus, the propagation of the velocity uncertainty is found by:

$$U_{u_{current,slope}} = \sqrt{\left(\frac{\partial u_{current,slope}}{\partial L} \cdot U_L\right)^2 + \left(\frac{\partial u_{current,slope}}{\partial \triangle I} \cdot U_{\triangle I}\right)^2} \tag{C.10}$$

The parameters contributing to the uncertainty of equation C.10 are less than the parameters contributing to equation C.7. The accuracy of measuring the current is almost

an order of magnitude higher than of measuring the conductivity. The current difference will contribute more to the uncertainty of finding the velocity from equation C.9. The uncertainty of the current difference $\triangle I = I_2 - I_1$ could be found from:

$$U_{\triangle I} = \sqrt{\left(\frac{\partial \triangle I}{\partial I1} \cdot U_{I_1}\right)^2 + \left(\frac{\partial \triangle I}{\partial I_2} \cdot U_{I_2}\right)^2} \tag{C.11}$$

For the same example presented for the conductivity difference, the 1XTBE buffer results, the high and low measured currents during the current-monitoring experiment were $I_1 = 11.400\mu A$ and $I_2 = 10.57\mu A$. Thus, the uncertainty of the measured current are:

$$U_{I_1} = 0.1\% \cdot (11.40) = 1.14 \times 10^{-2}\mu A$$

and

$$U_{I_1} = 0.1\% \cdot (10.57) = 1.057 \times 10^{-2}\mu A$$

The uncertainly of the current difference was:

$$U_{\triangle I} = \sqrt{(1.14 \times 10^{-2})^2 + (1.057 \times 10^{-2})^2} = 1.55 \times 10^{-2}\mu A$$

As a percentage, the uncertainty of the current difference is equal to :

$$\%U_{\triangle I} = \frac{1.55 \times 10^{-2}}{11.4 - 10.57} = 1.87\%$$

This is better than the case of using the conductivity measurement, since the uncertainty was previously found as 17.78 %. This result supports the use of the current-slope method over the regular slope method for finding the velocity in terms of reliability and confidence in the measurement. Both the conductivity difference and current difference were discussed in this section since the contribution of these two parameters was the highest uncertainty cause for the different variables found in this work.

An important point of consideration that for various experimental measurements it is highly recommended to avoid finding a dependent variable that needs a mathematical subtraction operation, since it will give the highest uncertainty of the all the mathematical operations. Unfortunately for some parameters found from this work the subtraction operation could not be avoided, such as the surface conductance and the current-slope velocity.

For the other dependent parameters measured in this thesis (i.e. the zeta potential, electroosmotic mobility surface conductance) the uncertainty propagation was done with the same approach as presented in this appendix. The uncertainty calculations were performed with a written Matlab algorithm.

References

[1] Patric Tabeling. *Introduction to Microfluidics*. Oxford University Press., 2005.

[2] Andrew J. deMello. Control and detection of chemical reactions in microfluidic systems. *Nature*, 442(7101):394–402, 2006.

[3] Nam-Trung Nguyen and Steven T. Wereley. *Fundamentals and Applications of Microfluidics*. Artech House, 2nd edition, 2006.

[4] Dongqing Li. *Electrokinetics in Microfluidics*. Elsevier, 2004.

[5] George M. Whitesides. The origins and the future of microfluidics. *Nature*, 442(7101):368–373, 2006.

[6] P. S. Dittrich and A. Manz. Lab-on-a-chip: Microfluidics in drug discovery. *Nature Reviews Drug Discovery*, 5(3):210–218, 2006.

[7] T. Vilkner, D. Janasek, and A. Manz. Micro total analysis systems. recent developments. *Anal. Chem.*, 76(12):3373–3386, 2004.

[8] Dirk Janasek, Joachim Franzke, and Andreas Manz. Scaling and the design of miniaturized chemical-analysis systems. *Nature*, 442(7101):374–380, 2006.

[9] Detlev Belder. Integrating chemical synthesis and analysis on a chip. *Analytical and Bioanalytical Chemistry*, 385(3):416–418, 2006.

[10] Sumita Pennathur. Flow control in microfluidics: are the workhorse flows adequate? *Lab on a Chip*, 8(3):383–387, 2008.

[11] Jacob H. Masliyah and Subir Bhattacharjee. *Electrokinetic and Colloid Transport Phenomena*. Wiley, 2006.

[12] Philip W. Miller, Nicholas J. Long, Andrew J. de Mello, Ramon Vilar, Jan Passchier, and Antony Gee. Rapid formation of amides via carbonylative coupling

reactions using a microfluidic device. *Chemical Communications*, (5):546–548, 2006.

[13] T. Pennell, T. Suchyna, J. Wang, J. Heo, J. D. Felske, F. Sachs, and S. Z. Hua. Microfluidic chip to produce temperature jumps for electrophysiology. *Anal. Chem.*, 2008.

[14] K. Fluri, G. Fitzpatrick, N. Chiem, and D. J. Harrison. Integrated capillary electrophoresis devices with an efficient postcolumn reactor in planar quartz and glass chips. *Analytical Chemistry*, 68(23):4285–4290, 1996.

[15] Stefan Haeberle and Roland Zengerle. Microfluidic platforms for lab-on-a-chip applications. *Lab on a Chip*, 7(9):1094–1110, 2007.

[16] Y. Sun, C. S. Lim, A. Q. Liu, T. C. Ayi, and P. H. Yap. Design, simulation and experiment of electroosmotic microfluidic chip for cell sorting. *Sensors and Actuators a-Physical*, 133(2):340–348, 2007.

[17] A. T. Woolley, D. Hadley, P. Landre, A. J. deMello, R. A. Mathies, and M. A. Northrup. Functional integration of pcr amplification and capillary electrophoresis in a microfabricated dna analysis device. *Anal. Chem.*, 68(23):4081–4086, 1996.

[18] Shin Young Shik, Cho Keunchang, Lim Sun Hee, Chung Seok, Park Sung-Jin, Chung Chanil, Han Dong-Chul, and Chang Jun Keun. Pdms-based micro pcr chip with parylene coating. *Journal of Micromechanics and Microengineering*, 13(5):768–74, 2003.

[19] Tomasz Glawdel. Design, fabrication and characterization of electrokinetically pumped microfluidic chips for cell culture applications. Master's thesis, University of Waterloo, 2007.

[20] Min-Cheol Kim, Zhanhui Wang, Raymond H. W. Lam, and Todd Thorsen. Building a better cell trap: Applying lagrangian modeling to the design of microfluidic devices for cell biology. *Journal of Applied Physics*, 103(4):044701, 2008.

[21] L. Kim, Y. C. Toh, J. Voldman, and H. Yu. A practical guide to microfluidic perfusion culture of adherent mammalian cells. *Lab on a Chip*, 7(6):681–694, 2007.

[22] Arash Dodge, Edouard Brunet, Suelin Chen, Jacques Goulpeau, Valerie Labas, Joelle Vinh, and Patrick Tabeling. Pdms-based microfluidics for proteomic analysis. *The Analyst*, 131(10):1122–1128, 2006.

[23] Dayu Liu, Ming Shi, Huaiqing Huang, Zhicheng Long, Xiaomian Zhou, Jianhua Qin, and Bingcheng Lin. Isotachophoresis preconcentration integrated microfluidic chip for highly sensitive genotyping of the hepatitis b virus. *Journal of Chromatography B: Analytical Technologies in the Biomedical and Life Sciences*, 844(1):32–38, 2006.

[24] Agilent Technologies. Hplc-chip/ms technology, 2008. http://www.chem.agilent.com/scripts/generic.asp?lPage=15400indcol=Yprodcol=Y.

[25] Jaap den Toonder, Femke Bos, Dick Broer, Laura Filippini, Murray Gillies, Judith de Goede, Titie Mol, Mireille Reijme, Wim Talen, Hans Wilderbeek, Vinayak Khatavkar, and Patrick Anderson. Artificial cilia for active micro-fluidic mixing. *Lab on a Chip*, 2008.

[26] Robert J. Hunter. *Zeta Potential in Colloid Science*. Academic Press, 1981.

[27] Xuan Xiangchun. Joule heating in electrokinetic flow. *Electrophoresis*, 29(1):33–43, 2008.

[28] A. D. Stroock, S. K. W. Dertinger, A. Ajdari, I. Mezic, H. A. Stone, and G. M. Whitesides. Chaotic mixer for microchannels. *Science*, 295(5555):647–651, 2002.

[29] J. B. Zhang, G. W. He, and F. Liu. Electro-osmotic flow and mixing in heterogeneous microchannels. *Physical Review E*, 73(5), 2006.

[30] P. H. Paul, M. G. Garguilo, and D. J. Rakestraw. Imaging of pressure- and electrokinetically driven flows through open capillaries. *Analytical Chemistry*, 70(13):2459–2467, 1998.

[31] Marc A. Unger, Hou-Pu Chou, Todd Thorsen, Axel Scherer, and Stephen R. Quake. Monolithic microfabricated valves and pumps by multilayer soft lithography. *Science*, 288(5463):113–116, 2000.

[32] Erwin Berthier and David J. Beebe. Flow rate analysis of a surface tension driven passive micropump. *Lab on a Chip*, 7(11):1475–1478, 2007.

[33] Bin Zhao, Jeffrey S. Moore, and David J. Beebe. Surface-directed liquid flow inside microchannels. *Science*, 291(5506):1023–1026, 2001.

[34] Ji Won Suk and Jun-Hyeong Cho. Capillary flow control using hydrophobic patterns. *Journal of Micromechanics and Microengineering*, 17(4):11–15, 2007.

[35] C. H. Chen and J. G. Santiago. A planar electroosmotic micropump. *Journal of Microelectromechanical Systems*, 11(6):672–683, 2002.

[36] Mohamed G. Al-Fandi, Shankar Sundaram, Steve Tung, Ajay P. Malshe, Jerry Jenkins, and Jin-Woo Kim. Simulation and design an e. coli-based rotary micropump for use in microfluidic systems: Integration of micro-nano-bio. volume 5 of *American Society of Mechanical Engineers, Micro-Electromechanical Systems Division Publication (MEMS)*, pages 485–490, Washington, DC, United States, 2003. American Society of Mechanical Engineers, New York, NY 10016-5990, United States.

[37] P. Gravesen, J. Branebjerg, and O. S. Jensen. Microfluidics-a review. *Journal of Micromechanics and Microengineering*, (4):168, 1993.

[38] D. J. Harrison, A. Manz, Z. H. Fan, H. Ludi, and H. M. Widmer. Capillary electrophoresis and sample injection systems integrated on a planar glass chip. *Analytical Chemistry*, 64(17):1926–1932, 1992.

[39] M. Washizu, Y. Nikaido, O. Kurosawa, and H. Kabata. Stretching yeast chromosomes using electroosmotic flow. *Journal of Electrostatics*, 57(3-4):395–405, 2003.

[40] M. Macka, P. Andersson, and P. R. Haddad. Changes in electrolyte ph due to electrolysis during capillary zone electrophoresis. *Analytical Chemistry*, 70(4):743–749, 1998.

[41] I. Rodriguez and N. Chandrasekhar. Experimental study and numerical estimation of current changes in electroosmotically pumped microfluidic devices. *Electrophoresis*, 26(6):1114–21, 2005.

[42] S. Arulanandam and D. Q. Li. Determining zeta potential and surface conductance by monitoring the current in electro-osmotic flow. *Journal of Colloid and Interface Science*, 225(2):421–428, 2000.

[43] D. Erickson, D. Q. Li, and C. Werner. An improved method of determining the zeta-potential and surface conductance. *Journal of Colloid and Interface Science*, 232(1):186–197, 2000.

[44] Bz J. Kirby and E. F. Hasselbrink. Zeta potential of microfluidic substrates: 1. theory, experimental techniques, and effects on separations. *Electrophoresis*, 25(2):187–202, 2004.

[45] B. J. Kirby and E. F. Hasselbrink. Zeta potential of microfluidic substrates: 2. data for ppolymers. *Electrophoresis*, 25(2):203–213, 2004.

[46] J. L. Pittman, C. S. Henry, and S. D. Gilman. Experimental studies of electroosmotic flow dynamics in microfabricated devices during current monitoring experiments. *Analytical Chemistry*, 75(3):361–370, 2003.

[47] X. H. Huang, M. J. Gordon, and R. N. Zare. Current-monitoring mehod for measuring the electroosmotic flow-rate in capillary zone electrophoresis. *Analytical Chemistry*, 60(17):1837–1838, 1988.

[48] L. Q. Ren, C. Escobedo-Canseco, and D. Q. Li. A new method of evaluating the average electro-osmotic velocity in microchannels. *Journal of Colloid and Interface Science*, 250(1):238–242, 2002.

[49] X. Q. Ren, M. Bachman, C. Sims, G. P. Li, and N. Allbritton. Electroosmotic properties of microfluidic channels composed of poly(dimethylsiloxane). *Journal of Chromatography B-Analytical Technologies in the Biomedical and Life Sciences*, 762(2):117–125, 2001.

[50] T. Sikanen, S. Tuomikoski, R. A. Ketola, R. Kostiainen, S. Franssila, and T. Kotiaho. Characterization of su-8 for electrokinetic microfluidic applications. *Lab on a Chip*, 5(8):888–96, 2005.

[51] D. Sinton, C. Escobedo-Canseco, L. Q. Ren, and D. Q. Li. Direct and indirect electroosmotic flow velocity measurements in microchannels. *Journal of Colloid and Interface Science*, 254(1):184–189, 2002.

[52] R. Venditti, X. C. Xuan, and D. Q. Li. Experimental characterization of the temperature dependence of zeta potential and its effect on electroosmotic flow velocity in microchannels. *Microfluidics and Nanofluidics*, 2(6):493–499, 2006.

[53] P. J. Scales, F. Grieser, T. W. Healy, L. R. White, and D. Y. C. Chan. Eelectrokinetics of the silica solution interface - a flat-plate streaming potential study. *Langmuir*, 8(3):965–974, 1992.

[54] D. G. Yan, C. Yang, N. T. Nguyen, and X. Y. Huang. A method for simultaneously determining the zeta potentials of the channel surface and the tracer particles using microparticle image velocimetry ttechnique. *Electrophoresis*, 27(3):620–627, 2006.

[55] A. Khademhosseini, J. Yeh, G. Eng, J. Karp, H. Kaji, J. Borenstein, O. C. Farokhzad, and R. Langer. Cell docking inside microwells within reversibly sealed microfluidic chanzels for fabricating multiphenotype cell arrays. *Lab on a Chip*, 5(12):1380–1386, 2005.

[56] H. Kinoshita, M. Oshima, J. W. Hong, T. Fujii, T. Saga, and T. Kobayashi. Piv measurement of pressure- and electrokinetically-driven flow in microchannels. volume 5058 of *Proceedings of SPIE - The International Society for Optical Engineering*, pages 113–118, Beijing, China, 2003. The International Society for Optical Engineering.

[57] G. R. Wang. Laser induced fluorescence photobleaching anemometer for microfluidic devices. *Lab on a Chip*, 5(4):450–456, 2005.

[58] A. Sze, D. Erickson, L. Q. Ren, and D. Q. Li. Zeta-potential measurement using the smoluchowski equation and the slope of the current-time relationship in electroosmotic flow. *Journal of Colloid and Interface Science*, 261(2):402–410, 2003.

[59] S. S. Hsieh, H. C. Lin, and C. Y. Lin. Electroosmotic flow velocity measurements in a square microchannel. *Colloid and Polymer Science*, 284(11):1275–1286, 2006.

[60] T. N. T. Duong, H. N. Cheang, D. N. Ghista, and A. Q. Liu. Stable and high-volume electroosmotic transport for microfluidic chip. volume 2006 of *NanoSingapore 2006: IEEE Conference on Emerging Technologies - Nanoelectronics - Proceedings*, pages 237–240. IEEE Computer Society, Piscataway, NJ 08855-1331, United States, 2006.

[61] D. G. Yan, C. Yang, and X. Y. Huang. Effect of finite reservoir size on electroosmotic flow in microchannels. *Microfluidics and Nanofluidics*, 3(3):333–340, 2007.

[62] David C. Duffy, J. Cooper McDonald, Olivier J. A. Schueller, and George M. Whitesides. Rapid prototyping of microfluidic systems in poly(dimethylsiloxane). *Analytical Chemistry*, 70(23):4974–4984, 1998.

[63] J. M. K. Ng, I. Gitlin, A. D. Stroock, and G. M. Whitesides. Components for integrated poly(dimethylsiloxane) microfluidic ssystems. *Electrophoresis*, 23(20):3461–3473, 2002.

[64] Xu Guojun, Yu Liyong, L. J. Lee, and K. W. Koelling. Experimental and numerical studies of injection molding with microfeatures. *Polymer Engineering and Science*, 45(6):866–75, 2005.

[65] Evandro Piccin, Wendell Karlos Tomazelli Coltro, Jose Alberto Fracassi da Silva, Salvador Claro Neto, Luiz Henrique Mazo, and Emanuel Carrilho. Polyurethane from biosource as a new material for fabrication of microfluidic devices by rapid prototyping. *Journal of Chromatography A*, 1173(1-2):151–158, 2007.

[66] H. Homma, T. Kuroyagi, K. Izumi, C. L. Mirley, J. Ronzello, and S. A. Boggs. Diffusion of low molecular weight siloxane from bulk to surface. *IEEE Transactions on Dielectrics and Electrical Insulation*, 6(3):370–375, 1999.

[67] Chou Hou-Pu, M. A. Unger, and S. R. Quake. A microfabricated rotary pump. *Biomedical Microdevices*, 3(4):323–30, 2001.

[68] J. N. Lee, C. Park, and G. M. Whitesides. Solvent compatibility of poly(dimethylsiloxane)-based microfluidic devices. *Anal. Chem.*, 75(23):6544–6554, 2003.

[69] *User Manual for Extended Plasma Cleaner*.

[70] I. Jane Chen and Erno Lindner. The stability of radio-frequency plasma-treated polydimethylsiloxane surfaces. *Langmuir*, 23(6):3118–3122, 2007.

[71] J. A. Vickers, M. M. Caulum, and C. S. Henry. Generation of hydrophilic poly(dimethylsiloxane) for high-performance microchip electrophoresis. *Analytical Chemistry*, 78(21):7446–7452, 2006.

[72] Adam R. Abate, Daeyeon Lee, Thao Do, Christian Holtze, and David A. Weitz. Glass coating for pdms microfluidic channels by sol-gel methods. *Lab on a Chip*, 2008.

[73] Dhananjay Bodas and Chantal Khan-Malek. Formation of more stable hydrophilic surfaces of pdms by plasma and chemical treatments. *Microelectronic Engineering*, 83(4-9 SPEC ISS):1277–1279, 2006.

[74] Dhananjay S. Bodas and Chantal Khan-Malek. Fabrication of long-term hydrophilic surfaces of poly(dimethyl siloxane) using 2-hydroxy ethyl methacrylate. *Sensors and Actuators, B: Chemical*, 120(2):719–723, 2007.

[75] David T. Eddington, John P. Puccinelli, and David J. Beebe. Thermal aging and reduced hydrophobic recovery of polydimethylsiloxane. *Sensors and Actuators, B: Chemical*, 114(1):170–172, 2006.

[76] S. Hu, X. Ren, M. Bachman, C. E. Sims, G. P. Li, and N. L. Allbritton. Surface-directed, graft polymerization within microfluidic channels. *Anal. Chem.*, 76(7):1865–1870, 2004.

[77] A. Karkhaneh, H. Mirzadeh, and A.R. Ghaffariyeh. Two-step plasma surface modification of pdms with mixture of hema and aac: Collagen immobilization and in vitro assays. In *Fifth IASTED international Conference on Biomedical Engineering*, 2007.

[78] Yiqi Luo, Bo Huang, Hongkai Wu, and Richard N. Zare. Controlling electroosmotic flow in poly(dimethylsiloxane) separation channels by means of prepolymer additives. *Analytical Chemistry*, 78(13):4588–4592, 2006.

[79] Jikun Liu and Milton L. Lee. Permanent s0urface modification of polymeric capillary electrophoresis microchips for protein and peptide analysis. *Electrophoresis*, 27(18):3533–3546, 2006.

[80] Quanguo He, Zhengchun Liu, Pengfeng Xiao, Rongqing Liang, Nongyue He, and Zuhong Lu. Preparation of hydrophilic poly(dimethylsiloxane) stamps by plasma-induced grafting. *Langmuir*, 19(17):6982–6986, 2003.

[81] B. Wang, L. Chen, Z. Abdulali-Kanji, J. H. Zorton, and R. D. Oleschuk. Aging effects on oxidized and amine-modified poly(dimethylsiloxane) surfaces studied with chemical force titrations: Effects on electroosmotic flow rate in microfluidic channels. *Langmuir*, 19(23), 2003.

[82] E.S. Choi and S.S. Yang. Improvement of electroosmotic flow characteristics in poly(dimethylsiloxane) channels via a long life chemical surface modification. In *Seventh International Conference on Miniaturized Chemical and Biochemical Analysis Systems*, CA, USA, 59 October, 2003.

[83] Brian C. Smith. *Fundamentals of Fourier Transform Infrared Spectroscopicy*. CRC press, 1996.

[84] Joseph B. Lambert, Herbert F. Shurvell, David Liightner, and R. Graham Cooks. *Introduction to Organic Spectroscopicy*. Macmillan, 1987.

[85] Ronald F. Probstein. *Physicochemical Hydrodynamics: An Introduction*. Wiley-Interscience, 1994.

[86] MicroChem. Su-8 2000 permanet epoxy negative photoresist processing guidelines.

[87] Norman E. Good, G. Douglas Winget, Wilhelmina Winter, Thomas N. Connolly, Seikichi Izawa, and Raizada M. M. Singh. Hydrogen ion buffers for biological research. *Biochemistry*, 5(2):467–477, 1966.

[88] Keithley. *Low Level Measurements Handbook, Precision DC Current, voltage, and resistance measurements*, volume 6th.

[89] Zeyad A. Almutairi, Tomasz Glawdel, Carolyn L. Ren, and David A. Johnson. A novel y-channel design for measuring the zeta potential using the current monitoring technique.

[90] M. S. Bello. Electrolytic modification of a buffer during a capillary electrophoresis run. *Journal of Chromatography A*, 744(1-2):81–91, 1996.

[91] A. V. Stoyanov and J. Pawliszyn. Buffer composition changes in background electrolyte during electrophoretic run in capillary zone electrophoresis. *Analyst*, 129(10):979–982, 2004.

[92] MathWorks TM. Matlab.

[93] Thomas G. Beckwith, Roy D. Marangon, and V. John H. Lienhard. *Mechanical Measurements*. Prentice Hall, 5th edition, 1993.

[94] Y. Liu, D. O. Wipf, and C. S. Henry. Conductivity detection for monitoring mixing reactions in microfluidic devices. *Analyst*, 126(8):1248–1251, 2001.

[95] N. C. Stellwagen, A. Bossi, C. Gelfi, and P. G. Righetti. Dna and buffers: Are there any noninteracting, neutral ph buffers? *Analytical Biochemistry*, 287(1):167–175, 2000.

[96] F. Bianchi, F. Wagner, P. Hoffmann, and H. H. Girault. Electroosmotic flow in composite microchannels and implications in microcapillary electrophoresis systems. *Anal. Chem.*, 73(4):829–836, 2001.

[97] Razim Farid Samy. Soft lithography for applications in microfluidic thermometry, isoelectric focusing, and micromixers. Master's thesis, University of Waterloo, 2007.